

UC San Diego

UC San Diego Electronic Theses and Dissertations

Title

The preparation and characterization of a new garnet $\text{CaEr}_2\text{Mg}_2\text{Si}_3\text{O}_{12}$ phosphor matrix for white LEDs

Permalink

<https://escholarship.org/uc/item/5cn459g2>

Author

Li, Xiang

Publication Date

2022

Peer reviewed|Thesis/dissertation

UNIVERSITY OF CALIFORNIA SAN DIEGO

The preparation and characterization of a new garnet $\text{CaEr}_2\text{Mg}_2\text{Si}_3\text{O}_{12}$ phosphor matrix for white LEDs

A Thesis submitted in partial satisfaction of the requirements
for the degree Master of Science

in

Materials Science and Engineering

by

Xiang Li

Committee in charge:

Professor Olivia A Graeve, Chair
Professor Shengqiang Cai
Professor Yu Qiao

2022

Copyright

Xiang Li, 2022

All rights reserved.

The Thesis of Xiang Li is approved, and it is acceptable in quality and form for publication on microfilm and electronically.

University of California San Diego

2022

TABLE OF CONTENTS

THESIS APPROVAL PAGE	iii
TABLE OF CONTENTS.....	iv
LIST OF FIGURES	v
LIST OF TABLES	ix
ACKNOWLEDGEMENTS	x
ABSTRACT OF THE THESIS	xi
1 INTRODUCTION & BACKGROUND.....	1
2 MATERIALS & METHODS	37
3 CONCLUSIONS & FUTURE WORK.....	64
REFERENCES	66

LIST OF FIGURES

Figure 1.1 Schematic structure of dichromatic pc-WLEDs[14].....	2
Figure 1.2 Three methods of generating white light from LEDs: (A)RGB (red + green + blue)-LEDs, (B) UV-LED + RGB phosphors, and (C) Binary complimentary (blue-LED + yellow phosphor)[14].	6
Figure 1.3 (A) XRD Rietveld refinement results of $Y_{1.94}Ce_{0.06}Mg_2Al_2Si_2O_{12}$, (B) XRD results of the Ce^{3+} doped $Y_2Mg_2Al_2Si_2O_{12}$ phosphors and the prescriptive XRD data of $Y_3Al_5O_{12}$ (JCPDs card no.72-1315).	9
Figure 1.4 (A) PL spectra of Ce^{3+} doped $Y_2Mg_2Al_2Si_2O_{12}$ phosphors; (B) CIE coordinates diagram of the LED device.....	10
Figure 1.5 Decay kinetics of Eu^{2+} luminescence in $Ca_3Ga_2Ge_3O_{12}: Eu$ ceramic.	11
Figure 1.6 (A) PL spectra of LCMV: xEu^{3+} phosphors under 336 nm excitation; (B) Excitation line of $BaSO_4$ and the emission spectrum of LCMV: $0.005Eu^{3+}$ phosphor.	12
Figure 1.7 (A) TEM micrograph of LuAG: Ce^{3+} nano-garnet powder; (B) Temperature dependent normalized integrated PL intensities of LuAG: Ce^{3+} nano-garnet together with YAG: Ce^{3+} nano-garnet.....	14
Figure 1.8 (A) Excitation spectrum of a YAG: Tb (20%) powder sintered for 4 h at 1100°C together with DUV, NUV and blue LEDs signals; (B) Evolution of relative luminescence yield for different Tb^{3+} -doped yttrium-based garnets regarding to the excitation wavelength.	14
Figure 1.9 (A) The standard $Na_2YMg_2V_3O_{12}$ (No. 79-0967) profile (a), the XRD patterns of the as-prepared $Na_2YMg_2V_3O_{12}$ (b), and $Na_2GdMg_2V_3O_{12}$ (c); (B) Optical properties of $Na_2YMg_2V_3O_{12}$ and $Na_2GdMg_2V_3O_{12}$: PLE ($\lambda_{em} = 520$ nm) and PL ($\lambda_{ex} = 330$ nm) spectra.	15
Figure 1.10 XRD patterns of $LaOCl: 0.03Eu^{3+}$, $LaOCl: 0.007Tm^{3+}$, and $LaOCl: 0.007Tm^{3+}, 0.01Eu^{3+}$ together with the standard reference of $LaOCl$ compound.	16
Figure 1.11 Dependence of emission intensity of the $NaLa(MoO_4)_2: Eu^{3+}$ at 276 nm	17

Figure 1.12 Illustration of the morphological evolution process of molybdate phosphor from sharp bipyramid to quasi-cube as a function of EDTA amount.	18
Figure 1.13 (A) XRD patterns of CSSG:xDy ³⁺ (x = 0.04, 0.2 at%) phosphors annealed at 1123 K and 1473 K in air; (B) The intensity ratio I(445–465 nm)/I(480–500 nm) as a function of temperature for CSSG: xDy (x = 0.085 and 0.17 at%) and CSSG:0.17 at% Dy:0.105 at% Ce single crystalline film (SCF).	19
Figure 1.14 (A) XRD patterns of Y ₂ CaAlGe(AlO ₄) ₃ : Ce (a) and Y ₂ CaAlGe(AlO ₄) ₃ : Ce (b), ..	20
Figure 1.15 (A) XRD pattern of CaAl ₂ Si ₄ O ₁₂ : Dy ³⁺ phosphor. (B) SEM Micrograph of CaAl ₂ Si ₄ O ₁₂ : Dy ³⁺ phosphor.	22
Figure 1.16 (A) XRD patterns of the Ca ₂ KMg ₂ V ₃ O ₁₂ prepared at different temperatures: (a) 600°C, (b) 700°C, (c) 800°C, (d) 900°C; (B) Excitation and emission spectra of the Ca ₂ KMg ₂ V ₃ O ₁₂ obtained at different ignition temperatures: (a) 700°C, (b) 800°C, (c) 900°C and those of the control sample KVO ₃ (d).	23
Figure 1.17 (A) XRD patterns of LuAG: Nd powders calcined at different temperatures (a. Precursor; b. 850°C; c. 875°C; d. 900°C; e. 950°C; f. 1000°C); (B) Fluorescence emission spectrum of Nd _{3x} Lu _{3-3x} Al ₅ O ₁₂ (x ranges from 0.03 to 0.07) powders.	24
Figure 1.18 (A) Temperature dependence of the relative emission intensities as a function of temperatures of Y _{2.94-x} La _x Ce _{0.06} Al ₅ O ₁₂ (x = 0, 0.02, 0.04, 0.06, 0.08, and 0.1) phosphors excited at 460 nm; (B) The local structure model of La ³⁺ -Ce ³⁺ co-doping YAG.	26
Figure 1.19 (A) Excitation and emission spectra of LuAG-nano and LuAG-micron; (B) relative emission intensity of LuAG phosphors.	27
Figure 1.20 (A) PL emission spectra of the Ca ₃ Sc ₂ Si ₃ O ₁₂ : Ce ³⁺ samples produced at different annealing ambient atmospheres; (B) Parameters describing the white LED with different mass ratio of Ca ₃ Sc ₂ Si ₃ O ₁₂ : Ce ³⁺ green phosphor(G) and Sr ₂ Si ₅ N ₈ : Eu red phosphor(R).	28
Figure 1.21 (A) XRD patterns of Lu ₂ CaMg _{2-x} Si ₃ O ₁₂ : xMn ²⁺ phosphors (x = 0.01– 0.8); (B) CIE chromaticity diagram for Lu ₂ CaMg _{2-x} Si ₃ O ₁₂ : xMn ²⁺ as a function of Mn ²⁺ content.	29

Figure 1.22 (A) The photoluminescence emission intensity (i), and the maximum emission wavelength (ii) for $\text{Lu}_{2-x}\text{CaMg}_2\text{Si}_{2.9}\text{Ti}_{0.1}\text{O}_{12}: x\text{Ce}$ phosphors under 467 nm excitation; (B) The chromaticity coordinates of $\text{Lu}_{2-x}\text{CaMg}_2\text{Si}_{2.9}\text{Ti}_{0.1}\text{O}_{12}: x\text{Ce}$ phosphors.	29
Figure 1.23 (A) Emission spectra of $\text{Lu}_2\text{Ca}_{1-x}\text{Mg}_2\text{Si}_3\text{O}_{12}: x\text{Eu}^{2+}$ phosphors with different amount of Eu ($\lambda_{\text{ex}} = 365$ nm); (B) Emission spectra of $\text{Lu}_2\text{CaMg}_2\text{Si}_3\text{O}_{12}: 0.03\text{Eu}^{2+}$ and $\text{BaMgAl}_{10}\text{O}_{17}: 0.1\text{Eu}^{2+}$ ($\lambda_{\text{ex}} = 365$ nm).	30
Figure 1.24 (A) Emission spectra of $\text{NaBaPO}_4:\text{Eu}^{2+}$ phosphors prepared by solid-state reaction (1) and combustion method (2); (B) Temperature dependence of emission spectra of $\text{NaBaPO}_4:\text{Eu}^{2+}$ obtained by combustion method. The insert illustrates a comparison between $\text{NaBaPO}_4:\text{Eu}^{2+}$ phosphors and $\text{YAG}:\text{Ce}^{3+}$ phosphors.	31
Figure 1.25 Photoluminescence excitation (PLE) and photoluminescence (PL) spectra of the $\text{LiCa}_{0.97}\text{PO}_4: 0.03\text{Eu}^{2+}$ phosphor; the inset illustrates the energy level diagram of the Eu^{2+} ions in $\text{LiCa}_{0.97}\text{PO}_4: 0.03\text{Eu}^{2+}$	31
Figure 1.26 Emission spectra of $\text{CaMoO}_4:\text{Eu}^{3+}$ and sulfide phosphors.	33
Figure 1.27 (A) Emission spectra of $\text{Y}_{0.95}\text{Eu}_{0.05}\text{Al}_3(\text{BO}_3)_4$ phosphors calcined at 1100°C; (B) Emission intensity of Eu^{3+} in $\text{Y}_{0.95-x}\text{Gd}_x\text{Eu}_{0.05}\text{Al}_3(\text{BO}_3)_4$ series phosphors.	34
Figure 1.28 (A) The excitation (a) and emission (b) spectra of $\text{LiSr}_{4-x}\text{Pb}_x(\text{BO}_3)_3$ ($x = 0.005, 0.015, \text{ and } 0.03$) at room temperature; (B) Emission spectra of pure and $\text{LiSr}_{4-x}\text{Pb}_x(\text{BO}_3)_3$ ($x = 0.05, 0.1, 0.25, 0.5, 1, 1.5, 2, 3, 4, \text{ and } 5$ mol%).	35
Figure 1.29 (A) PL spectra of $\text{YCa}_4\text{O}(\text{BO}_3)_3: \text{Eu}^{3+}$. (a) Excitation by 613 nm. (b) Emission for 254 nm; (B) UV PL spectra of $\text{YCa}_4\text{O}(\text{BO}_3)_3: \text{Tb}^{3+}$. (a) Excitation by 547 nm. (b) Emission for 254 nm.	35
Figure 2.1 Theoretical XRD pattern of $\text{CaEr}_2\text{Mg}_2\text{Si}_3\text{O}_{12}$ calculated by VESTA software.	39
Figure 2.2 XRD spectra of CEMSO1 and CEMSO2 samples.	41
Figure 2.3 XRD spectra of CEMSO3 and CEMSO4 samples.	43
Figure 2.4 XRD spectra of CEMSO2 and CEMSO4 samples.	44

Figure 2.5 XRD spectra of CEMSO5 and CEMSO6 samples.	46
Figure 2.6 XRD spectra of CEMSO7 and CEMSO8 samples.	48
Figure 2.7 XRD spectra of CEMSO9, CEMSO10, and CEMSO11 samples.....	50
Figure 2.8 XRD pattern of CEMSO12 sample together with the theoretical $\text{CaEr}_2\text{Mg}_2\text{Si}_3\text{O}_{12}$ pattern.	52
Figure 2.9 XRD spectra of CEMSO13 sample.	53
Figure 2.10 XRD spectra of CEMSO14 and CEMSO15 samples.	55
Figure 2.11 XRD spectra of CEMSO16 sample.	57
Figure 2.12 XRD spectra of CEMSO17 and CEMSO18 samples.	58
Figure 2.13 XRD spectra of CEMSO21 and CEMSO22 samples.	59
Figure 2.14 XRD spectra of CEMSO12, CEMSO16, CEMSO21 and CEMSO22 samples....	60
Figure 2.15 XRD spectra of CEMSO23.....	61

LIST OF TABLES

Table 1-1 Comparison of excitation and emission intensity of $\text{LiEu}(\text{WO}_4)_{2-x}(\text{MoO}_4)_x$ phosphors.....	33
Table 2-1 Information on the starting reagents.	37
Table 2-2 Mass of the starting reagents (fuel-to-oxidizer ratio = f/o ratio).....	38
Table 2-3 The experimental parameters for CEMSO1 and CEMSO2 samples.	40
Table 2-4 The experimental parameters for CEMSO3 and CEMSO4 samples.	42
Table 2-5 The experimental parameters for CEMSO5 and CEMSO6 samples.	45
Table 2-6 The experimental parameters for CEMSO7 and CEMSO8 samples.	47
Table 2-7 The experimental parameters for CEMSO9, CEMSO10, and CEMSO11 samples.	49
Table 2-8 The experimental parameters for CEMSO12 and CEMSO13 samples.	51
Table 2-9 The experimental parameters for CEMSO14 and CEMSO15 samples.	54
Table 2-10 The experimental parameters for CEMSO16, CEMSO17, CEMSO18, CEMSO19, and CEMSO20 samples.....	56
Table 2-11 The calcination parameters for CEMSO12, CEMSO16, CEMSO21, and CEMSO22 samples.	60
Table 2-12 Phase composition of all the prepared samples.	62
Table 3-1 The experimental parameters for sample CEMSO23.	64

ACKNOWLEDGEMENTS

At the very first, I would like to extend my sincere gratitude to my Faculty Advisor, Dr. Olivia A Graeve. I am deeply grateful for her approval of my attendance in the research group and her valuable guidance for my research.

Then, I would like to express my heartfelt gratitude to Dr. Ekaterina Novitskaya. She has offered me insightful comments on my experiments and valuable suggestions for my thesis writing.

Last but not least, I would like to express my gratitude to my family for their supports and consideration.

ABSTRACT OF THE THESIS

The preparation and characterization of a new garnet $\text{CaEr}_2\text{Mg}_2\text{Si}_3\text{O}_{12}$ phosphor matrix for white LEDs

by

Xiang Li

Master of Science in Materials Science and Engineering

University of California San Diego, 2022

Professor Olivia A Graeve, Chair

White light-emitting diode (WLED) has been widely used because of its excellent performance in solid-state lighting. Among all the white LEDs (WLEDs), the phosphor-converted WLED is the most popular one, and its performance depends on the characteristics of the phosphor to a great extent. For this reason, it is necessary to study new phosphors for their potential use in WLEDs. In this thesis, a new garnet $\text{CaEr}_2\text{Mg}_2\text{Si}_3\text{O}_{12}$ matrix for phosphors was prepared by a solution combustion synthesis. Parameters of the synthesis, such as fuel-to-oxidizer ratio, amounts of precursors, order of mixing, as well as combustion and calcination parameters were optimized during this process. The garnet structure was successfully obtained and confirmed by X-ray diffraction characterization technique.

1 INTRODUCTION & BACKGROUND

White LEDs

White light-emitting diode (WLED) is a popular semiconductor light-emitting device, which belongs to one of the solid-state light sources. It has the advantages of small volume, low energy consumption, long service life, high luminous efficiency, and low environmental pollution[1-3]. Therefore, WLED has been widely used, and it recently became a new generation of all-solid-state lighting sources in the lighting industry[4].

The WLED started with the development of LED. LED is a stable and efficient semiconductor light-emitting device for photoelectric conversion.

Holonyak and Bevaqua[5] made the world's first red LED with the semiconductor compound material GaAsP at the 1960s. The luminous efficiency of this first red LED was less than 0.1 lm/W, which was very low compared with that of an unfiltered incandescent source (around 15 lm/W). In the following decade, a nitrogen-doped GaAsP(GaAsP:N) was reported, which could generate ten times brighter red emitters as well as orange and yellow emitters[6].

In the 1980s, the LED's lumen efficiency reached 10 lm/W because of the application of the GaAlAs material synthesized by a liquid phase epitaxy (LPE) method. This lumen efficiency exceeded the liquid crystal efficiency for the first time, and it pointed out the direction for the research and development of high brightness LEDs[7]. In 1993, the double-heterostructure blue LED chip[8] was successfully prepared for the first time, taking a big step toward the short-wavelength light-emitting area.

Since the entire visible spectrum was realized with the development of the different LEDs, it made it possible to yield white light by LEDs. The first white LED based on $Y_3Al_5O_{12}: Ce$ (YAG:

Ce) was then successfully offered for sale in 1996[9]. This white LED can emit polychromatic light, while the traditional LED can only emit monochromatic light.

In summary, with the improvement of brightness and luminous efficiency of LED materials, their application field became more extensive. They are now widely used in lighting sources, display screens, indicator lamps, among others[10-12]. Therefore, the realization of high-performance white LED light sources has always been the goal of researchers all over the world[13].

Structure and luminous principle of white LED

Structure

For the widely-used white LED, the fluorescence conversion is the main implementation method which emits light through the combination of chips and phosphors. This structural principle is shown on Figure 1.1 for dichromatic phosphor-converted white LED (pc-WLED).

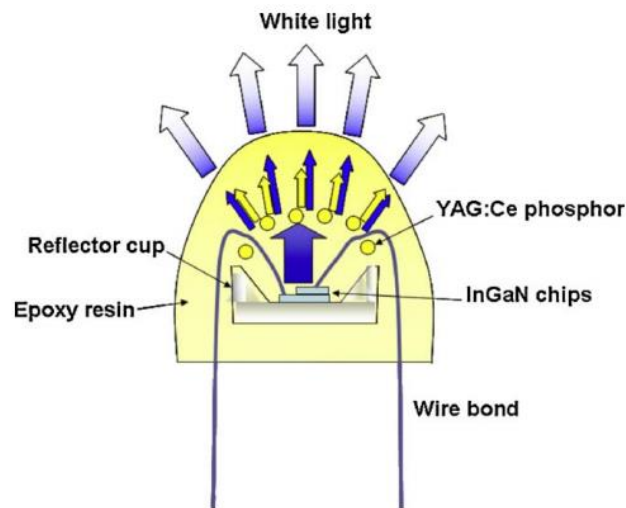


Figure 1.1 Schematic structure of dichromatic pc-WLEDs[14].

As seen on Figure 1.1, the white LED device mainly consists of two parts:

1. The bottom part is composed of two aluminum supports which are the cathode and anode.

2. For the upper part, a reflector cup is to control the light quality and quantity. To fix the LED chip on the reflector, the crystal glue is coated on the bottom layer; the outer layer of the chip is coated with silica gel and phosphor. Also, in order to protect the white LED device from damage, a layer of epoxy resin is wrapped around the periphery of the white LED device[14].

Luminous principle

The LED chip is composed of a p-type semiconductor, n-type semiconductor, and p-n junction. The electron deficient holes (h^+ , positive charge carrier) are dominant in the p-type semiconductors, while the free electrons (e^- , negative charge carrier) are dominant in the n-type semiconductors. A p-n junction in the LED chip is known as the active region, which can emit light when an electric field is applied. As a result, the process of electricity-to-light conversion can be realized. When there is no bias voltage applied, the p-type and n-type semiconductors will get in contact with each other and form a p-n junction. When the bias voltage is applied in the forward direction to the p-n junction, the electrons flow from the n-type to the p-type, and the holes flow from the p-type to the n-type. When the electrons in the n-type combine with the holes in the p-type at the p-n junction, the excess energy is released in the form of light and heat, so as to convert electricity into the light[15]. When the reverse biased voltage is applied to the p-n junction, the electrons are difficult to move to the p-type, so the electrons cannot combine with the holes, and cannot emit light at this time.

In addition, the luminous principle of white LED mainly includes two processes: electroluminescence and photoluminescence[16]. For example, for the LED device shown on Figure 1.1, after the current is applied, the blue indium gallium nitride (InGaN) LED chip can emit blue light, and one part of the emitted blue light can excite the $Y_3Al_5O_{12}: Ce^{3+}$ phosphor coated on

the chip to emit yellow light, and then the yellow light is combined with the other part of the blue light emitted by the chip to form white light.

Implementation methods of white LED

RGB LEDs

This method is mainly based on the principle of spatial color mixing, combining the RGB (red, green, and blue) LED chips within the same device, and then controlling the current of these three chips and the ratio of the emitted tricolor lights to obtain white light (generally, the ratio of red, green, and blue is 3:6:1) [17]. This method has the advantages of high luminous efficiency, less energy loss, and high color rendering index. However, due to the complexity of the circuit design, the cost is high[18]. In addition, with the increase in the working temperature, the RGB LED chips will have diversities in quantum efficiency (the ratio of the average number of photons to the number of photons produced under a specific wavelength), which will cause differences in the performance (decay time and chromatic aberration). Also, environmental changes can affect its luminescence properties, so the luminescence properties become unstable by using this method[19]. This method is summarized on Figure 1.2(A).

UV LED chip + RGB phosphor

This method takes ultraviolet (UV) or near-ultraviolet (NUV) LED as the excitation source, excites the RGB phosphors at the same time, or excites the single matrix white-light phosphor. Then, after adjusting the ratio of the RGB phosphors, white light can be obtained. This method has the advantages of high color rendering index, high luminous efficiency, and controllable color temperature. However, to excite the RGB phosphors, high-power chips need to be used in this method, so it brings difficulties to the fabrication of the device, and also the cost is relatively high[20]. Secondly, in this method, the blue light emitted can be re-absorbed by the red and green

phosphors, and this will cause a low color rendering index. In addition, the accidental leakage of ultraviolet light may endanger human health, so there are also potential security risks by using this method[21, 22]. This method is summarized on Figure 1.2(B).

Binary complimentary = Blue LED chip + yellow phosphor

For this method, the blue LED is used as the excitation source. As mentioned above, some of the blue light excites the yellow phosphor to emit yellow light, which can be combined with the rest of the directly-emitted blue light to obtain white light[14]. It has the advantages of a simple operation, low cost, good stability, high luminous efficiency, and non-production of UV radiation pollution. However, this method mainly produces white light by combining the blue and yellow light, which lacks the red-light component, therefore, the resultant white LED has several main disadvantages, such as high color temperature, and low color rendering index. In addition, both packaging materials and phosphors may age with the extension of LED service time, resulting in the gradual drift of the color temperature[23]. This method is summarized on Figure 1.2(C).

What's more, nowadays, the commercial production of white LED only adopts the way of blue LED chip + yellow phosphor (see Figure 1.2(C)). In order to improve on this method, the corresponding yellow phosphor can be further doped, and the red components can be supplemented by mixing red phosphor with the yellow phosphor[24, 25]. Also, the way of UV LED chip + RGB phosphor is also a promising way to produce white light. In order to solve the serious problem of mutual re-absorption of the RGB phosphors, single matrix phosphors with tunable emission spectrum have been widely studied in recent years[26, 27]. Furthermore, the white LED implemented by using phosphors is defined as phosphor-converted white LED (pc-WLED), and it has the requirements of high-performance phosphors. Therefore, it is important to

study novel phosphors with excellent properties to improve the properties of the pc-WLED made by these two promising ways.

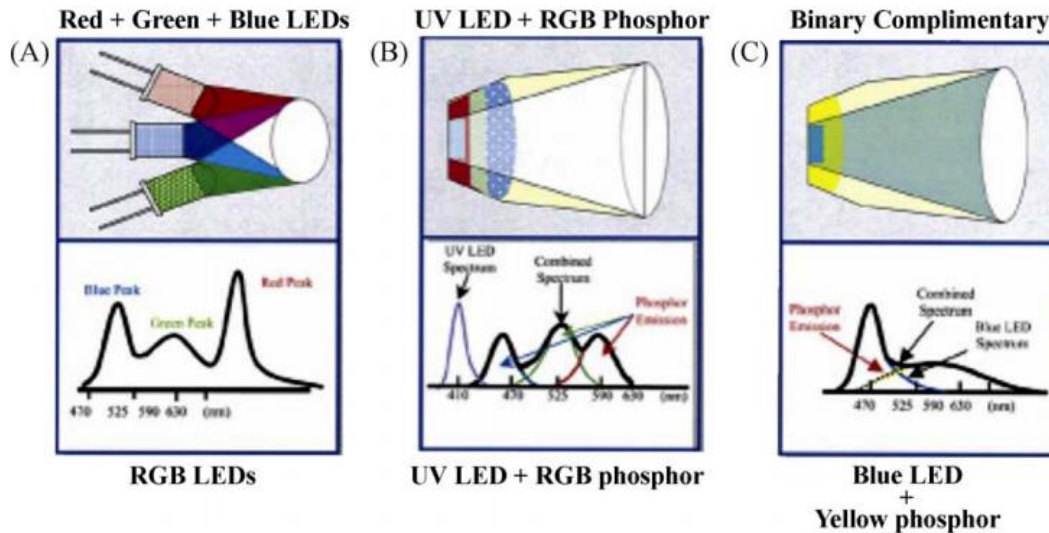


Figure 1.2 Three methods of generating white light from LEDs: (A)RGB (red + green + blue)-LEDs, (B) UV-LED + RGB phosphors, and (C) Binary complimentary (blue-LED + yellow phosphor)[14].

White-light phosphor

As mentioned above, phosphors play an important role in the realization of phosphor-converted white LEDs. After an enormous amount of investigations by the researchers, the phosphors used to achieve excellent white LED should have the following characteristics[28]:

- (1) Since most of the phosphor needs to be excited by LED chips, the excitation spectrum should be located in the wavelength range of ultraviolet (UV) or near-ultraviolet (NUV).
- (2) Heat is generated in the working process of the white LED device, so the phosphor should have good thermal stability to avoid performance degradation when the temperature is increased.
- (3) The phosphor should have both excellent physical and chemical stability, to avoid causing physical and chemical reactions with the packaging materials.
- (4) The phosphor should have a relatively high quantum efficiency.

For the composition of the phosphor, it is mainly composed of matrix, activator, and sensitizer. The matrix has a specific crystal structure to form a basic energy band structure. It does not participate in the luminescent process but can provide a sufficiently stable lattice environment for the luminescence of the activator[29]. Generally, rare-earth ions and transition metal ions can work as activators. How does the activator work? The lattice of the ions in the matrix is occupied by the activator to generate the luminescence center, and the luminescence is accomplished by the transition between the energy levels of the ground state and the excited state[30]. The energy-level structure of the sensitizer is usually similar to that of the activator. It can transfer the absorbed energy to the luminescence center (activator) and improve the luminescence performance of the phosphor by improving the energy excitation efficiency of the phosphor[31].

Characterization of the phosphor

X-ray diffraction (XRD) analysis: XRD can effectively study the phases and crystal structure of the phosphor. The XRD pattern obtained from the test is compared with the standard PDF card to determine whether the prepared phosphors contain impurities.

Scanning electron microscope (SEM) analysis: SEM can study the surface morphology and particle size of the phosphor.

Fluorescence spectroscopy analysis: by measuring the excitation and emission spectra, the excitation wavelength, emission wavelength, and luminous intensity of the phosphor can be studied.

Concentration quenching[32, 33] analysis: the doping concentration of rare-earth ions has a decisive influence on the luminescence intensity of the phosphor. Generally, with the increase in doping concentration of rare-earth ions, the fluorescence intensity will first increase and then decrease.

Thermal stability[34, 35] analysis: by comparing the relative intensities of emission spectra at different temperatures during the heating process, the thermal stability of the phosphor can be studied.

Chromaticity coordinates[36, 37]: by analyzing the chromaticity coordinates of the phosphor, the luminous color and color temperature can be obtained. Also, according to the comparison between the coordinates of the phosphor and standard color, the color rendering index can be studied.

Preparation methods for phosphor

Solid-state method

Solid-state method is the most traditional and widely-used method for the preparation of the phosphors[38, 39]. At present, most phosphors on market are synthesized by the solid-state method. The basic operation steps of this method are to mix the raw materials according to the chemical composition, then heat them at a certain temperature for a certain time.

That is to say, the main part of this method is to melt the raw materials, conduct the reaction in the molten state, and heat the reactants in a high-temperature furnace. After these operations, it is taken out and ground to finally obtain the product phosphor[40-42]. In the heating process, the reactants conduct the ionic diffusion or the recombination of chemical bonds at the interface contact firstly, and then gradually diffuse to the interior of the material.

Several examples of phosphors prepared by the solid-state method are summarized below.

In order to realize the partial substitution of Mg^{2+} - Si^{4+} to Y^{3+} - Al^{3+} in the $Y_3Al_5O_{12}$ (YAG) matrix, Z. Wei et al.[43] successfully prepared a new cubic-type garnet $Y_2Mg_2Al_2Si_2O_{12}$ by solid-state method. For the synthesis process, the raw materials were mingled and ground together and

then sintered in a muffle furnace at 1400°C, finally, the as-prepared powders were collected and reground.

The authors compared the raw XRD data for their new phosphor with both the calculated data (based on the crystallographic data of $Y_3Al_5O_{12}$) and the standard PDF card for the YAG material, and concluded the successful preparation of the pure $Y_2Mg_2Al_2Si_2O_{12}: Ce^{3+}$ phosphor (see Figure 1.3). In addition, as shown on Figure 1.4, the excitation band of $Y_2Mg_2Al_2Si_2O_{12}: Ce^{3+}$ phosphor was found to be located at 400–525 nm, which is suitable for applying this phosphor in the WLEDs based on a blue LED chip. Also, the LED device using the phosphors mentioned above can emit white light with the CIE coordinates of (0.3548, 0.3150), and the CCT value of 4363K. These results clearly indicate that the $Y_2Mg_2Al_2Si_2O_{12}: Ce^{3+}$ phosphors can be served as blue light excited phosphors in warm WLEDs.

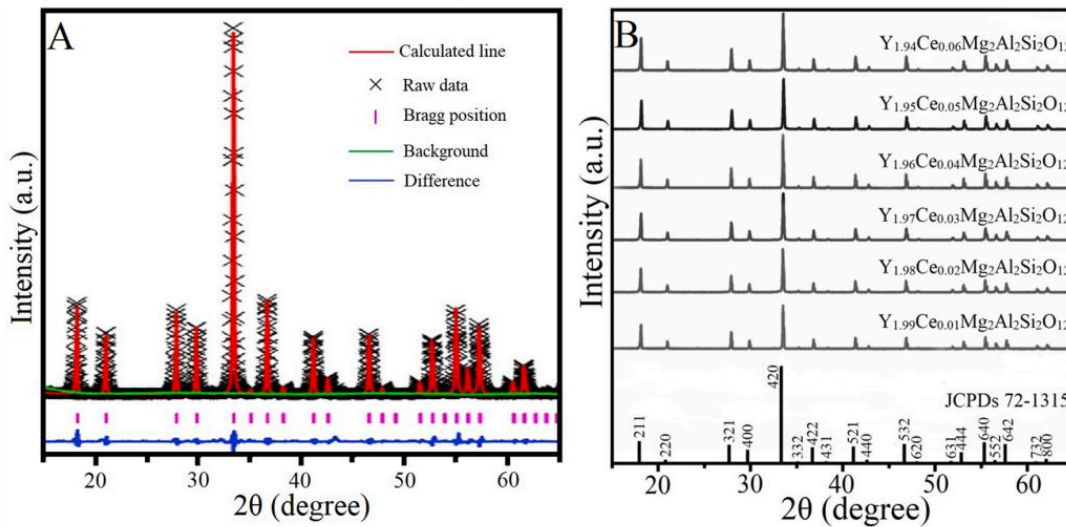


Figure 1.3 (A) XRD Rietveld refinement results of $Y_{1.94}Ce_{0.06}Mg_2Al_2Si_2O_{12}$, (B) XRD results of the Ce^{3+} doped $Y_2Mg_2Al_2Si_2O_{12}$ phosphors and the prescriptive XRD data of $Y_3Al_5O_{12}$ (JCPDs card no.72-1315).

T. Zorenko et al.[44] successfully prepared the $\text{Ca}_3\text{Ga}_2\text{Ge}_3\text{O}_{12}:\text{Eu}$ by solid-state method. For the synthesis process, the raw materials were heated at a temperature of 1100°C in a N_2+H_2 atmosphere.

For the characterization, the XRD analysis confirmed the phase formation by comparing the XRD pattern of the synthesized sample with the $\text{Ca}_3\text{Ga}_2\text{Ge}_3\text{O}_{12}:\text{Eu}$ ceramic sample. In addition, the luminescence of the Eu^{2+} ions was found to be located at the 450–460 nm range, which is due to the 4f-5d transitions of the Eu^{3+} ions. As a result, it was concluded that the luminescence of Eu^{3+} can be excited via the Eu^{2+} luminescence. After further investigation of the Eu-related luminescence centers by the decay kinetics of Eu^{2+} and Eu^{3+} luminescence, the Eu^{2+} to Eu^{3+} energy transfer was verified (see Figure 1.5).

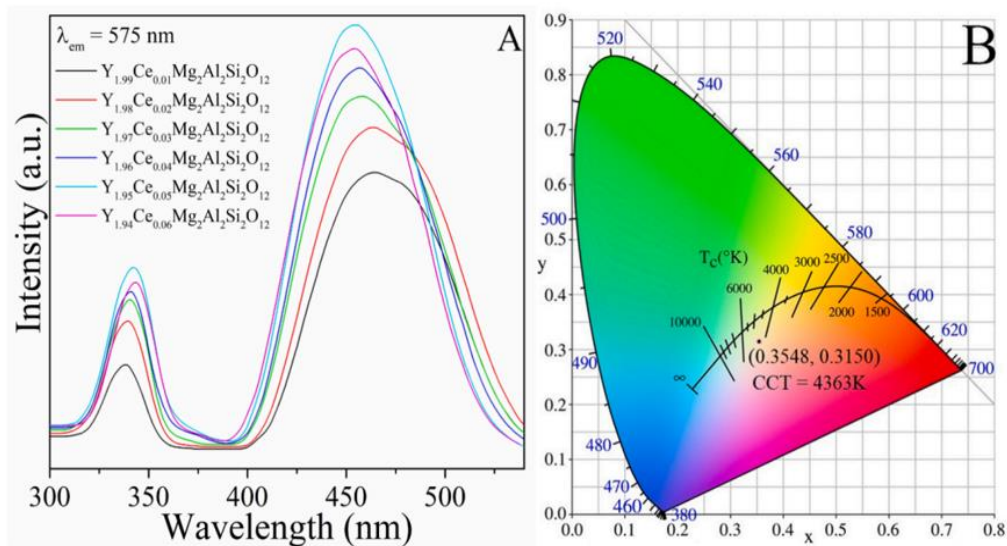


Figure 1.4 (A) PL spectra of Ce^{3+} doped $\text{Y}_2\text{Mg}_2\text{Al}_2\text{Si}_2\text{O}_{12}$ phosphors; (B) CIE coordinates diagram of the LED device.

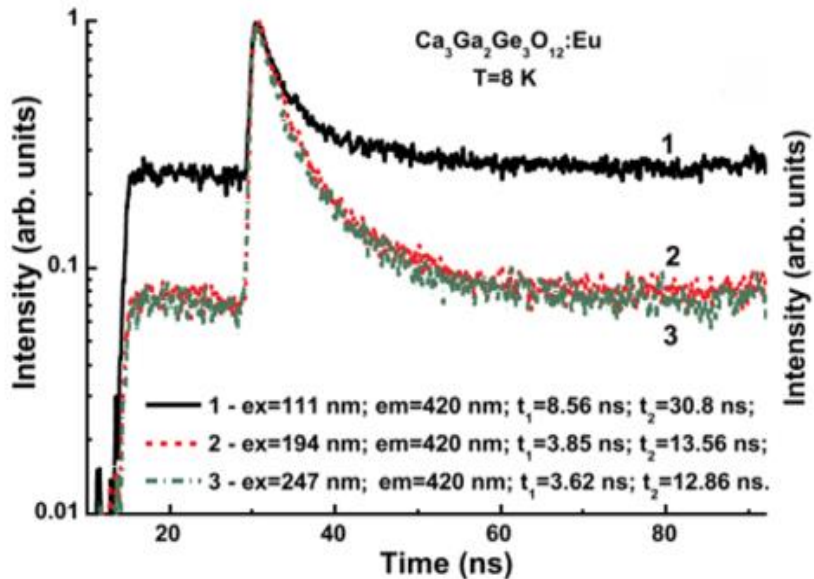


Figure 1.5 Decay kinetics of Eu^{2+} luminescence in $\text{Ca}_3\text{Ga}_2\text{Ge}_3\text{O}_{12}:\text{Eu}$ ceramic.

X. Huang et al.[45] prepared the $\text{LiCa}_3\text{MgV}_3\text{O}_{12}(\text{LCMV}):\text{Eu}^{3+}$ phosphor by the high-temperature solid-state method. For the synthesis process, the starting materials were mixed homogeneously and then calcined in a tubular furnace at 750°C for 6 h. Finally, the samples were reground and put into a furnace for a further calcination at 850°C for 6 h in air.

The prepared phosphors can increase the strong broadband bluish-green emission in the visible range, and the phosphors demonstrate the tunable bluish-green-to-white-to-red photoluminescence after increasing the Eu^{3+} concentrations (see Figure 1.6(A)). Specifically, the $\text{LCMV}:0.005\text{Eu}^{3+}$ sample can emit white light and showed a high internal quantum efficiency, which is 53% as demonstrated on Figure 1.6(B).

The advantages of the solid-state method are a simple process, few experimental steps, and simple equipment used, therefore, it is suitable for mass industrial production. However, this method has several disadvantages: high energy consumption, large amounts of impurities, and also, the grinding treatment will sometimes affect the fluorescence characteristics of the prepared sample.

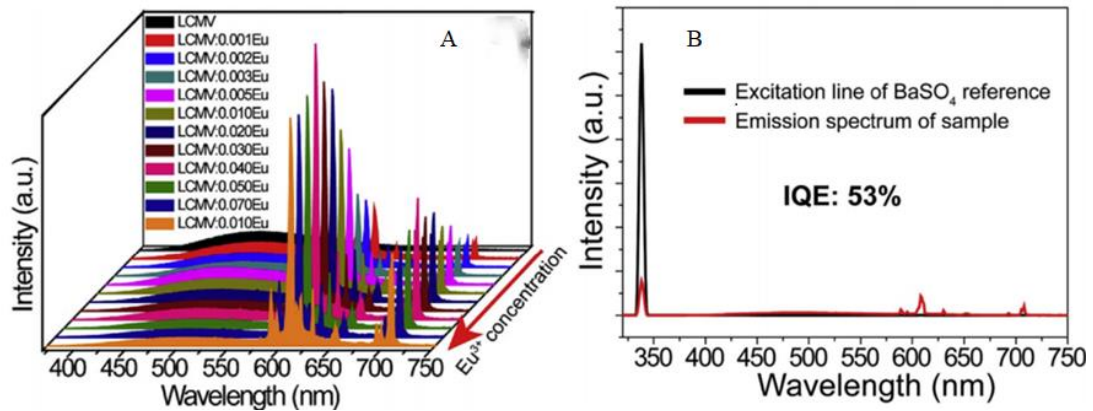


Figure 1.6 (A) PL spectra of LCMV: $x\text{Eu}^{3+}$ phosphors under 336 nm excitation; (B) Excitation line of BaSO_4 and the emission spectrum of LCMV: 0.005Eu^{3+} phosphor.

Sol-gel method

At present, this method is very common in the preparation of phosphors. The basic steps of this method are listed as follows[39]:

1. Inorganic salts, metal alkoxides, and metal salts solution are used as precursors, the precursors are dissolved in a nitric acid solution. Then the cross-linking agents (ethylene glycol and polyethylene glycol) are added into the solution.

2. Then the solution is stirred while heating and the transparent gel is formed then.

3. The gel with a network structure is calcinated at a low temperature.

4. The final product is obtained.

Furthermore, the preparation of the gel in the above-mentioned step 1 can be further divided into three kinds: (a) The precursor is an inorganic compound, which needs to adjust the pH value or add an electrolyte. (b) The precursor is a metal alkoxide, which needs to add chelating agent. (c) The precursor is a metal salt, which a complexing agent needs to be added. In addition, choosing suitable calcination parameters can also adjust the particle size and enhance the luminous intensity of the resultant phosphor[46].

Several phosphors prepared by sol-gel method are taken as examples below.

R. Praveena et al.[47] successfully prepared the $\text{Lu}_3\text{Al}_5\text{O}_{12}:\text{Ce}^{3+}$ (LuAG: Ce^{3+}) nano-garnet by the sol-gel method, and also investigated the structure and the thermal stability of photoluminescence of that phosphors. For the synthesis process, citric acid was added to the solution of $\text{Lu}(\text{NO}_3)_3$, $\text{Al}(\text{NO}_3)_3$, $\text{Ce}(\text{NO}_3)_3$, and HNO_3 , and then the polyethylene glycol (PEG) was added as a cross-linking agent. After drying, the gel was fired at 500°C for 2 h and annealed at 900°C for 16 h in the air.

As shown on Figure 1.7(A), the prepared nano-garnet was found that there were agglomerated particles with an average grain size of 22 nm. Also, the thermal stability of the prepared LuAG: Ce^{3+} was found to be much better than the one of the commercially available $\text{Y}_3\text{Al}_5\text{O}_{12}$ (YAG): Ce^{3+} , which can be seen on Figure 1.7(B). This indicates that LuAG: Ce^{3+} phosphor can be potentially used in the WLED applications.

A. Potdevin et al.[48] also used the sol-gel method and prepared both $\text{Y}_3\text{Al}_5\text{O}_{12}$ (YAG) and $\text{Y}_3\text{Ga}_5\text{O}_{12}$ (YGG) samples with Tb^{3+} dopants. For the synthesis process, after the gel was obtained, it was sintered at 1100°C for 4 h in a muffle furnace. For the characterization, the excitation spectra of the YAG: Tb (20%) powder, deep-ultraviolet (DUV) LED signal, near-UV LED signal, and blue LED signal can be seen on Figure 1.8(A). It indicates that several excitation bands between 200 and 500 nm match well with the DUV LED signal and the near-UV LED signal. Furthermore, on Figure 1.8(B), the evolution of relative luminescence yield for different Tb^{3+} -doped yttrium-based garnets regarding to the excitation wavelength; the efficiency of those materials clearly depends on the corresponding excitation wavelength was summarized. In summary, by tuning the composition, the optimized luminescence properties for prospective LEDs applications can be obtained.

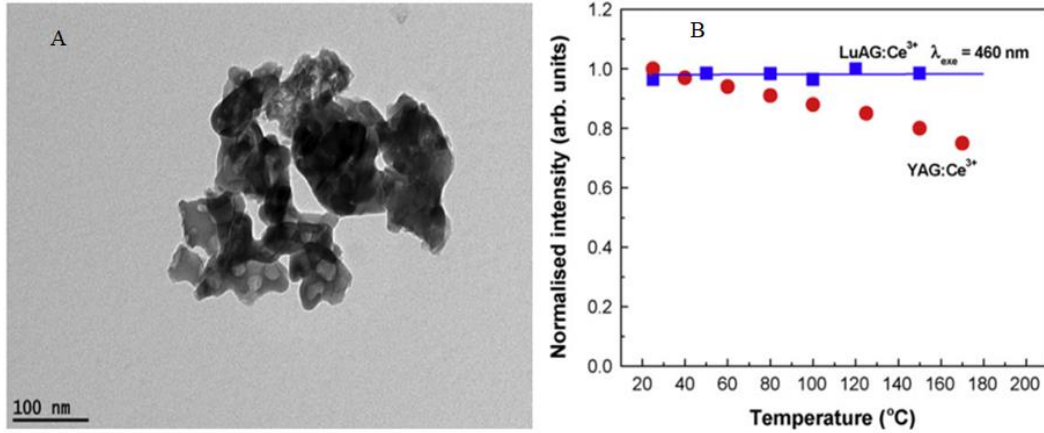


Figure 1.7 (A) TEM micrograph of LuAG: Ce³⁺ nano-garnet powder; (B) Temperature dependent normalized integrated PL intensities of LuAG: Ce³⁺ nano-garnet together with YAG: Ce³⁺ nano-garnet.

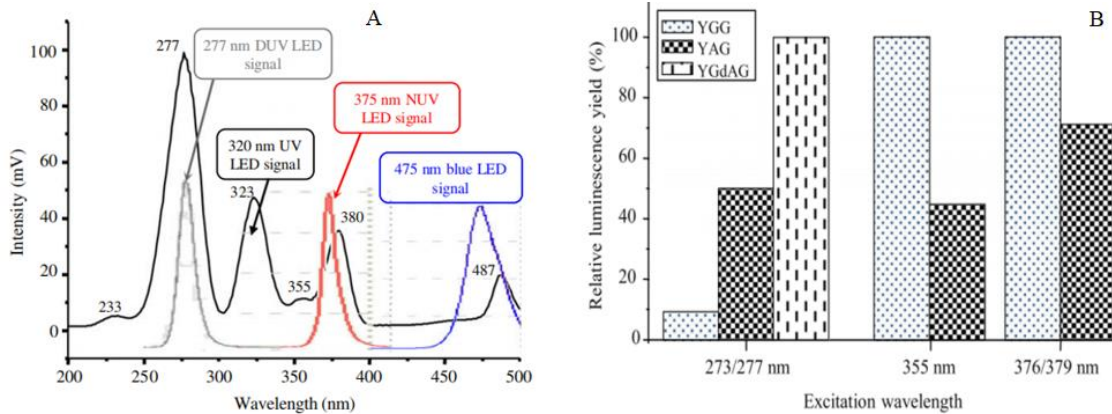


Figure 1.8 (A) Excitation spectrum of a YAG: Tb (20%) powder sintered for 4 h at 1100°C together with DUV, NUV and blue LEDs signals; (B) Evolution of relative luminescence yield for different Tb³⁺-doped yttrium-based garnets regarding to the excitation wavelength.

D. Song et al.[49] prepared the garnet vanadate phosphors Na₂LnMg₂V₃O₁₂ (Ln = Y, Gd) by a modified sol-gel method. For the experimental procedure, they made a metal complex after adding the citric acid C₆H₈O₇ with a molar ratio of 1:2 (metal ions and citric acid) first, and then the raw materials were mixed to obtain the solution. Next, the gel was formed after a gradually 48 h -drying process, and finally, the gel was ground and preheated in a muffle furnace at 500°C for 5 h and then sintered at 800°C for 5 h under ambient atmospheres. The prepared phosphors had a well-crystallized single garnet structure (see Figure 1.9(A)). The phosphors also showed a broad

temperature and time. Finally, the resultant product is washed, filtered, and dried to obtain the final product. Some phosphors prepared by hydrothermal method will be discussed below.

H. Bai et al.[50] prepared the $\text{LaOCl: Tm}^{3+}, \text{Eu}^{3+}$ by the hydrothermal method. For the synthesis process, $\text{La}(\text{NO}_3)_3$, $\text{Eu}(\text{NO}_3)_3$, and $\text{Tm}(\text{NO}_3)_3$ were dissolved in deionized water and mixed homogeneously according to the corresponding doping proportions. Then sodium citrate and urea were added into the mixture, and the pH of the mixture was adjusted to 10 by dropping ammonia. Finally, the obtained aqueous solution was transferred to the high-pressure hydrothermal reactor to fill 80% of its total volume. The hydrothermal reactor was tightly sealed and heated at 180°C for 24 h.

As can be seen from Figure 1.10, the XRD patterns of Tm^{3+} single-doped, Eu^{3+} single-doped, and $\text{Tm}^{3+}/\text{Eu}^{3+}$ co-doped LaOCl were all consistent with those of pure phase LaOCl , and there was no second phase detected. The result shows that the sample prepared by this method has less impurities.

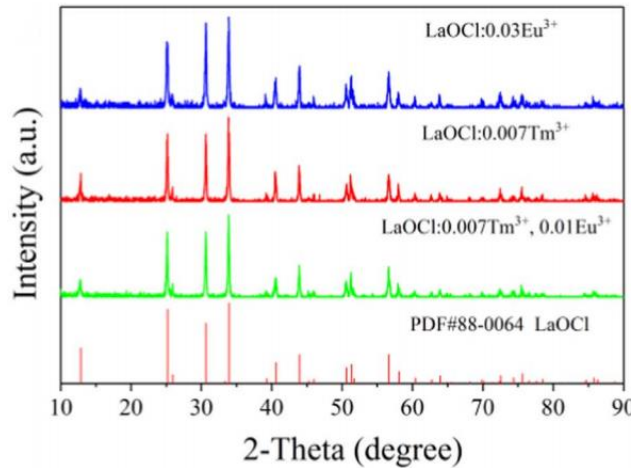


Figure 1.10 XRD patterns of $\text{LaOCl: 0.03Eu}^{3+}$, $\text{LaOCl: 0.007Tm}^{3+}$, and $\text{LaOCl: 0.007Tm}^{3+}, 0.01\text{Eu}^{3+}$ together with the standard reference of LaOCl compound.

M. Yang et al.[51] systematically studied the effects of different process parameters on $\text{NaLa}(\text{MoO}_4)_2: \text{Eu}^{3+}$ phosphor prepared by hydrothermal synthesis. The dependence of

luminescent intensity on the Eu^{3+} concentration was also studied. As shown on Figure 1.11, it can be seen that the emission intensity of the Eu^{3+} ions first increases with increasing Eu^{3+} concentrations, after that the intensity reaches a maximum when the percentage of Eu-doped product is 4%, and then it decreases with a further increasing of Eu^{3+} concentration due to the concentration quenching of the Eu^{3+} ions.

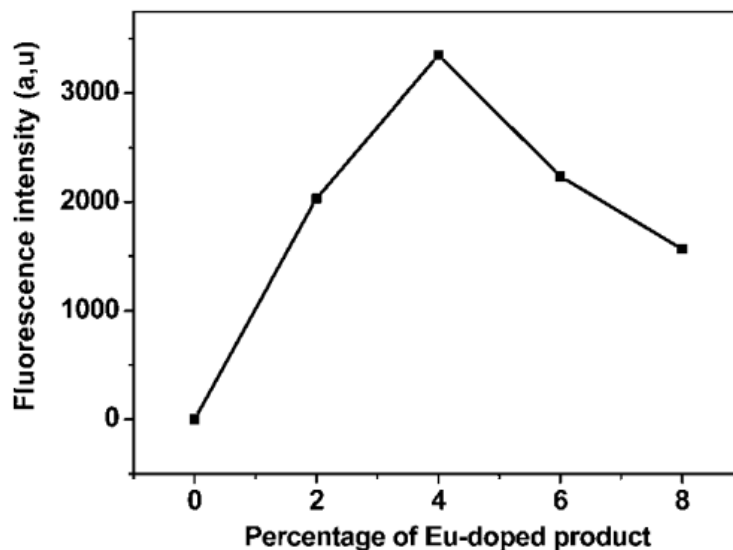


Figure 1.11 Dependence of emission intensity of the $\text{NaLa}(\text{MoO}_4)_2: \text{Eu}^{3+}$ at 276 nm excitation on the Eu^{3+} concentration.

L. Xu et al.[52] tuned the surface morphology of molybdate phosphor by adjusting the concentration of ethylene diamine tetraacetic acid (EDTA) in the hydrothermal method. As shown on Figure 1.12, with the increase of the concentration of EDTA, the crystal shape changed from a regular double pyramid type to round headed double pyramid type, and finally to the shape similar to a cubic sheet.

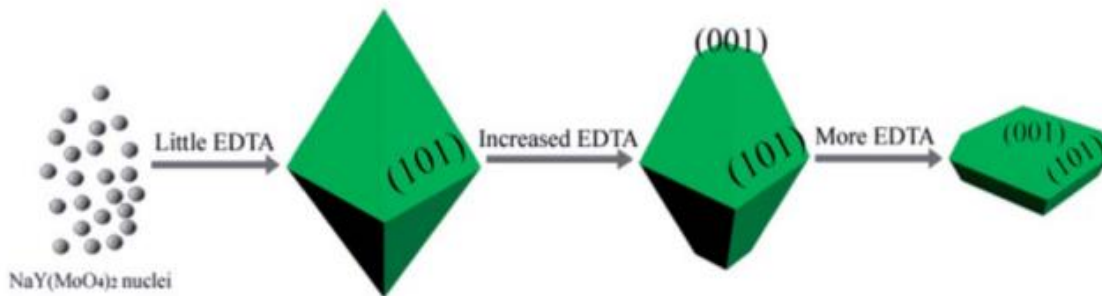


Figure 1.12 Illustration of the morphological evolution process of molybdate phosphor from sharp bipyramid to quasi-cube as a function of EDTA amount.

The reaction temperature required by the hydrothermal method is relatively low, and the prepared phosphor has a good morphology and a controllable crystal shape[53]. However, this method has high requirements for the equipment. For example, the special sealed vessels are required and are needed to be produced at high pressure and temperature[54]. Furthermore, mass production is difficult to realize by using this method due to the small volume of the reaction container.

Precipitation method

The precipitation method can be divided into three types: direct precipitation method[55], homogeneous precipitation method[56], and co-precipitation method[57]. Since the preparation of phosphors often involves a variety of metal elements, the co-precipitation method is the most widely-used one among the above three types.

The basic steps for the co-precipitation method[58-60] are:

1. The raw materials are fully mixed in the aqueous solution, then the precipitant is added slowly to produce chemical precipitation.
2. The obtained precursor is washed, dried and annealed to obtain the final phosphor product.

Next, several examples of phosphors' production by the co-precipitation method are discussed.

L. M. Chepyga et al.[61] prepared both $\text{Ca}_3\text{Sc}_2\text{Si}_3\text{O}_{12}$ (CSSG): $x\text{Dy}^{3+}$ and $\text{Ca}_3\text{Sc}_2\text{Si}_3\text{O}_{12}$: Dy, Ce phosphors as well as their single crystalline films (SCFs) counterparts by a fatty acid-assisted co-precipitation method and liquid phase epitaxy method. For the co-precipitation synthesis process, the related metal nitrites were fully dissolved in the distilled water. Then the water solution of SiO_2 nanoparticles (NPs) was added. In order to obtain the precipitate of metal oleates with SiO_2 NPs, the water solution of sodium oleate was added drop-by-drop with continuous stirring. After the precipitate was formed, it was then centrifuged, dried, and annealed.

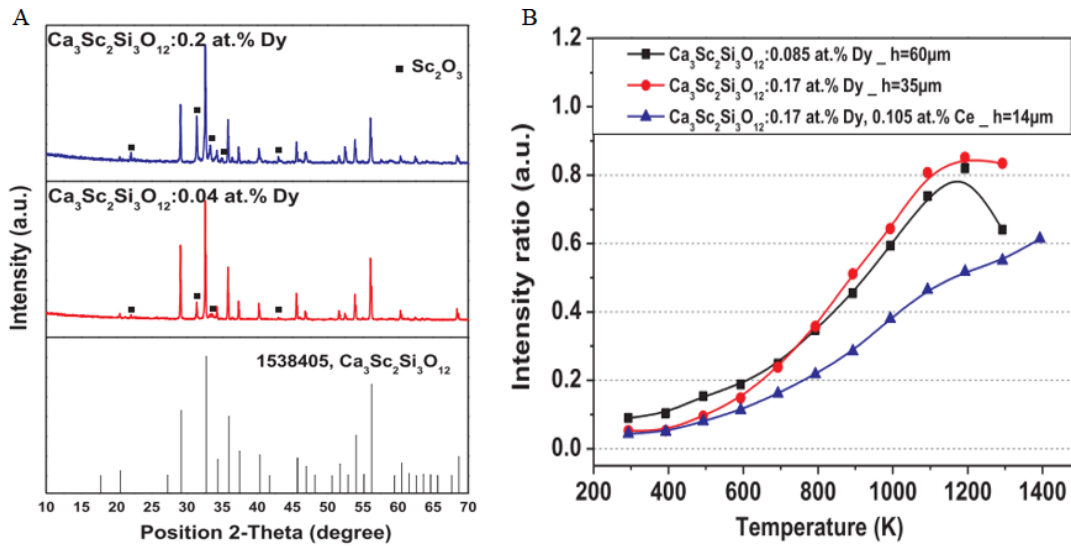


Figure 1.13 (A) XRD patterns of CSSG: $x\text{Dy}^{3+}$ ($x = 0.04, 0.2$ at%) phosphors annealed at 1123 K and 1473 K in air; (B) The intensity ratio $I(445\text{--}465\text{ nm})/I(480\text{--}500\text{ nm})$ as a function of temperature for CSSG: $x\text{Dy}$ ($x = 0.085$ and 0.17 at%) and CSSG: 0.17 at% Dy: 0.105 at% Ce single crystalline film (SCF).

For the XRD characterization shown on Figure 1.13(A), the synthesized phosphors matched well with the standard card of $\text{Ca}_3\text{Sc}_2\text{Si}_3\text{O}_{12}$, but a minor secondary Sc_2O_3 phase was also observed. In addition, it was found that the intensity ratio between $I(445\text{--}465\text{ nm})/I(480\text{--}500\text{ nm})$ for $\text{Ca}_3\text{Sc}_2\text{Si}_3\text{O}_{12}$: 0.17 at% Dy sample was increased to 0.85 at 1200K as shown on Figure 1.13(B), which demonstrated that the studied phosphors can be a promising candidate for high-temperature phosphor applications.

Y. Tratsiak et al.[62] prepared the $Y_2CaAlGe(AlO_4)_3: Ce$ and $Y_2MgAlGe(AlO_4)_3: Ce$ garnet phosphors by a co-precipitation method. For the synthesis process, powdered $Ce(NO_3)_3$ and $Ca(NO_3)_2$ (or $Mg(NO_3)_2$) were dissolved into the mixture of $Y(NO_3)_3$, $Al(NO_3)_3$ and GeO_2 solutions under stirring. Next, the obtained solution was added to the ammonium bicarbonate (precipitant solution) drop-by-drop, and finally, the obtained precipitate was centrifuged, dried, and further thermally treated for 2 h at 600 °C, and then for 2 h at 1500 °C.

As shown on Figure 1.14(A), the XRD patterns of both samples agreed well with the Powder Diffraction File (PDF) reference [33-0040], and this result confirmed the garnet structure. Furthermore, both prepared phosphors have similar sub-micrometer scale structures with porosity, which is due to the gases released during the heat treatment or the heat-facilitated sintering of small particles (see Figure 1.14(B)).

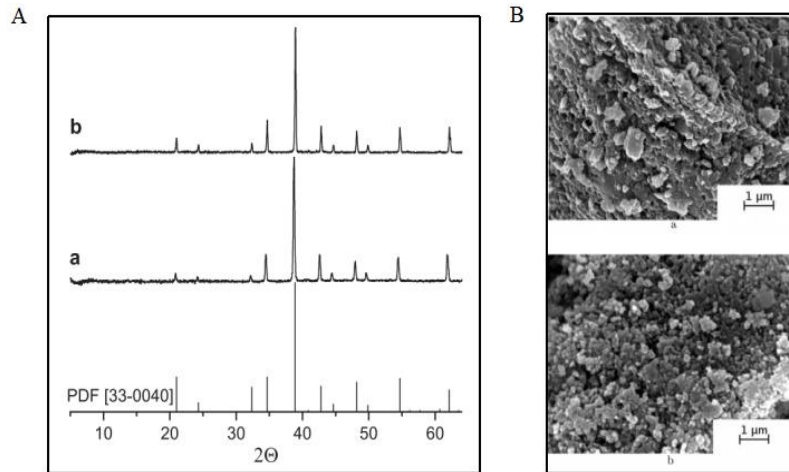


Figure 1.14 (A) XRD patterns of $Y_2CaAlGe(AlO_4)_3: Ce$ (a) and $Y_2CaAlGe(AlO_4)_3: Ce$ (b), PDF [33-0040] is added for reference. (B) SEM images of $Y_2CaAlGe(AlO_4)_3: Ce$ (a); $Y_2MgAlGe(AlO_4)_3: Ce$ (b).

The co-precipitation method has several advantages[59, 63, 64] such as: controllable reaction conditions, low energy consumption, uniform crystallinity, and small particle sizes. The disadvantage is that the morphology of the resultant material can be easily affected by the experimental conditions (such as pH value, choice of precipitating agent, stirring rate, and the

order of addition of the starting materials)[39, 65, 66], therefore the scope of potential applications has certain limitations.

Solution combustion method

The basic principle of this method is to dissolve a certain amount of organic fuel and metal nitrate raw materials in the deionized water and then obtain an aqueous solution. After that the prepared solution is ignited, and a large amount of heat is also released during the combustion[67, 68]. Finally, the powder is calcinated under a certain temperature and a final powder is obtained. This method has the advantages of simple operation, fast reaction speed, and no external energy consumption[69, 70].

C. M. Mehare et al.[71] successfully prepared a new phosphor: $\text{CaAl}_2\text{Si}_4\text{O}_{12}:\text{Dy}^{3+}$ by the solution combustion synthesis. $\text{Ca}(\text{NO}_3)_2$, $\text{Al}(\text{NO}_3)_3$, SiO_2 , $\text{Dy}(\text{NO}_3)_3$, and urea (organic fuel) was used as the starting materials, and then all the reactants were dissolved in deionized water under stirring to form a homogeneous solution. After that, the obtained solution was transferred into a furnace and maintained at 550°C , and a foamy powder was obtained after reaction. Next, the temperature was increased to 1100°C - 1200°C suddenly to obtain a fine and stable product.

For the characterization of the structural properties and morphology, the phase formation was confirmed (see Figure 1.15(A)) by comparing with the standard JCPDS card no. (01-086-1548). The particle size of the prepared phosphor was found to be irregular and inhomogeneous (see Figure 1.15(B)). In addition, the photoluminescence emission spectra, the concentration quenching properties, and the color coordinate were also investigated in this study. These results indicate that the prepared phosphor is suitable for white LEDs applications.

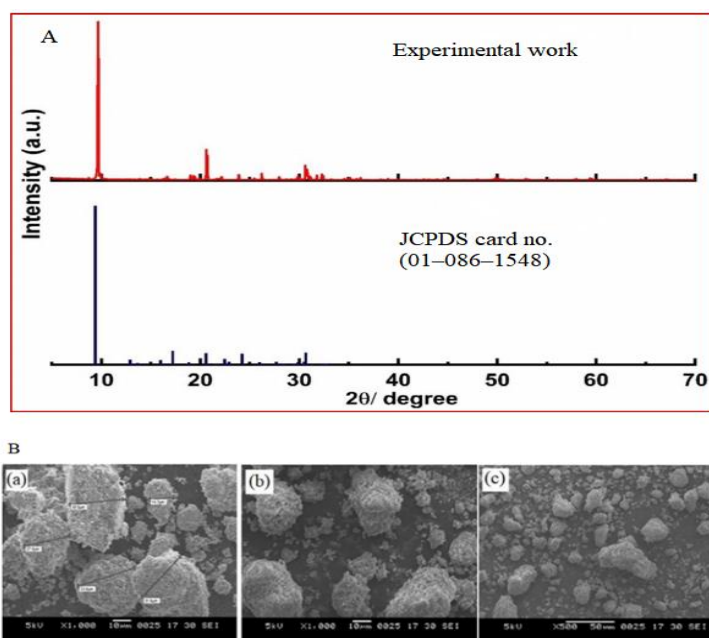


Figure 1.15 (A) XRD pattern of $\text{CaAl}_2\text{Si}_4\text{O}_{12}:\text{Dy}^{3+}$ phosphor. (B) SEM Micrograph of $\text{CaAl}_2\text{Si}_4\text{O}_{12}:\text{Dy}^{3+}$ phosphor.

J. Li et al.[72] prepared a new phosphor $\text{Ca}_2\text{KMg}_2\text{V}_3\text{O}_{12}$ by a solution combustion method. For the synthesis, the stoichiometric ratio of $\text{Ca}(\text{NO}_3)_2 \cdot 4\text{H}_2\text{O}$, $\text{Mg}(\text{NO}_3)_2 \cdot 6\text{H}_2\text{O}$, and KNO_3 were dissolved and mixed in the deionized water, then $\text{C}_6\text{H}_8\text{O}_7 \cdot \text{H}_2\text{O}$ and NH_4VO_3 aqueous solution was added under stirring and heated at around $70\text{--}80^\circ\text{C}$. After that, the solution was transferred into a preheated furnace at different temperatures (600°C , 700°C , 800°C , and 900°C) and then calcinated for 1 h to obtain the final powder.

XRD results obtained from the resultant powder were summarized on Figure 1.16(A), and matched well with the standard card of the $\text{Ca}_2\text{KMg}_2\text{V}_3\text{O}_{12}$ phase, but there was also an obvious KVO_3 phase causing the effect on the excitation spectrum (by introducing a new shoulder peak into the corresponding excitation spectrum, see Figure 1.16(B)). The good white color luminescent property of the $\text{Ca}_2\text{KMg}_2\text{V}_3\text{O}_{12}$ phosphors can be promising for prospective illumination applications.

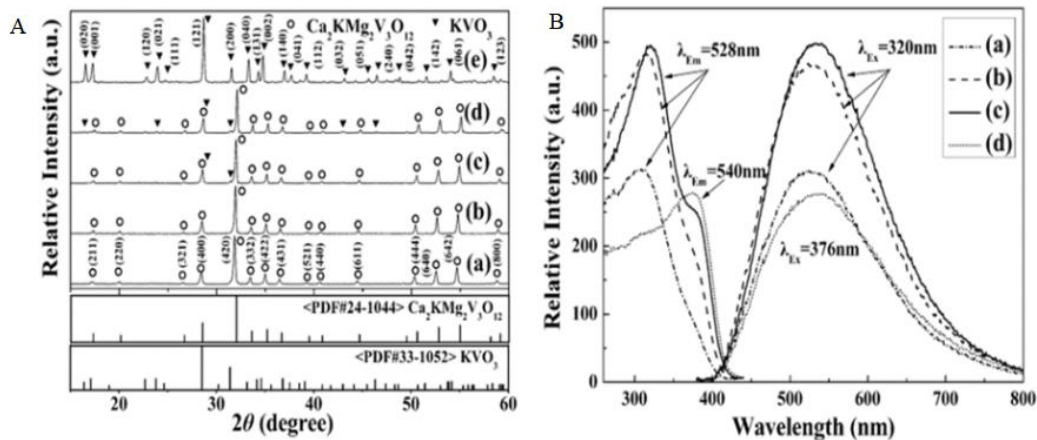


Figure 1.16 (A) XRD patterns of the $\text{Ca}_2\text{KMg}_2\text{V}_3\text{O}_{12}$ prepared at different temperatures: (a) 600°C, (b) 700°C, (c) 800°C, (d) 900°C; (B) Excitation and emission spectra of the $\text{Ca}_2\text{KMg}_2\text{V}_3\text{O}_{12}$ obtained at different ignition temperatures: (a) 700°C, (b) 800°C, (c) 900°C and those of the control sample KVO_3 (d).

Sometimes, solution combustion method can also be combined with other methods for preparation of phosphor materials.

For example, C. Zhao et al.[73] prepared $\text{Lu}_3\text{Al}_5\text{O}_{12}(\text{LuAG}): \text{Nd}^{3+}$ by a microwave-induced solution combustion method. For the synthesis procedure, $\text{Lu}(\text{NO}_3)_3$, $\text{Nd}(\text{NO}_3)_3$, and $\text{Al}(\text{NO}_3)_3 \cdot 9\text{H}_2\text{O}$ were fully dissolved into the deionized water, and followed by the addition of glycine. After that, the prepared solution was placed into a domestic microwave and underwent quick combustion. The dried powders could be formed in the microwave within a few minutes. Finally, the obtained powders were placed into a muffle furnace at 800-1000°C for 2 h for the subsequent calcination step.

The XRD analysis is shown on Figure 1.17(A), and the XRD patterns of the samples calcinated at 900°C were consistent with the JCPDS card (No.73-1368). This result confirmed the formation of a cubic phase and indicated that the optimal temperature for the synthesis of LuAG is 900°C. Also, with the increase of the calcination temperature, only the peak intensity increased.

Fluorescence emission of the samples with different Nd^{3+} concentrations summarized on Figure 1.17(B), the optimum Nd^{3+} concentration in the synthesized matrix was found to be 5mol%.

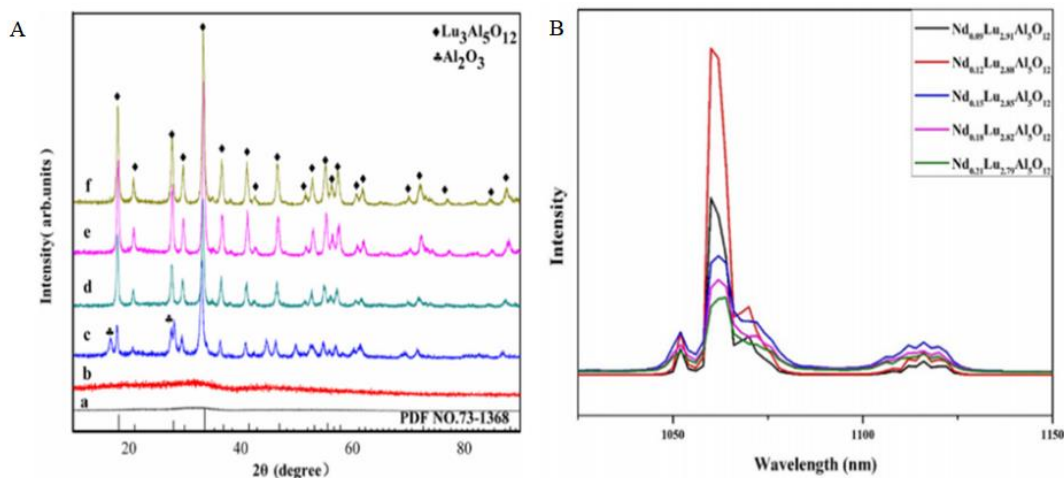


Figure 1.17 (A) XRD patterns of LuAG: Nd powders calcined at different temperatures (a. Precursor; b. 850°C; c. 875°C; d. 900°C; e. 950°C; f. 1000°C); (B) Fluorescence emission spectrum of $\text{Nd}_3\text{xLu}_3-3\text{xAl}_5\text{O}_{12}$ (x ranges from 0.03 to 0.07) powders.

Other methods: microwave method & spray pyrolysis method

The process of the microwave method[74-76] is outlined here. (1) Powders of the relevant oxides are weighed according to a certain stoichiometric ratio and milled together in a ball mill. (2) A fraction of the mixed powder is then pelletized. (3) The pellet is then put into an insulating vessel made of silica wool. (4) The insulating vessel is transferred into a domestic microwave oven for heat. (5) The sample is taken out and cooled to room temperature. (6) The sample is ground to obtain powder products. This method makes use of the action of a microwave electric field to intensify the molecular thermal motion, and rapidly heat up the material. It is environmental-friendly and has the advantages of low energy consumption, as well as good morphology of the resultant materials. However, the reaction mechanism between raw materials in this method is not clear and needs to be further investigated.

The basic process of the spray pyrolysis method[77, 78] is outlined here: (1) The reaction raw materials and solvent are mixed in a solution. (2) The above solution is atomized under the condition of ultrasonic vibration to obtain liquid droplets. (3) Then the droplets are introduced into the high-temperature pyrolytic furnace for drying, pyrolysis, or combustion. (4) Finally, the phosphor product is obtained. This method does not need grinding, and the phosphor product has controllable morphology and uniform size. However, the operation of this method is relatively complex, and the particles obtained are porous, which will decrease the corresponding luminous intensity.

Matrix of the phosphor

Aluminate phosphor

Phosphors that use the aluminates as matrices are widely used in white LEDs because of their excellent properties. They have the advantages of good color rendering performance, wide excitation spectrum, high-temperature resistance, corrosion resistance, and no toxicity[79-81]. Their luminous efficiency and quantum efficiency are usually high, and there is almost no radiation-free transition in the whole luminous process. At present, the most widely used aluminate phosphor is Ce^{3+} doped $\text{Y}_3\text{Al}_5\text{O}_{12}$ (YAG: Ce^{3+}) phosphor. On this basis, scholars have carried out a lot of research work on this series of phosphors[82, 83]. For example, a study on YAG: Ce^{3+} phosphor was conducted by J. Zhong et al.[84]. The blue-shift of the spectrum and the enhanced luminescent properties of YAG: Ce^{3+} phosphor, was also induced by a small amount of La^{3+} incorporation.

Specifically, the luminescent efficiency and thermal quenching properties were improved by the incorporation of La^{3+} as demonstrated on Figure 1.18(A); the blue-shift of the spectrum shown on this figure might be attributed to the local structural (see Figure 1.18(B)) variation around Ce^{3+}

ions. The results also demonstrate that an appropriate amount of La^{3+} co-doping can be helpful for the improvement of the luminescent properties of the $\text{YAG}:\text{Ce}^{3+}$ phosphor.

J. Xu et al.[85] proposed a carbon-free sol-gel method to synthesize $\text{Lu}_3\text{Al}_5\text{O}_{12}(\text{LuAG})$: Ce phosphor, which mainly contained two samples: LuAG-micron(annealed at 1100°C) and LuAG-nano(annealed at 950°C).

After the investigation of the luminescence properties, shown on Figure 1.19(A), it was found that both micron-scale and nano-scale phosphors showed broad emission spectra, and the relative intensity of the LuAG-micron sample reached 80% of the commercial LuAG phosphor (see Figure 1.19(B)). Therefore, the mainly prepared two phosphors can meet the requirements of the white LED.

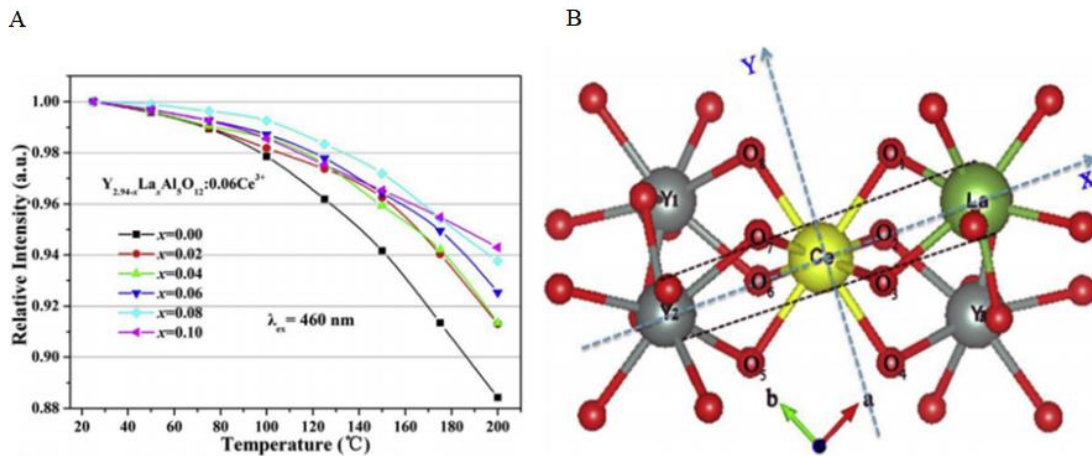


Figure 1.18 (A) Temperature dependence of the relative emission intensities as a function of temperatures of $\text{Y}_{2.94-x}\text{La}_x\text{Ce}_{0.06}\text{Al}_5\text{O}_{12}$ ($x = 0, 0.02, 0.04, 0.06, 0.08, \text{ and } 0.1$) phosphors excited at 460 nm ; (B) The local structure model of La^{3+} - Ce^{3+} co-doping YAG.

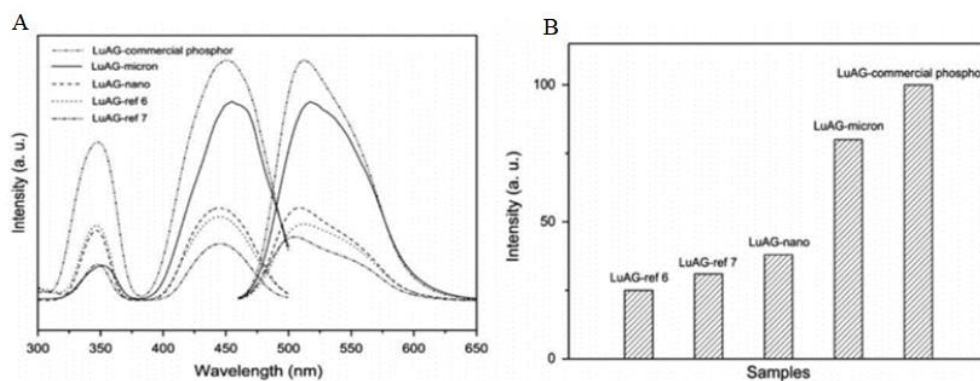


Figure 1.19 (A) Excitation and emission spectra of LuAG-nano and LuAG-micron; (B) relative emission intensity of LuAG phosphors.

Silicate phosphor

Because of the rich raw material resources, low price, and easy access, the silicate matrix material[86] has laid a solid foundation for the popularization and application of silicate phosphors. The phosphor based on silicate has the advantages[87-91] of simple synthesis, good chemical stability, good thermal stability, easy adjustment of matrix components, and stable matrix structure. Compared with other phosphors, it has indispensable characteristics and is suitable for rare-earth ion doping, therefore, it has become an ideal luminescent material.

Furthermore, Y. Liu et al.[92] successfully synthesized the $\text{Ca}_3\text{Sc}_2\text{Si}_3\text{O}_{12}:\text{Ce}^{3+}$ phosphors by a gel-combustion method and studied their photoluminescence properties. Particularly, the intensity of PL emission was increased with reducing atmospheres as shown on Figure 1.20(A). In addition, after combining a blue LED with prepared $\text{Ca}_3\text{Sc}_2\text{Si}_3\text{O}_{12}:\text{Ce}^{3+}$ green phosphor and $\text{Sr}_2\text{Si}_5\text{N}_8:\text{Eu}$ red phosphor, the white LED has a relatively higher color rendering index (Ra) and a lower correlated color temperature (CCT), as demonstrated on Figure 1.20(B). These results indicate that the obtained phosphors are promising candidates for the white LED applications.

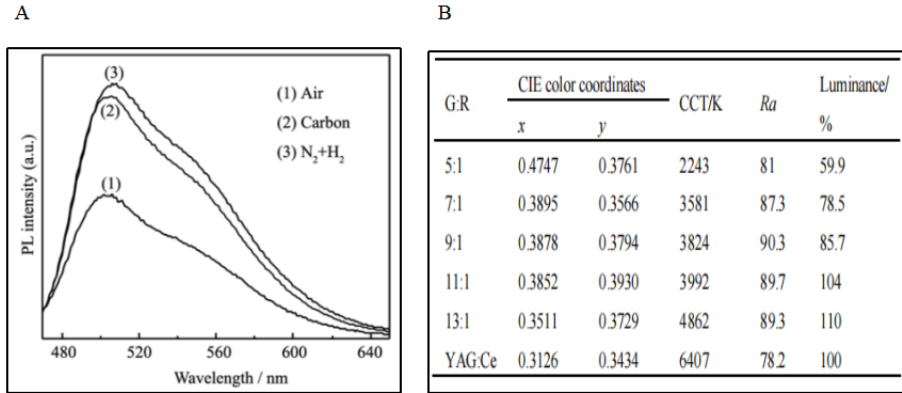


Figure 1.20 (A) PL emission spectra of the $\text{Ca}_3\text{Sc}_2\text{Si}_3\text{O}_{12}:\text{Ce}^{3+}$ samples produced at different annealing ambient atmospheres; (B) Parameters describing the white LED with different mass ratio of $\text{Ca}_3\text{Sc}_2\text{Si}_3\text{O}_{12}:\text{Ce}^{3+}$ green phosphor(G) and $\text{Sr}_2\text{Si}_5\text{N}_8:\text{Eu}$ red phosphor(R).

G. Li et al.[93] prepared the Mn^{2+} doped $\text{Lu}_2\text{CaMg}_2\text{Si}_3\text{O}_{12}$ garnet phosphors by a high-temperature solid-state method and the corresponding luminescent properties were also investigated. The XRD analysis shown on Figure 1.21(A) proved that the phosphors mainly present a garnet structure with a few weak peaks of impurity phases. After that, the effects of Mn^{2+} concentrations on the emission spectra were also investigated in this study. In addition, through the study of the variation of chromaticity coordinates with different Mn^{2+} concentrations, which is shown on Figure 1.21(B), it was found that the color-tunable phosphors ranging from orange to red could be realized by appropriately adjusting the content of Mn^{2+} .

Y. Chu et al.[94] further used a solid-state reaction under a reductive atmosphere to study a new orange emitting garnet phosphor $\text{Lu}_{2-x}\text{CaMg}_2\text{Si}_{2.9}\text{Ti}_{0.1}\text{O}_{12}:\text{xCe}$. After the pure garnet structure was confirmed, the photoluminescence properties were also investigated. The prepared phosphors can absorb blue light efficiently and exhibit bright yellow-orange emission. As shown on Figure 1.22(A), the concentration quenching was found at the Ce^{3+} concentration higher than 0.04. In addition, the $\text{Lu}_{1.96}\text{CaMg}_2\text{Si}_{2.9}\text{Ti}_{0.1}\text{O}_{12}:0.04\text{Ce}$ phosphors have a good color temperature (2430 K), which can be seen on Figure 1.22(B).

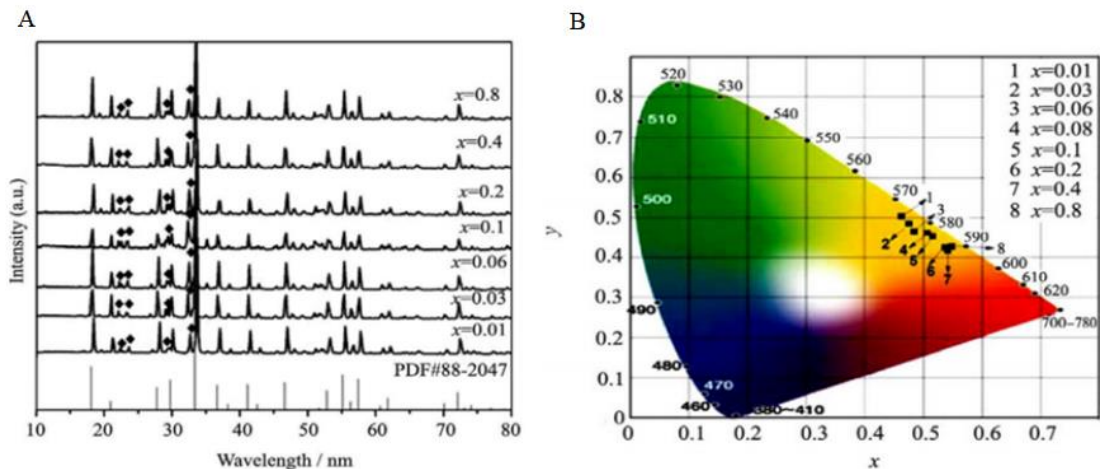


Figure 1.21 (A) XRD patterns of $\text{Lu}_2\text{CaMg}_{2-x}\text{Si}_3\text{O}_{12}: x\text{Mn}^{2+}$ phosphors ($x = 0.01-0.8$); (B) CIE chromaticity diagram for $\text{Lu}_2\text{CaMg}_{2-x}\text{Si}_3\text{O}_{12}: x\text{Mn}^{2+}$ as a function of Mn^{2+} content.

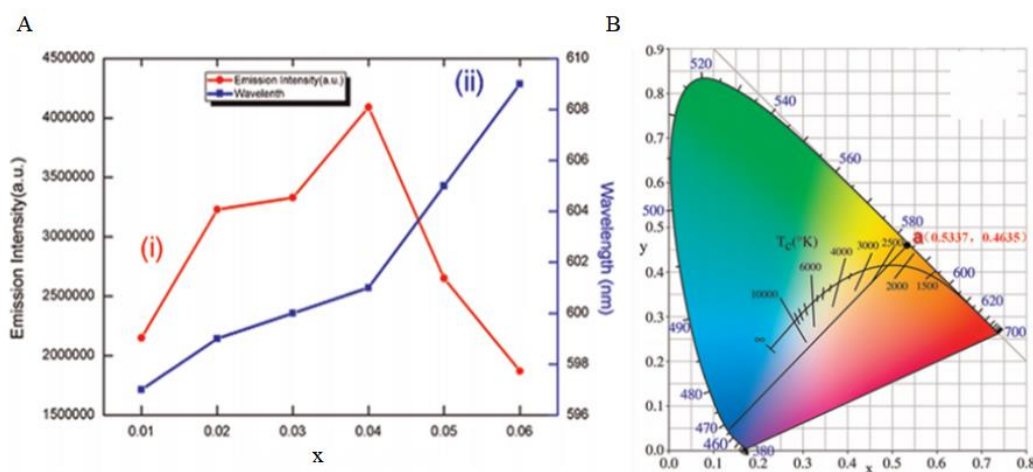


Figure 1.22 (A) The photoluminescence emission intensity (i), and the maximum emission wavelength (ii) for $\text{Lu}_{2-x}\text{CaMg}_2\text{Si}_{2.9}\text{Ti}_{0.1}\text{O}_{12}: x\text{Ce}$ phosphors under 467 nm excitation; (B) The chromaticity coordinates of $\text{Lu}_{2-x}\text{CaMg}_2\text{Si}_{2.9}\text{Ti}_{0.1}\text{O}_{12}: x\text{Ce}$ phosphors.

Y. Chen et al.[95] prepared a series of $\text{Lu}_2\text{Ca}_{1-x}\text{Mg}_2\text{Si}_3\text{O}_{12}: x\text{Eu}^{2+}$ by a solid-state method. The prepared phosphors can be effectively excited by near-UV light and emitted strong blue light. A concentration quenching occurs at $x = 0.03$ for the emission spectra of the resultant materials, which is demonstrated on Figure 1.23(A). Additionally, the emission intensity of the $\text{Lu}_2\text{CaMg}_2\text{Si}_3\text{O}_{12}: 0.03\text{Eu}^{2+}$ was found to be stronger than that of the widely-used $\text{BaMgAl}_{10}\text{O}_{17}(\text{BAM}): \text{Eu}^{2+}$ blue phosphor (as demonstrated on Figure 1.23(B)). All the results

indicate that the preparation of blue-emitting phosphors can be promising for near-UV based white LEDs.

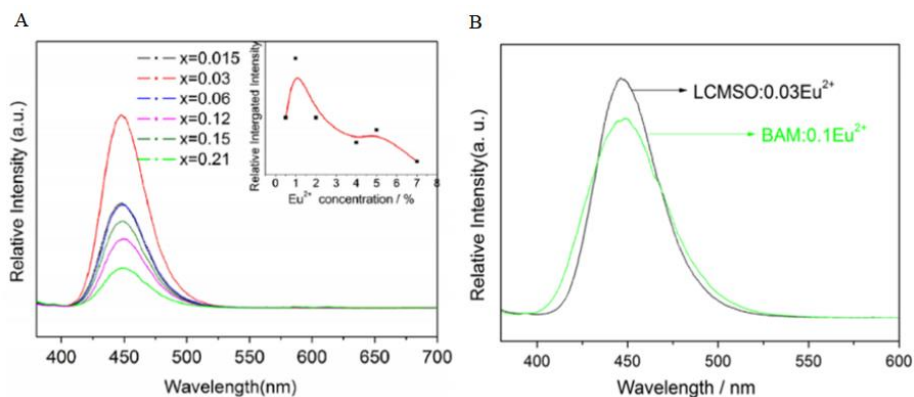


Figure 1.23 (A) Emission spectra of $\text{Lu}_2\text{Ca}_{1-x}\text{Mg}_2\text{Si}_3\text{O}_{12}: x\text{Eu}^{2+}$ phosphors with different amount of Eu ($\lambda_{\text{ex}} = 365 \text{ nm}$); (B) Emission spectra of $\text{Lu}_2\text{CaMg}_2\text{Si}_3\text{O}_{12}: 0.03\text{Eu}^{2+}$ and $\text{BaMgAl}_{10}\text{O}_{17}: 0.1\text{Eu}^{2+}$ ($\lambda_{\text{ex}} = 365 \text{ nm}$).

Phosphate phosphor

In recent years, phosphate phosphors have been widely studied in the matrix of luminescent materials[96, 97]. Phosphate phosphors have advantages[98-100] of easy crystallization, high conversion efficiency, and stable physical and chemical properties.

J. Sun et al.[101] prepared a blue-emitting phosphor $\text{NaBaPO}_4: \text{Eu}^{2+}$ by both combustion method and solid-state method. The SEM images of the $\text{NaBaPO}_4: \text{Eu}^{2+}$ obtained by both methods indicated that the combustion method can effectively prevent the formation of a larger agglomeration of the particles in this study.

In addition, as shown on Figure 1.24(A), $\text{NaBaPO}_4: \text{Eu}^{2+}$ phosphor prepared by solution combustion synthesis has a higher relative emission intensity than the phosphor obtained by the solid-state method. Also, the thermally stable luminescence of the Eu^{2+} -doped NaBaPO_4 phosphor was found to be higher than that of the commercial $\text{Y}_3\text{Al}_5\text{O}_{12}: \text{Ce}^{3+}$ (YAG: Ce^{3+}) phosphor (see

Figure 1.24(B) insert). Therefore, the prepared phosphor can be a good candidate for white LEDs application.

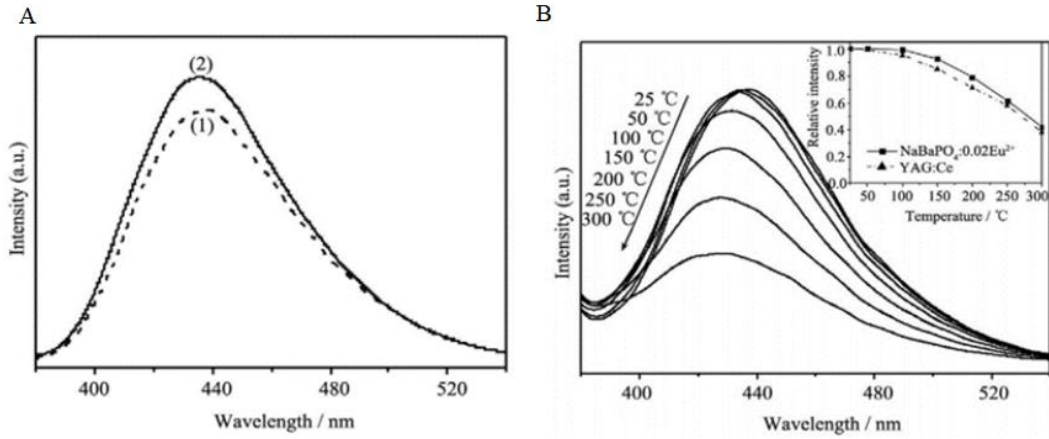


Figure 1.24 (A) Emission spectra of NaBaPO₄:Eu²⁺ phosphors prepared by solid-state reaction (1) and combustion method (2); (B) Temperature dependence of emission spectra of NaBaPO₄:Eu²⁺ obtained by combustion method. The insert illustrates a comparison between NaBaPO₄:Eu²⁺ phosphors and YAG:Ce³⁺ phosphors.

X. Yang et al.[102] studied the LiCaPO₄:Eu²⁺ blue phosphor. As shown on Figure 1.25, that phosphor has a wide excitation band of 220-450 nm, and can produce a blue light under 395 nm excitation. It can also be successfully mixed with red and green phosphors, and then combined with a near UV LED chip to form warm white LED device with excellent performance.

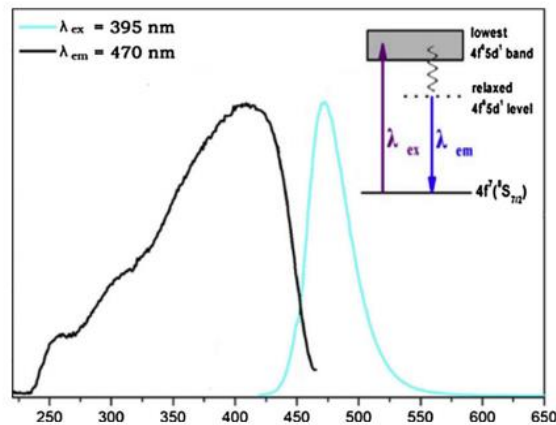


Figure 1.25 Photoluminescence excitation (PLE) and photoluminescence (PL) spectra of the LiCa_{0.97}PO₄:0.03Eu²⁺ phosphor; the inset illustrates the energy level diagram of the Eu²⁺ ions in LiCa_{0.97}PO₄:0.03Eu²⁺.

D. Kim et al.[103] studied the $(\text{Ca}_{1-x}\text{Sr}_x)_9\text{La}(\text{PO}_4)_7: \text{Eu}^{2+}$ phosphor. By adjusting the Ca/Sr ratio, the luminescence can change from yellowish-green to blue, and the prepared phosphors have very high quantum efficiency and good thermal stability.

Tungstate molybdate phosphor

Tungstate and molybdate are new phosphor substrates developed in recent years, and they have attracted more and more attentions[104-106]. The reasons can be summarized into two main points: (1) Tungstate and molybdate can effectively absorb the blue and purple light from the LED chip and transfer a part of the energy to the activator. (2) In the matrix of the system, the activators have higher quenching concentration and higher luminous efficiency.

Y. Hu et al.[107] prepared the $\text{CaMoO}_4: \text{Eu}^{3+}$ phosphors by solid-state reaction. The emission spectra of the prepared $\text{CaMoO}_4: \text{Eu}^{3+}$ and commercial sulfide phosphors (conventional sulfide used as red phosphor in white LEDs) are shown on Figure 1.26. Under the excitation of 394 nm and 464 nm corresponding to the near-ultraviolet and blue wavelengths, respectively, the emission spectrum showed that the luminescence intensity of the $\text{CaMoO}_4: \text{Eu}^{3+}$ was slightly stronger than that of the sulfide under blue light excitation. Under near UV excitation, the luminous intensity of the $\text{CaMoO}_4: \text{Eu}^{3+}$ was several times stronger than that of the sulfide, and it was a linear narrow-band emission, which had the potential to be used in UV excited LED.

C.-H. Chiu et al.[108] synthesized the composite phosphor $\text{LiEu}(\text{WO}_4)_{2-x}(\text{MoO}_4)_x$. It was found that adjusting the molybdenum to tungsten ratio in the matrix can change the emission intensity of the sample (see Table 1-1). Specifically, when the $\text{Mo}/\text{W} = 2/0$, the emission peak at 615 nm was found to be the strongest. The reason is that the ion radii of W^{6+} and Mo^{6+} in a tetrahedral coordination environment are different, resulting in different distances between Eu^{3+} in their matrix, which is 3.91 Å and 3.86 Å, respectively. The energy transfer efficiency of the

molybdate group to Eu^{3+} is higher, therefore, the $\text{LiEu}(\text{MoO}_4)_2$ has the highest luminous intensity. However, the reason for this phenomenon needs to be further studied, because when the distance between Eu^{3+} decreases, the probability of concentration quenching increases, which will lead to a decrease of luminescence intensity.

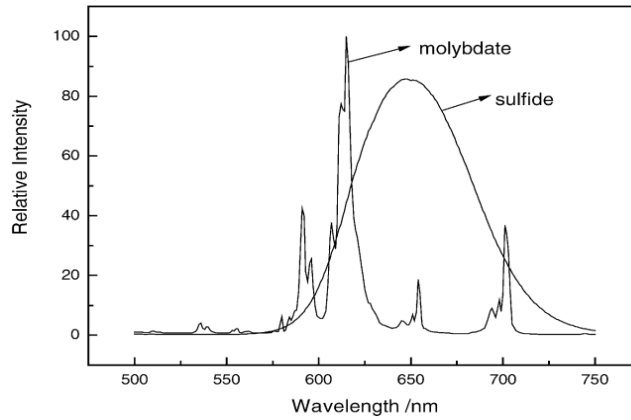


Figure 1.26 Emission spectra of $\text{CaMoO}_4:\text{Eu}^{3+}$ and sulfide phosphors.

Table 1-1 Comparison of excitation and emission intensity of $\text{LiEu}(\text{WO}_4)_{2-x}(\text{MoO}_4)_x$ phosphors.

Compositions	Intensity (10^7 cps)	
	$\lambda_{\text{em}} = 615 \text{ nm}$	$\lambda_{\text{ex}} = 394 \text{ nm}$
$\text{LiEu}(\text{WO}_4)_2$	1.582	1.215
$\text{LiEu}(\text{WO}_4)_{1.6}(\text{MoO}_4)_{0.4}$	1.803	1.612
$\text{LiEu}(\text{WO}_4)_{1.2}(\text{MoO}_4)_{0.8}$	1.817	1.742
$\text{LiEu}(\text{WO}_4)_{0.8}(\text{MoO}_4)_{1.2}$	1.820	1.746
$\text{LiEu}(\text{WO}_4)_{0.4}(\text{MoO}_4)_{1.6}$	1.824	1.794
$\text{LiEu}(\text{MoO}_4)_2$	1.885	1.889
$\text{NaEu}(\text{MoO}_4)_2$	1.864	1.885
$\text{KEu}(\text{MoO}_4)_2$	1.800	1.800

Borate phosphor

Borate phosphors have the characteristics of good thermal stability, good chemical stability, and high luminescence efficiency[109, 110].

G. Li et al.[111] prepared the $(\text{Y}, \text{Gd})\text{Al}_3(\text{BO}_3)_4:\text{Eu}^{3+}$ phosphors by a solution combustion method, and the luminescence properties were also investigated.

The XRD and SEM analysis confirmed that the pure phase was obtained under the calcination temperature of 1000°C and the particle size was varied with different calcination temperatures. The highest peak of the emission spectrum was observed at 612 nm, which is due to the $^5D_0-^7F_2$ electric dipole transition of Eu^{3+} (see Figure 1.27(A)). It was also verified that the luminescence intensity of Eu^{3+} can be affected by simultaneous adding of Gd^{3+} , and the optimum concentration of the introduced Gd^{3+} was found to be $x = 0.75$ (see Figure 1.27 (B)).

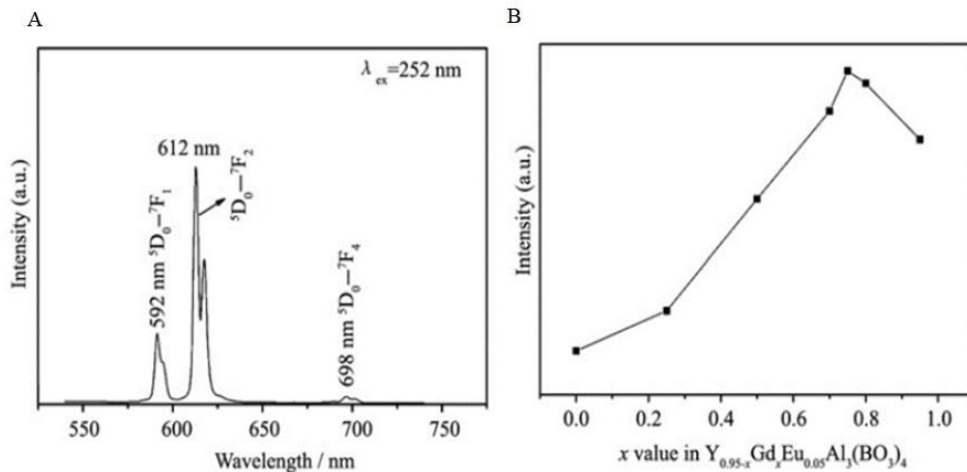


Figure 1.27 (A) Emission spectra of $\text{Y}_{0.95}\text{Eu}_{0.05}\text{Al}_3(\text{BO}_3)_4$ phosphors calcined at 1100°C; (B) Emission intensity of Eu^{3+} in $\text{Y}_{0.95-x}\text{Gd}_x\text{Eu}_{0.05}\text{Al}_3(\text{BO}_3)_4$ series phosphors.

İ. Pekgözlü et al.[112] prepared both pure and Pb^{2+} doped $\text{LiSr}_4(\text{BO}_3)_3$ by a solution combustion synthesis method.

The excitation and emission bands of the prepared samples were observed at 284 and 328 nm, and these two bands were assigned to $^1S_0-^3P_1$ transition and $^3P_1-^1S_0$, respectively (see Figure 1.28(A)). The concentration quenching of Pb^{2+} in $\text{LiSr}_{4-x}\text{Pb}_x(\text{BO}_3)_3$ was also investigated and found to be 0.005 mol (see Figure 1.28(B)). The results show that the studied phosphor is promising for white LED applications.

J. T. Ingle et al.[113] prepared the $\text{YCa}_4\text{O}(\text{BO}_3)_3: \text{RE}^{3+}$ ($\text{RE} = \text{Eu}^{3+}, \text{Tb}^{3+}$) phosphors by a solution combustion synthesis method.

The study of the optical properties indicates that the prepared samples have a strong absorption and also show intense red and green emissions when they were excited by 254 nm UV and 147 nm VUV radiation (see Figure 1.29). The results show that both phosphors can be promising candidates for white LED applications.

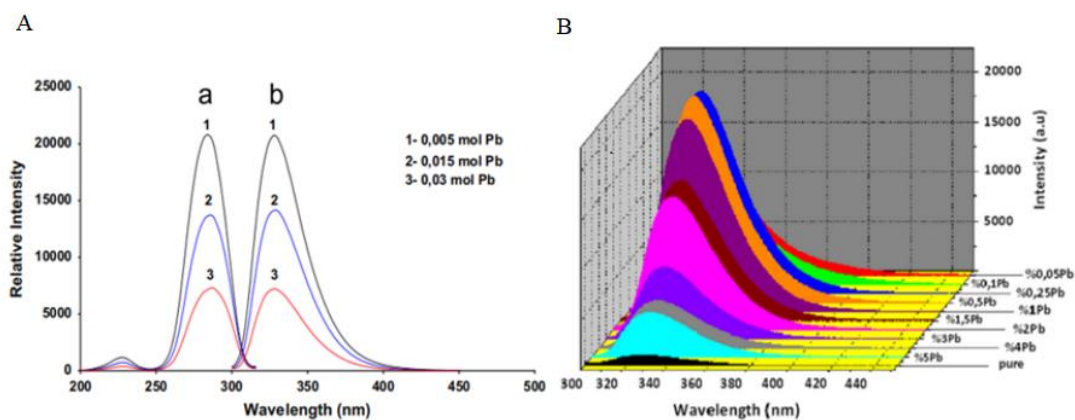


Figure 1.28 (A) The excitation (a) and emission (b) spectra of $\text{LiSr}_{4-x}\text{Pb}_x(\text{BO}_3)_3$ ($x = 0.005, 0.015,$ and 0.03) at room temperature; (B) Emission spectra of pure and $\text{LiSr}_{4-x}\text{Pb}_x(\text{BO}_3)_3$ ($x = 0.05, 0.1, 0.25, 0.5, 1, 1.5, 2, 3, 4,$ and 5 mol%).

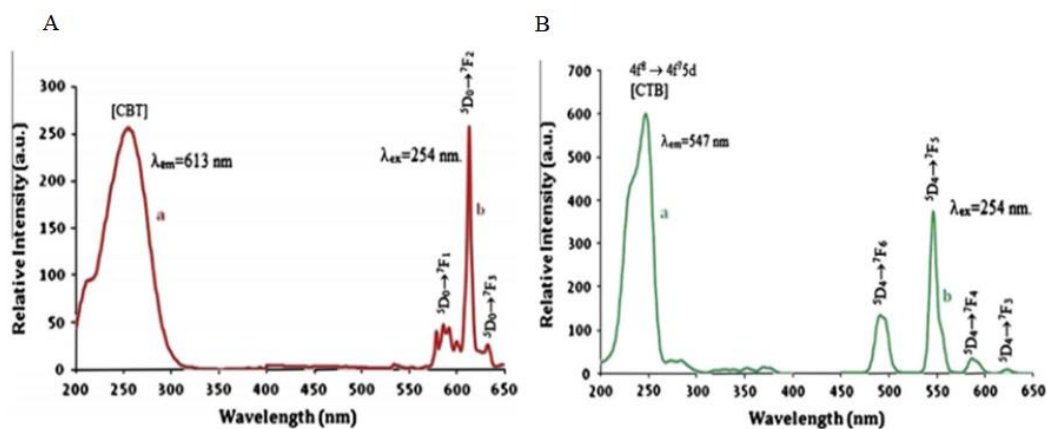


Figure 1.29 (A) PL spectra of $\text{YCa}_4\text{O}(\text{BO}_3)_3: \text{Eu}^{3+}$. (a) Excitation by 613 nm. (b) Emission for 254 nm; (B) UV PL spectra of $\text{YCa}_4\text{O}(\text{BO}_3)_3: \text{Tb}^{3+}$. (a) Excitation by 547 nm. (b) Emission for 254 nm.

Research content and purpose

As was described above, garnet phosphors are the one of the most important candidates for WLEDs due to their excellent performance on stability and luminescent efficiency[114]. For

example, YAG: Ce³⁺ is one of the most commonly used phosphor materials. However, the lack of red-light components in their emission spectrum, low color rendering index, and high color temperature greatly restrict the further applications of this phosphor in lighting applications. Therefore, additional research has to be performed to develop novel garnet-type phosphors.

In addition, among all the phosphors mentioned above, the silicate-based phosphors have the advantages of simple synthesis, good stability, and great suitability for rare-earth ion doping, which make them ideal luminescent materials. Also, Lu₂CaMg₂Si₃O₁₂, Ca₃Sc₂Si₃O₁₂, and Ca₂NaMg₂V₃O₁₂ garnet phosphors have been successfully prepared as was discussed before. This is an inspiring sign for researchers to look for ways of developing new silicate-based garnet phosphors to meet various spectral requirements.

Furthermore, among all the preparation methods mentioned above, the solution combustion method has the advantages of simple operation and energy saving.

Therefore, the current research content is to explore the proper experimental conditions for the preparation of a novel CaEr₂Mg₂Si₃O₁₂ garnet matrix by a solution combustion synthesis method. Specifically, several conditions have been optimized for the synthesis, such as fuel-to-oxidizer ratio, order of mixing, combustion parameters (time and temperature), amounts of precursors, as well as calcination parameters. The obtained powders were also characterized by XRD analysis for proper phase examination.

In summary, the main goal for this research is to prepare the single-phased CaEr₂Mg₂Si₃O₁₂ garnet matrix for prospective white LED applications by a solution combustion method.

2 MATERIALS & METHODS

Reagents and equipment

Reagents

The information on the starting materials is listed in Table 2-1 below.

Table 2-1 Information on the starting reagents.

Name	Chemical Formula	Purity	Company
Calcium nitrate tetrahydrate	$\text{Ca}(\text{NO}_3)_2 \cdot 4\text{H}_2\text{O}$	99.0-103.0%	SIGMA-ALDRICH
Erbium nitrate pentahydrate	$\text{Er}(\text{NO}_3)_3 \cdot 5\text{H}_2\text{O}$	99.9%	SIGMA-ALDRICH
Carbohydrazide	$(\text{H}_2\text{NNH})_2\text{C}=\text{O}$	97%	Alfa Aesar
Silica, fumed	SiO_2	99.0%	SIGMA-ALDRICH
Magnesium nitrate hexahydrate	$\text{Mg}(\text{NO}_3)_2 \cdot 6\text{H}_2\text{O}$	98.0-102.0%	SIGMA-ALDRICH

Equipment

The solution combustion synthesis was conducted by using a muffle furnace (ST-1200C-242424, Sentro Tech, Strongsville, OH, USA), and the calcination process was conducted by a high-temperature furnace (HT-04/18, Nabertherm, Lilienthal, Germany).

Sample preparation

In this experiment, a solution combustion synthesis method was adopted for the preparation of the targeted $\text{CaEr}_2\text{Mg}_2\text{Si}_3\text{O}_{12}$. Specifically, a stoichiometric amount of the starting reagents was weighed as shown in Table 2-2. Next, the starting reagents were added to 50 ml of deionized water following a certain order (described in Result & Discussion part) under continuous stirring. It

should be pointed out that only when the previous reagent was thoroughly dissolved, the next reagent was added. After all the starting reagents were added, the obtained solution was further stirred for different times (30 min, 1 h, and 2 h) at room temperature for a full dissolution. When the preparation of the solution was completed, the obtained solution was transferred into the preheated muffle furnace and maintained at different temperatures (500°C, 550°C, and 600°C) for 15 min to conduct the combustion process. After that, the precursor powders were removed from the furnace and thoroughly ground in an agate mortar. Next, the ground powders were placed into a crucible and transferred into the high-temperature furnace for the calcination. In calcination process, the powders were heated up to different temperatures (1000°C, 1200°C, 1225°C, 1250°C, 1275°C, 1300°C, and 1400°C) in 2 h, and steadied for different time (2 h, 5 h, 10 h, 20 h, 30 h, and 40 h), then cooled down in 2 h. Finally, after the calcination process was finished, the obtained powders were taken out and reground to get the final fine powders for further investigation.

Table 2-2 Mass of the starting reagents (fuel-to-oxidizer ratio = f/o ratio).

Reagent	Mass
$\text{Ca}(\text{NO}_3)_2 \cdot 4\text{H}_2\text{O}$	0.3376g
$\text{Er}(\text{NO}_3)_3 \cdot 5\text{H}_2\text{O}$	1.2677g
$(\text{H}_2\text{NNH})_2\text{C}=\text{O}$	0.3220g (f/o ratio = 0.5) 0.4830g (f/o ratio = 0.75) 0.5152g (f/o ratio = 0.8) 0.6440g (f/o ratio = 1.0)
SiO_2	0.2577g
$\text{Mg}(\text{NO}_3)_2 \cdot 6\text{H}_2\text{O}$	0.7331g 1.4662g (doubled) 2.1994g (tripled)

Characterization

The XRD patterns of the samples were recorded using a D2 Phaser [Bruker AXS, Madison, WI] using a step size of 0.014 degrees 2θ and a count time of 0.3 s by scanning from 10 to 80 degrees 2θ . Cu-K α radiation ($\lambda = 1.54184 \text{ \AA}$) was used as the X-ray source.

Results & Discussion

Theoretical XRD pattern of the $\text{CaEr}_2\text{Mg}_2\text{Si}_3\text{O}_{12}$

The crystal structure of the $\text{CaEr}_2\text{Mg}_2\text{Si}_3\text{O}_{12}$ was simulated, and the theoretical XRD pattern was obtained by using VESTA software ($\lambda = 1.54184 \text{ \AA}$). The indexed theoretical XRD pattern is shown on Figure 2.1, and the crystal plane of each peak is also labeled. This theoretical spectrum was later used to compare with the experimental patterns to confirm the formation of the targeted garnet phase.

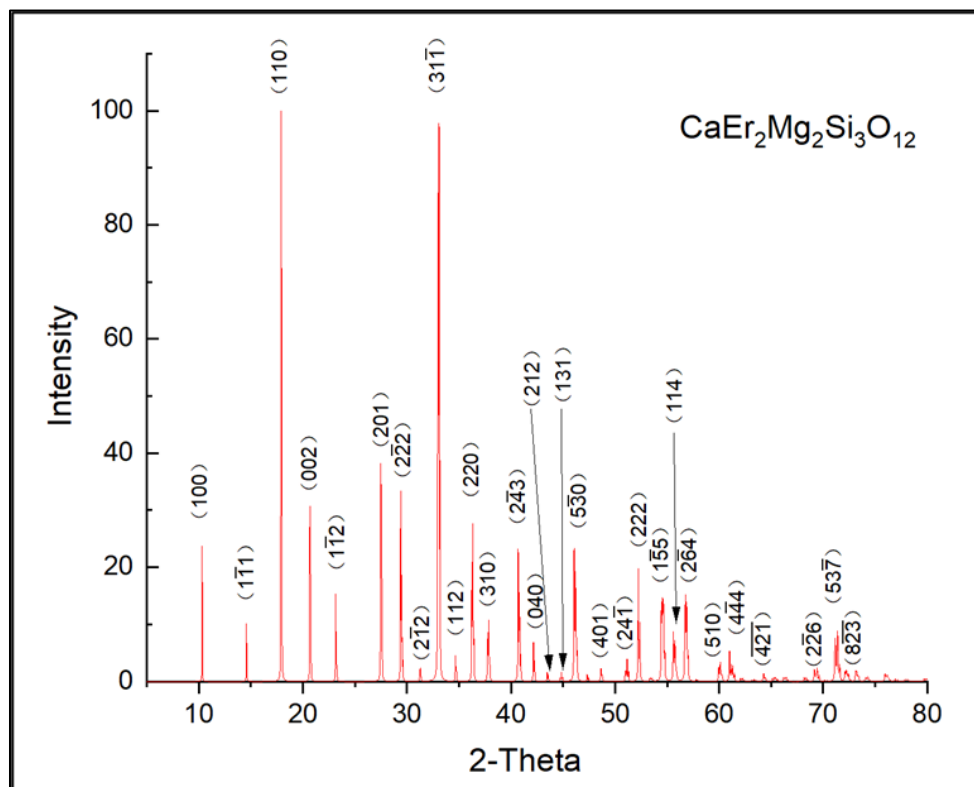


Figure 2.1 Theoretical XRD pattern of $\text{CaEr}_2\text{Mg}_2\text{Si}_3\text{O}_{12}$ calculated by VESTA software.

All the prepared samples are named as CEMSO ($\text{CaEr}_2\text{Mg}_2\text{Si}_3\text{O}_{12}$) in this thesis.

Different fuel-to-oxidizer ratios and calcination temperatures

CEMSO1 & CEMSO2 samples

For the following two samples: CEMSO1 and CEMSO2, the related experimental parameters such as the fuel-to-oxidizer ratio, order of reactants, stirring time, combustion synthesis time and temperature, and calcination temperature and time are listed in Table 2-3. To be specific, these two samples have the same parameters as follows: the reactants were added by the order of $\text{Ca}(\text{NO}_3)_2 + \text{Mg}(\text{NO}_3)_2 + \text{Er}(\text{NO}_3)_3 + \text{SiO}_2 + \text{CH}_6\text{N}_4\text{O}$, the stirring time was 30 min, the combustion temperature was 500°C , the combustion reaction time was 15 min, and the calcination was conducted for 2 h. In addition, for CEMSO1 and CEMSO2, the fuel-to-oxidizer ratio was 0.5, and they were under the calcination at 1000°C and 1200°C , respectively.

Table 2-3 The experimental parameters for CEMSO1 and CEMSO2 samples.

Sample Name	CEMSO1	CEMSO2
f/o Ratio	0.5	0.5
Order	1. $\text{Ca}(\text{NO}_3)_2$ 2. $\text{Mg}(\text{NO}_3)_2$ 3. $\text{Er}(\text{NO}_3)_3$ 4. SiO_2 5. $\text{CH}_6\text{N}_4\text{O}$	1. $\text{Ca}(\text{NO}_3)_2$ 2. $\text{Mg}(\text{NO}_3)_2$ 3. $\text{Er}(\text{NO}_3)_3$ 4. SiO_2 5. $\text{CH}_6\text{N}_4\text{O}$
Stirring Time	30 min	30 min
Combustion Synthesis Parameters	500°C 15 min	500°C 15 min
Calcination Temperature	1000°C	1200°C
Calcination Time	2 h	2 h

Phase analysis by XRD: CEMSO1 & CEMSO2 samples

The XRD patterns of the sample CEMSO1 and sample CEMSO2, which were calcinated at 1000°C and 1200°C, respectively, are shown on Figure 2.2. From the XRD patterns, it can be seen that the predominant peaks in both XRD patterns are mainly consistent with the $\text{Ca}_2\text{Er}_8(\text{SiO}_4)_6\text{O}_2$ phase, and there are also some impurity phases that belong to Ca_2SiO_4 , Mg_2SiO_4 and MgO . However, the appropriate-phase of the targeted garnet $\text{CaEr}_2\text{Mg}_2\text{Si}_3\text{O}_{12}$ did not appear in these XRD patterns, therefore the experimental procedures used for production of samples CEMSO1 and CEMSO2 cannot be used for the synthesis of the $\text{CaEr}_2\text{Mg}_2\text{Si}_3\text{O}_{12}$.

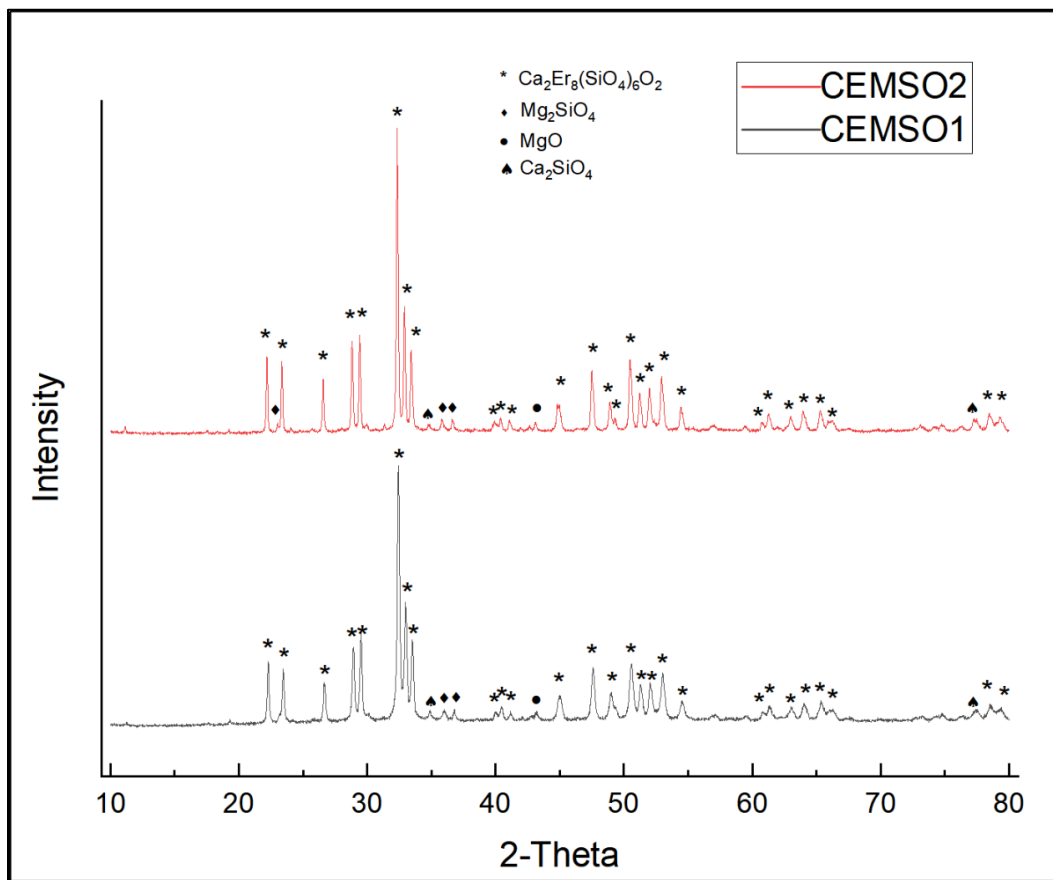


Figure 2.2 XRD spectra of CEMSO1 and CEMSO2 samples.

Since the process with the fuel-to-oxidizer ratio of 0.5 did not successfully synthesize the targeted garnet $\text{CaEr}_2\text{Mg}_2\text{Si}_3\text{O}_{12}$, two experiments with an increased fuel-to-oxidizer ratio of 0.75,

have been performed. The fuel-to-oxidizer ratio is an important parameter to the combustion reaction, which can determine the reaction speed, thus, a higher fuel-to-oxidizer may benefit the synthesis.

CEMSO3 & CEMSO4 samples

Specifically, for the samples CEMSO3 and CEMSO4, the fuel-to-oxidizer ratio was increased to 0.75, and the calcination temperature was at 1000°C and 1200°C, respectively. Other conditions were the same as that for samples CEMSO1 and CEMSO2, all the parameters are listed in Table 2-4. The reactants were added in the order of $\text{Ca}(\text{NO}_3)_2 + \text{Mg}(\text{NO}_3)_2 + \text{Er}(\text{NO}_3)_3 + \text{SiO}_2 + \text{CH}_6\text{N}_4\text{O}$, the stirring time was 30 min, the combustion temperature was 500°C, the combustion reaction time was 15 min, and the calcination was maintained at 1000°C and 1200°C for 2 h.

Table 2-4 The experimental parameters for CEMSO3 and CEMSO4 samples.

Sample Name	CEMSO3	CEMSO4
f/o Ratio	0.75	0.75
Order	1. $\text{Ca}(\text{NO}_3)_2$ 2. $\text{Mg}(\text{NO}_3)_2$ 3. $\text{Er}(\text{NO}_3)_3$ 4. SiO_2 5. $\text{CH}_6\text{N}_4\text{O}$	1. $\text{Ca}(\text{NO}_3)_2$ 2. $\text{Mg}(\text{NO}_3)_2$ 3. $\text{Er}(\text{NO}_3)_3$ 4. SiO_2 5. $\text{CH}_6\text{N}_4\text{O}$
Stirring Time	30 min	30 min
Combustion Synthesis Parameters	500°C 15 min	500°C 15 min
Calcination Temperature	1000°C	1200°C
Calcination Time	2 h	2 h

Phase analysis by XRD: CEMSO3 & CEMSO4 samples

The XRD patterns of samples CEMSO3 and CEMSO4 are shown on Figure 2.3. After analyzing these XRD patterns, it can be seen that the predominant peaks in the XRD pattern are still consistent with the $\text{Ca}_2\text{Er}_8(\text{SiO}_4)_6\text{O}_2$ phase, and some impurity phases of Ca_2SiO_4 , Mg_2SiO_4 and MgO appear. However, the related phase of the targeted garnet did not appear in the XRD patterns, so the experimental procedure of samples CEMSO3 and CEMSO4 cannot be adopted for the synthesis of the $\text{CaEr}_2\text{Mg}_2\text{Si}_3\text{O}_{12}$.

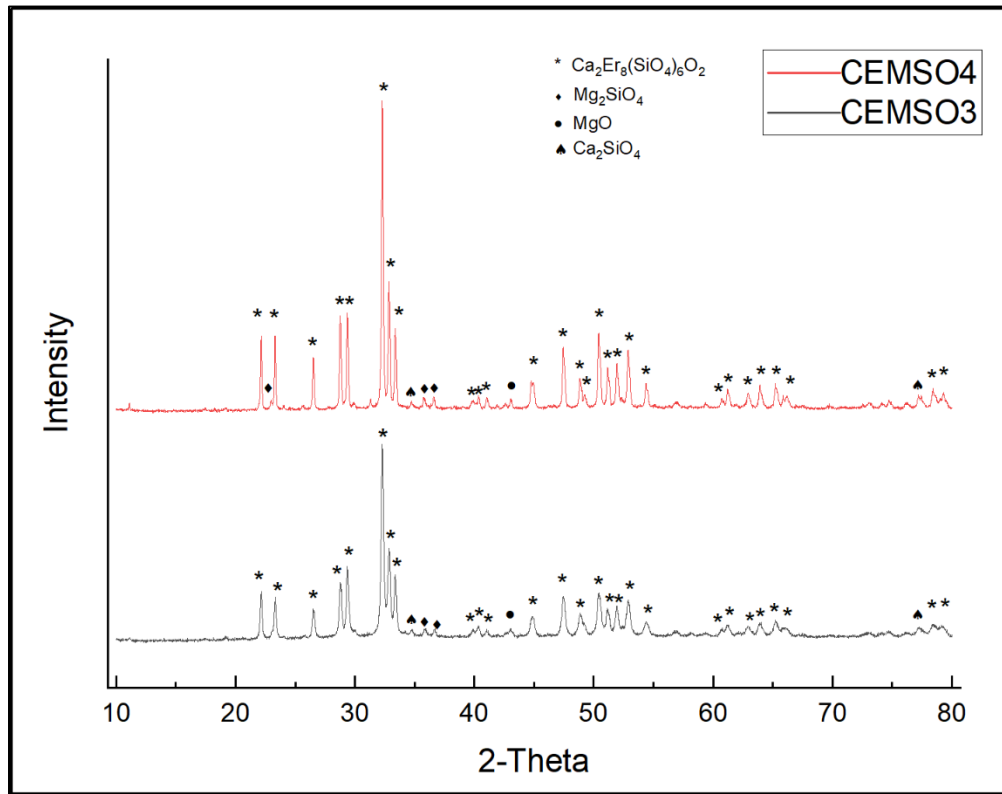


Figure 2.3 XRD spectra of CEMSO3 and CEMSO4 samples.

Summary

XRD patterns of samples CEMSO2 (fuel-to-oxidizer ratio = 0.5) and CEMSO4 (fuel-to-oxidizer ratio = 0.75) are shown on Figure 2.4. These two samples have the same phase composition, which indicates that the speed of the reaction at these two fuel-to-oxidizer ratios is

insufficient to make the $\text{Mg}(\text{NO}_3)_2$ take a part in the reaction. Therefore, a 0.25 increase in fuel-to-oxidizer ratio is not enough, and the fuel-to-oxidizer ratio has to be continuously increased.

Although different calcination temperatures do not cause any changes in phase formation, a higher calcination temperature can potentially improve the crystallinity of powder[115, 116]. Therefore, the calcination temperature of 1200°C may benefit the phase formation. Under this situation, the calcination temperature of 1200°C was determined for the follow-up experiments.

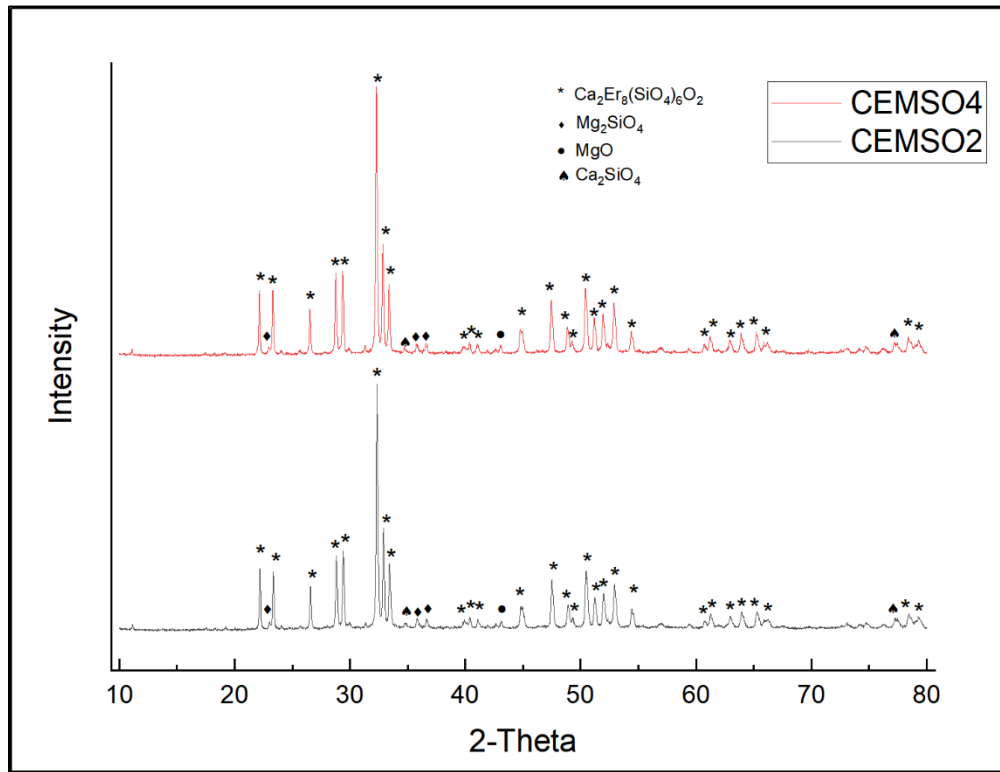


Figure 2.4 XRD spectra of CEMSO2 and CEMSO4 samples.

Further increase of the fuel-to-oxidizer ratio, different orders of mixing & excess $\text{Mg}(\text{NO}_3)_2$

CEMSO5 & CEMSO6 samples

For samples CEMSO5 and CEMSO6, the fuel-to-oxidizer ratio was increased to 1.0. Also, the order of the reactants was different. The reactants were added by the order of $\text{Ca}(\text{NO}_3)_2 + \text{Er}(\text{NO}_3)_3 + \text{CH}_6\text{N}_4\text{O} + \text{SiO}_2 + \text{Mg}(\text{NO}_3)_2$ for the sample CEMSO5, and $\text{Ca}(\text{NO}_3)_2 + \text{Er}(\text{NO}_3)_3 +$

$\text{CH}_6\text{N}_4\text{O} + \text{Mg}(\text{NO}_3)_2 + \text{SiO}_2$ for the sample CEMSO6. All experimental parameters are listed in Table 2-5. The stirring time was 30 min, the combustion process was conducted at 500°C for 15 min, and the calcination process was maintained at 1200°C for 2 h.

Table 2-5 The experimental parameters for CEMSO5 and CEMSO6 samples.

Sample Name	CEMSO5	CEMSO6
f/o Ratio	1.0	1.0
Order	1.Ca(NO ₃) ₂ 2.Er(NO ₃) ₃ 3.CH ₆ N ₄ O 4.SiO ₂ 5.Mg(NO ₃) ₂	1.Ca(NO ₃) ₂ 2.Er(NO ₃) ₃ 3.CH ₆ N ₄ O 4.Mg(NO ₃) ₂ 5.SiO ₂
Stirring Time	30 min	30 min
Combustion Synthesis Parameters	500°C 15 min	500°C 15 min
Calcination Temperature	1200°C	1200°C
Calcination Time	2 h	2 h

Phase analysis by XRD: CEMSO5 & CEMSO6 samples

The XRD patterns of the sample CEMSO5 and CEMSO6 are shown on Figure 2.5. It can be seen that most for the peaks of both the samples are consistent with the peaks of the $\text{Ca}_2\text{Er}_8(\text{SiO}_4)_6\text{O}_2$, Mg_2SiO_4 , Ca_2SiO_4 , and MgO , but the desired garnet phase of $\text{CaEr}_2\text{Mg}_2\text{Si}_3\text{O}_{12}$ was still not detected in these two samples. Thus, further optimization of the experimental conditions needs to be performed. Specifically, the content of $\text{Mg}(\text{NO}_3)_2$ was decided to be

doubled since the magnesium was found to be difficult to be synthesized into the resultant garnet structure.

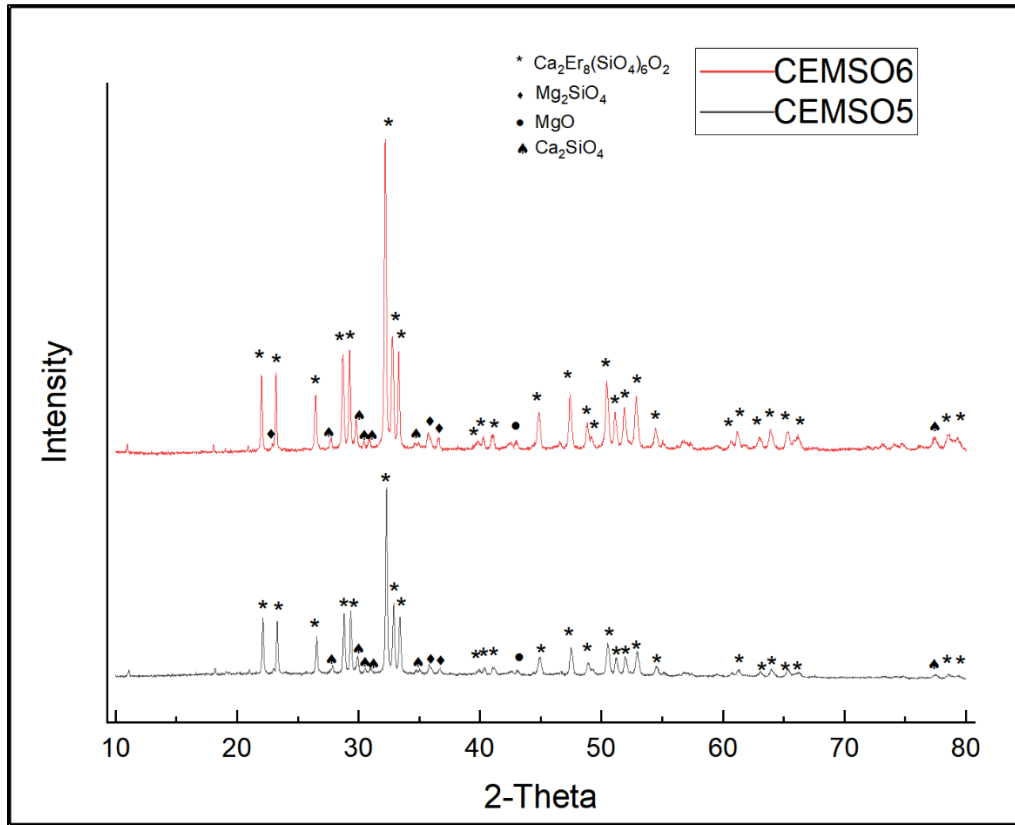


Figure 2.5 XRD spectra of CEMSO5 and CEMSO6 samples.

CEMSO7 & CEMSO8 samples

For samples CEMSO7 and CEMSO8, the content of $\text{Mg}(\text{NO}_3)_2$ was doubled (1.4662g), and different orders of reactants' addition were still investigated in these two experiments. For both samples, the fuel-to-oxidizer ratio was 1.0, the stirring time of the reactants were 30 min, the combustion was conducted at 500°C for 15 min, and the calcination process was maintained at 1200°C for 2 h. The sample CEMSO7 used the order of $\text{Ca}(\text{NO}_3)_2 + \text{Er}(\text{NO}_3)_3 + \text{CH}_6\text{N}_4\text{O} + \text{SiO}_2 + \text{Mg}(\text{NO}_3)_2$, and the sample CEMSO8 used the order of $\text{Ca}(\text{NO}_3)_2 + \text{Er}(\text{NO}_3)_3 + \text{CH}_6\text{N}_4\text{O} + \text{Mg}(\text{NO}_3)_2 + \text{SiO}_2$. All the experimental parameters are listed in Table 2-6.

Table 2-6 The experimental parameters for CEMSO7 and CEMSO8 samples.

Sample Name	CEMSO7	CEMSO8
f/o Ratio	1.0	1.0
Order	1.Ca(NO ₃) ₂ 2.Er(NO ₃) ₃ 3.CH ₆ N ₄ O 4.SiO ₂ 5.Mg(NO ₃) ₂ *2	1.Ca(NO ₃) ₂ 2.Er(NO ₃) ₃ 3.CH ₆ N ₄ O 4.Mg(NO ₃) ₂ *2 5.SiO ₂
Stirring Time	30 min	30 min
Combustion Synthesis Parameters	500°C 15 min	500°C 15 min
Calcination Temperature	1200°C	1200°C
Calcination Time	2 h	2 h

Phase analysis by XRD: CEMSO7 & CEMSO8 samples

Both of the XRD patterns for samples CEMSO7 and CEMSO8 are shown on Figure 2.6. It is clear that the main peaks in these XRD patterns still belong to the Ca₂Er₈(SiO₄)₆O₂, Mg₂SiO₄, MgO, and Ca₂SiO₄.

The targeted composition of CaEr₂Mg₂Si₃O₁₂ was also not obtained after the above treatments for these samples, which suggests that the optimal amount of magnesium still cannot be added into the structure. As a result, three times of the content amount of the Mg(NO₃)₂ was decided to be added during the synthesis as the last reactant. In addition, the calcination time of 5 h, 10 h, and 15 h were also introduced into the corresponding experiments (see Table 2-7). Due to a violent

reaction with the fuel-to-oxidizer ratio of 1.0, a fuel-to-oxidizer ratio of 0.8 was applied in the following experiments.

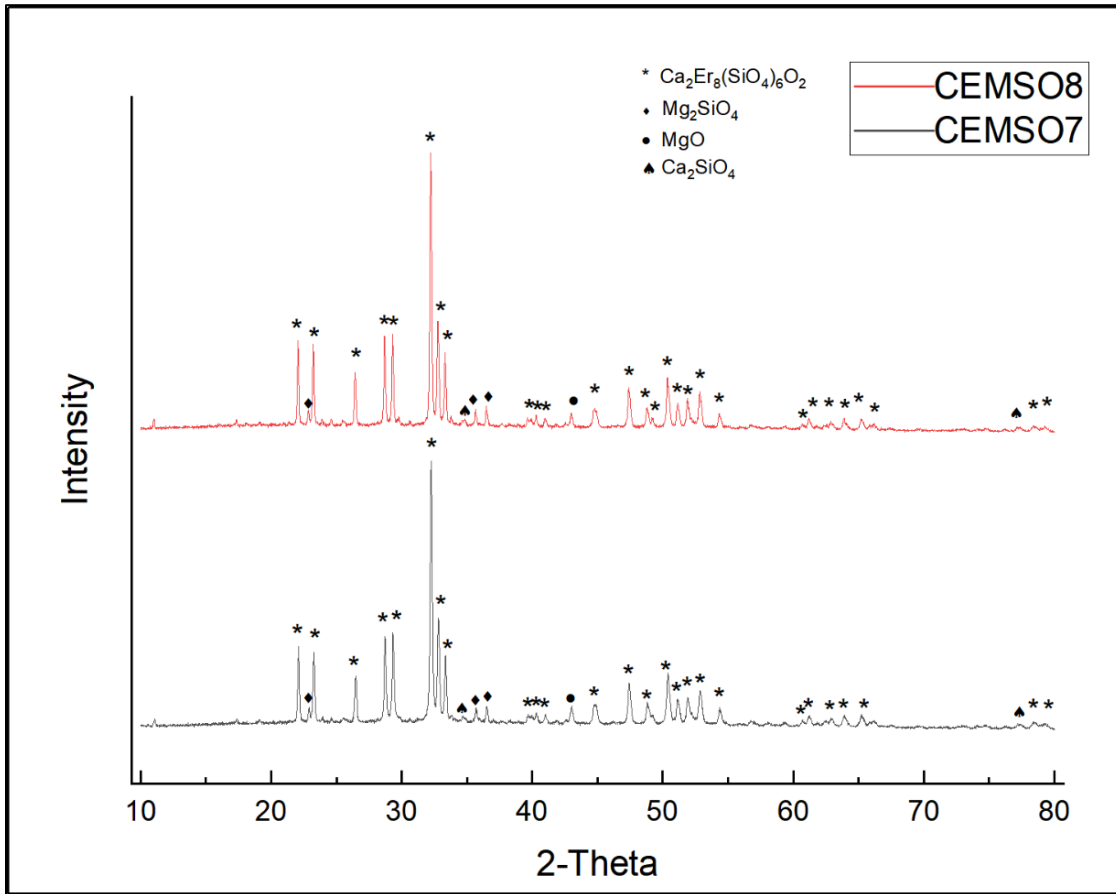


Figure 2.6 XRD spectra of CEMSO7 and CEMSO8 samples.

Longer calcination time and more $Mg(NO_3)_2$

CEMSO9, CEMSO10 & CEMSO11 samples

The fuel-to-oxidizer ratio was decreased to 0.8, the content of the $Mg(NO_3)_2$ was tripled (2.1994g), and the calcination time was different for these three samples(5 h, 10 h, and 15 h). As for other experimental conditions, the reactants were added in the order of $Ca(NO_3)_2 + Er(NO_3)_3 + CH_6N_4O + SiO_2 + Mg(NO_3)_2$, the stirring time was 30 min, the combustion reaction was conducted at 500°C for 15 min, and the calcination temperature was 1200°C. The detailed parameters are listed in Table 2-7.

Table 2-7 The experimental parameters for CEMSO9, CEMSO10, and CEMSO11 samples.

Sample Name	CEMSO9	CEMSO10	CEMSO11
f/o Ratio	0.8	0.8	0.8
Order	1.Ca(NO ₃) ₂ 2.Er(NO ₃) ₃ 3.CH ₆ N ₄ O 4.SiO ₂ 5.Mg(NO ₃) ₂ *3	1.Ca(NO ₃) ₂ 2.Er(NO ₃) ₃ 3.CH ₆ N ₄ O 4.SiO ₂ 5.Mg(NO ₃) ₂ *3	1.Ca(NO ₃) ₂ 2.Er(NO ₃) ₃ 3.CH ₆ N ₄ O 4.SiO ₂ 5.Mg(NO ₃) ₂ *3
Stirring Time	30 min	30 min	30 min
Combustion Synthesis Parameters	500°C 15 min	500°C 15 min	500°C 15 min
Calcination Temperature	1200°C	1200°C	1200°C
Calcination Time	5 h	10 h	15 h

Phase analysis by XRD: CEMSO9, CEMSO10 & CEMSO11 samples

All the XRD patterns are shown on Figure 2.7. These three patterns are similar except for the intensity of the peaks. The main peaks are consistent with the Ca₂Er₈(SiO₄)₆O₂ compound, and other peaks can be fitted with the Mg₂SiO₄, MgO, and Ca₂SiO₄ phases.

Similar to the previous experiments discussed above, the phase of the CaEr₂Mg₂Si₃O₁₂ was not obtained for these three samples. Therefore, adding a tripled content of Mg(NO₃)₂ and changing the calcination time were not promising ways to synthesize the magnesium into the CaEr₂Mg₂Si₃O₁₂ structure.

Summary

Since all the previous experiments cannot successfully prepare the targeted compound of $\text{CaEr}_2\text{Mg}_2\text{Si}_3\text{O}_{12}$ but mainly the apatite[117] $\text{Ca}_2\text{Er}_8(\text{SiO}_4)_6\text{O}_2$ compound, we decided to increase the combustion temperature and a stirring time. In order to avoid a violent reaction when the combustion temperature is increased, the fuel-to-oxidizer ratio was decided to be 0.5. Also, the doubled content of the $\text{Mg}(\text{NO}_3)_2$ and a last addition of the $\text{Mg}(\text{NO}_3)_2$ into the solution were used. The calcination process was determined to be conducted at 1200°C for 10 h.

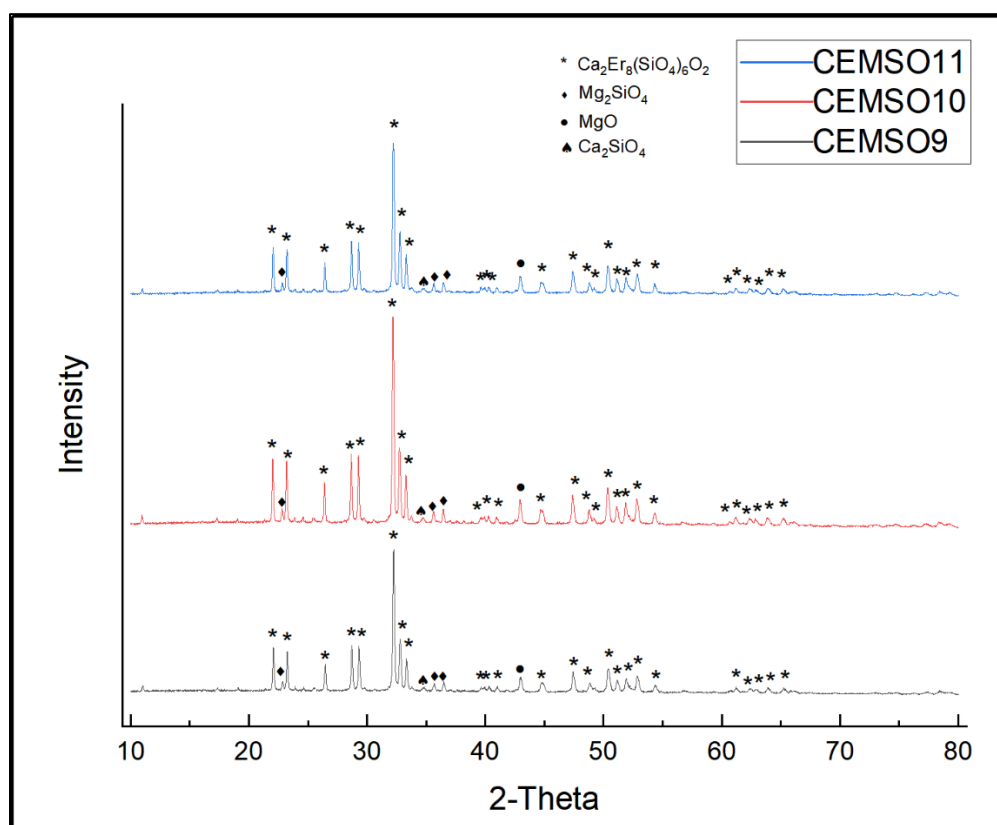


Figure 2.7 XRD spectra of CEMSO9, CEMSO10, and CEMSO11 samples.

Different stirring times and different combustion temperatures (550°C & 600°C)

CEMSO12 & CEMSO13 samples

For these two samples, the combustion temperature was increased to 550°C , and the stirring time was increased to 1 h for CEMSO12 and 2 h for CEMSO13, respectively. In addition, for both

samples, the reactants were added in the order of $\text{Ca}(\text{NO}_3)_2 + \text{Er}(\text{NO}_3)_3 + \text{CH}_6\text{N}_4\text{O} + \text{SiO}_2 + \text{Mg}(\text{NO}_3)_2$, the content of the $\text{Mg}(\text{NO}_3)_2$ was doubled, the fuel-to-oxidizer ratio was 0.5, the calcination was conducted at 1200°C for 10 h. The detailed summary of the experimental parameters is listed in Table 2-8.

Table 2-8 The experimental parameters for CEMSO12 and CEMSO13 samples.

Sample Name	CEMSO12	CEMSO13
f/o Ratio	0.5	0.5
Order	1. $\text{Ca}(\text{NO}_3)_2$ 2. $\text{Er}(\text{NO}_3)_3$ 3. $\text{CH}_6\text{N}_4\text{O}$ 4. SiO_2 5. $\text{Mg}(\text{NO}_3)_2*2$	1. $\text{Ca}(\text{NO}_3)_2$ 2. $\text{Er}(\text{NO}_3)_3$ 3. $\text{CH}_6\text{N}_4\text{O}$ 4. SiO_2 5. $\text{Mg}(\text{NO}_3)_2*2$
Stirring Time	1 h	2 h
Combustion Synthesis Parameters	550°C 15 min	550°C 15 min
Calcination Temperature	1200°C	1200°C
Calcination Time	10 h	10 h

Phase analysis by XRD: CEMSO12 & CEMSO13 samples

CEMSO12 sample

The XRD pattern of the CEMSO12 and the theoretical pattern of the $\text{CaEr}_2\text{Mg}_2\text{Si}_3\text{O}_{12}$ are shown on Figure 2.8. A comparison with the theoretical XRD pattern of the $\text{CaEr}_2\text{Mg}_2\text{Si}_3\text{O}_{12}$ prove that most of the peaks fit well with the theoretical pattern; peaks of the $\text{Ca}_2\text{Er}_8(\text{SiO}_4)_6\text{O}_2$ phase are also presented in that spectrum. This result indicates that the garnet structure $\text{CaEr}_2\text{Mg}_2\text{Si}_3\text{O}_{12}$ was successfully obtained with some impurities of $\text{Ca}_2\text{Er}_8(\text{SiO}_4)_6\text{O}_2$.

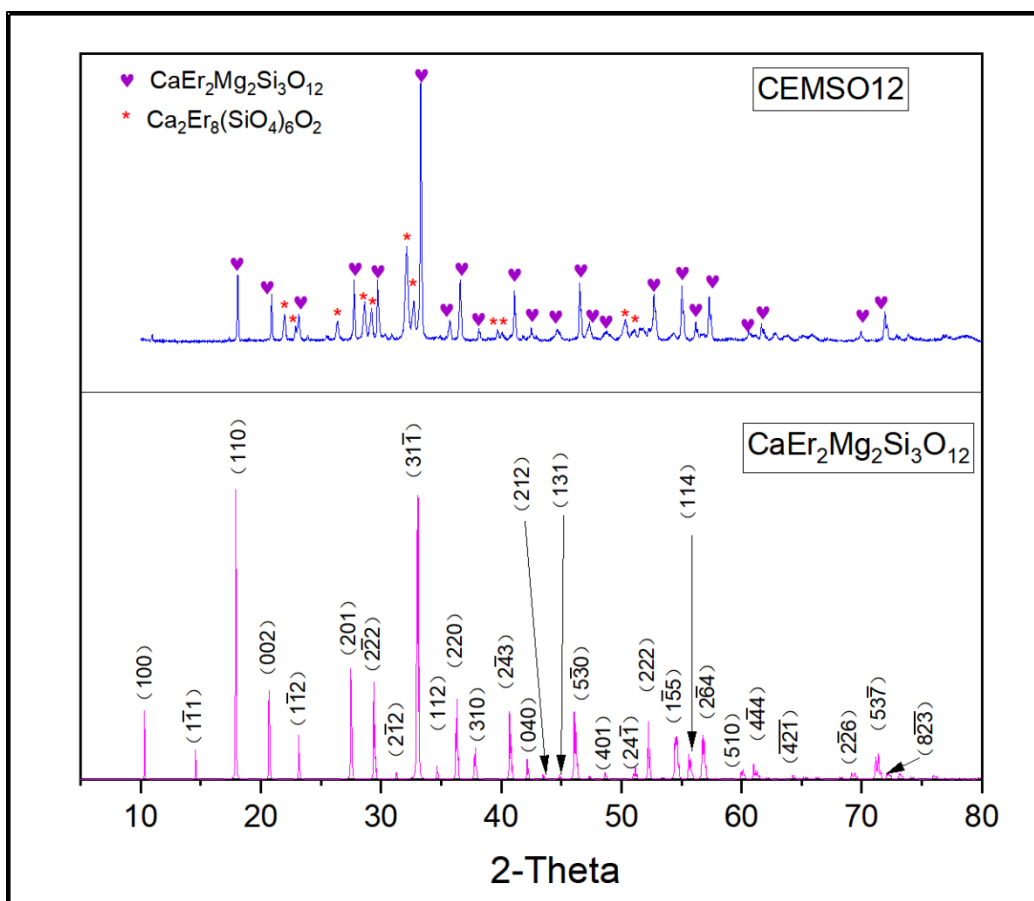


Figure 2.8 XRD pattern of CEMSO12 sample together with the theoretical $\text{CaEr}_2\text{Mg}_2\text{Si}_3\text{O}_{12}$ pattern.

CEMSO13 sample

The XRD pattern of the sample CEMSO13 is presented on Figure 2.9. For this 2-hour stirring sample, the XRD pattern changes back to the apatite $\text{Ca}_2\text{Er}_8(\text{SiO}_4)_6\text{O}_2$ phase together with other impurities that have been discussed before.

According to these results, a combustion temperature of 550°C was a promising condition for the synthesis of $\text{CaEr}_2\text{Mg}_2\text{Si}_3\text{O}_{12}$ compound.

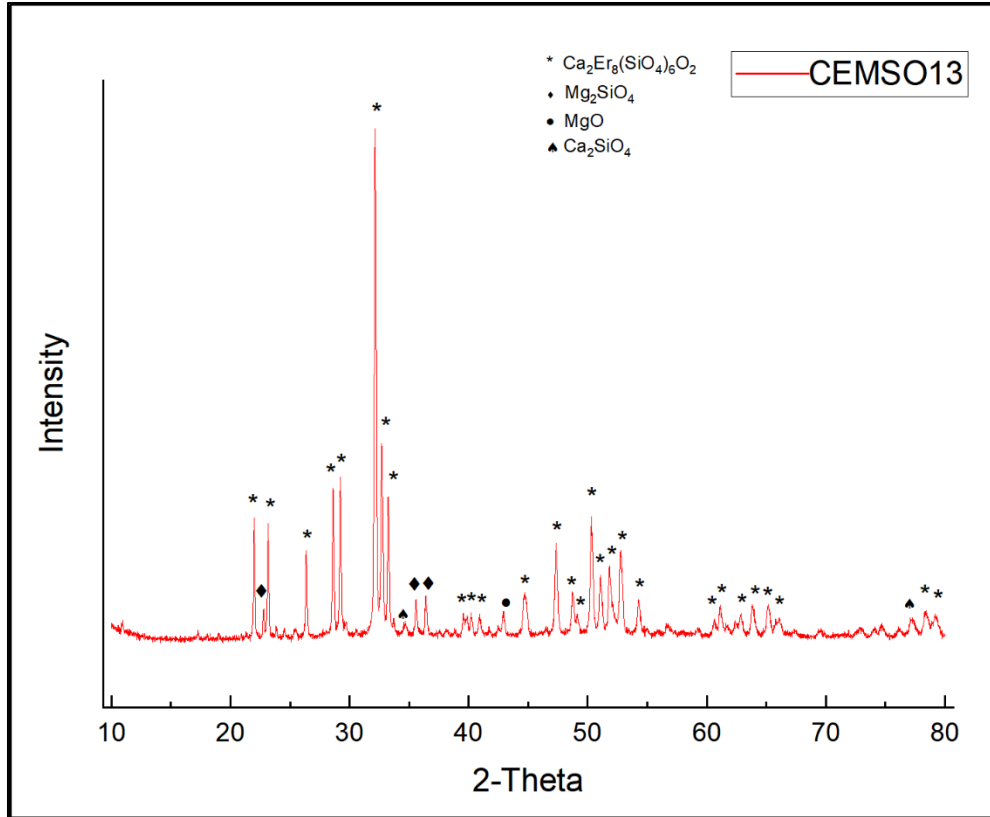


Figure 2.9 XRD spectra of CEMSO13 sample.

CEMSO14 & CEMSO15 samples

These two samples were treated with a combustion temperature of 600°C for 15 min. The stirring process lasted for 1 h and 2 h for CEMSO14 and CEMSO15, respectively. For other experimental parameters, the fuel-to-oxidizer ratio was 0.5, the starting reagents were added with the order of $\text{Ca}(\text{NO}_3)_2 + \text{Er}(\text{NO}_3)_3 + \text{CH}_6\text{N}_4\text{O} + \text{SiO}_2 + \text{Mg}(\text{NO}_3)_2$, and the calcination process was conducted at 1200°C for 10 h. All the experimental parameters are listed in Table 2-9.

Phase analysis by XRD: CEMSO14 & CEMSO15 samples

The XRD patterns of these two samples are shown on Figure 2.10. The XRD result indicates that the apatite $\text{Ca}_2\text{Er}_8(\text{SiO}_4)_6\text{O}_2$ phase was mainly formed under a combustion temperature of 600°C. Mg_2SiO_4 , MgO , and Ca_2SiO_4 phases were also detected. According to this result, the combustion temperature of 600°C was not promising for the preparation of the targeted

CaEr₂Mg₂Si₃O₁₂ compound. This may result from a faster reaction at a higher combustion temperature, which makes the magnesium difficult to be synthesized into the resultant targeted structure.

Table 2-9 The experimental parameters for CEMSO14 and CEMSO15 samples.

Sample Name	CEMSO14	CEMSO15
f/o Ratio	0.5	0.5
Order	1.Ca(NO ₃) ₂ 2.Er(NO ₃) ₃ 3.CH ₆ N ₄ O 4.SiO ₂ 5.Mg(NO ₃) ₂ *2	1.Ca(NO ₃) ₂ 2.Er(NO ₃) ₃ 3.CH ₆ N ₄ O 4.SiO ₂ 5.Mg(NO ₃) ₂ *2
Stirring Time	1 h	2 h
Combustion Synthesis Parameters	600°C 15 min	600°C 15 min
Calcination Temperature	1200°C	1200°C
Calcination Time	10 h	10 h

Summary

In summary, the experimental parameters of the sample CEMSO12 can be used for the synthesis of the targeted CaEr₂Mg₂Si₃O₁₂ compound. Specifically, the experimental conditions are listed here: the fuel-to-oxidizer ratio is 0.5, the reactants are added following the order of Ca(NO₃)₂ + Er(NO₃)₃ + CH₆N₄O + SiO₂ + Mg(NO₃)₂, the content of the Mg(NO₃)₂ is doubled (1.4662g), the

stirring time is 1 h, the combustion process is conducted at 550°C for 15 min, and the calcination is conducted at 1200°C for 10 h.

Although the desired phase was obtained under these conditions, the apatite $\text{Ca}_2\text{Er}_8(\text{SiO}_4)_6\text{O}_2$ phase still needs to be removed. Next, several experiments were performed in order to remove this apatite phase.

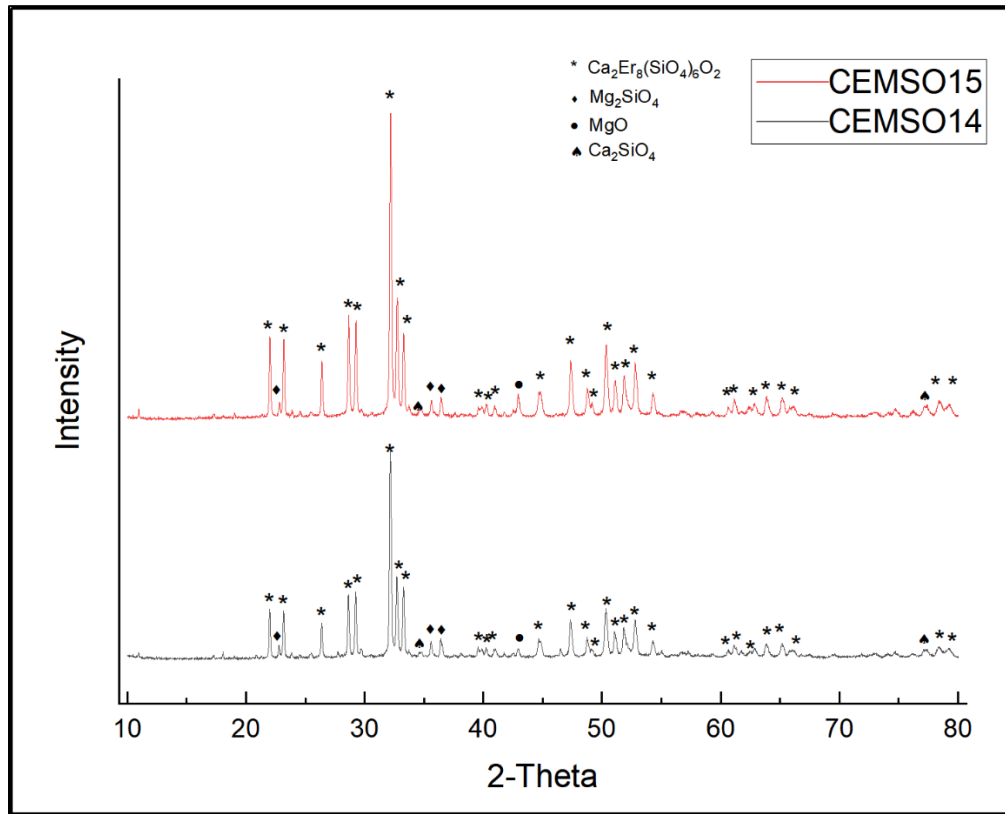


Figure 2.10 XRD spectra of CEMSO14 and CEMSO15 samples.

Removal of the apatite $\text{Ca}_2\text{Er}_8(\text{SiO}_4)_6\text{O}_2$ phase

Increase of the calcination temperature

Different calcination temperatures of 1225°C, 1250°C, 1275°C, 1300°C, and 1400°C were used to find ways to remove the $\text{Ca}_2\text{Er}_8(\text{SiO}_4)_6\text{O}_2$ phase from the resultant material (see Figure 2.8), and the detailed information is listed in Table 2-10.

Phase analysis by XRD

CEMSO16 sample

The XRD pattern of the sample CEMSO16 is shown on Figure 2.11. The result indicates that the $\text{Ca}_2\text{Er}_8(\text{SiO}_4)_6\text{O}_2$ apatite phase still existed when the calcination temperature was increased to 1225°C.

Table 2-10 The experimental parameters for CEMSO16, CEMSO17, CEMSO18, CEMSO19, and CEMSO20 samples.

Sample Name	CEMSO16	CEMSO17	CEMSO18	CEMSO19	CEMSO20
f/o Ratio	1.0	1.0	1.0	1.0	1.0
Order	1.Ca(NO ₃) ₂ 2.Er(NO ₃) ₃ 3.CH ₆ N ₄ O 4.SiO ₂ 5.Mg(NO ₃) ₂ *2	1.Ca(NO ₃) ₂ 2.Er(NO ₃) ₃ 3.CH ₆ N ₄ O 4.SiO ₂ 5.Mg(NO ₃) ₂ *2	1.Ca(NO ₃) ₂ 2.Er(NO ₃) ₃ 3.CH ₆ N ₄ O 4.SiO ₂ 5.Mg(NO ₃) ₂ *2	1.Ca(NO ₃) ₂ 2.Er(NO ₃) ₃ 3.CH ₆ N ₄ O 4.SiO ₂ 5.Mg(NO ₃) ₂ *2	1.Ca(NO ₃) ₂ 2.Er(NO ₃) ₃ 3.CH ₆ N ₄ O 4.SiO ₂ 5.Mg(NO ₃) ₂ *2
Stirring Time	1 h	1 h	1 h	1 h	1 h
Combustion Synthesis Parameters	550°C 15 min				
Calcination Temperature	1225°C	1250°C	1275°C	1300°C	1400°C
Calcination Time	10 h				

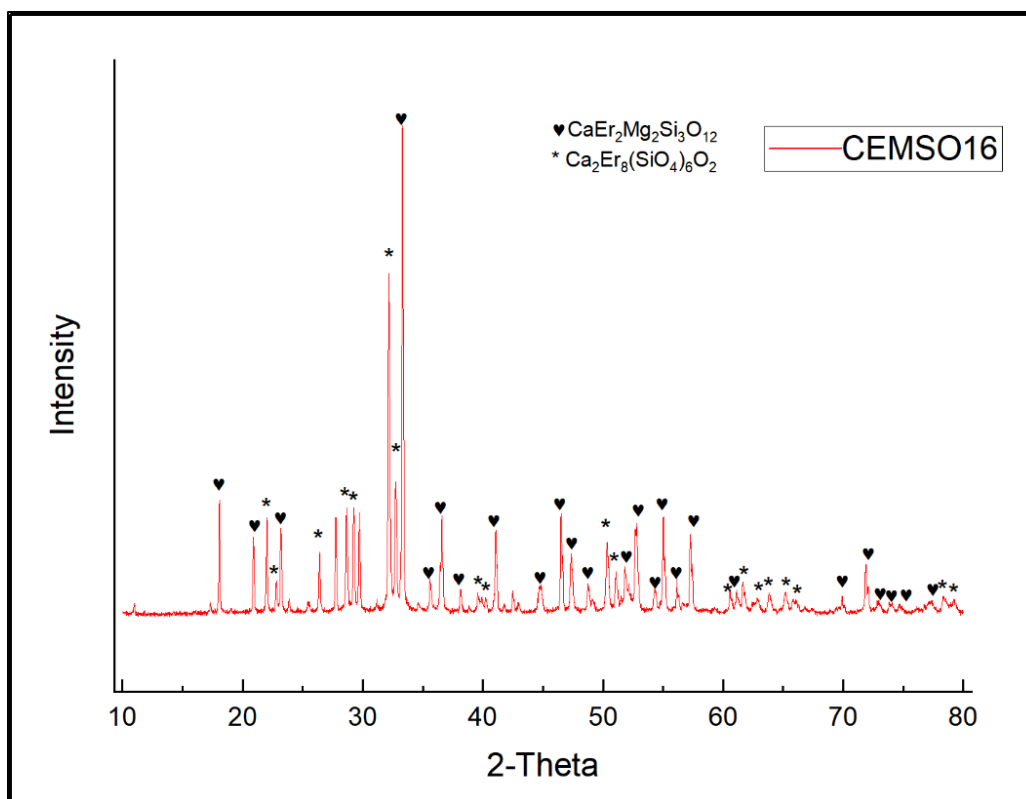


Figure 2.11 XRD spectra of CEMSO16 sample.

CEMSO17 & CEMSO18 samples

The XRD results of the sample CEMSO17 and CEMSO18 are presented on Figure 2.12. It is shown that the main peaks returned to fit with the apatite phase, thus the calcination temperatures of 1250°C and 1275°C also did not work for the removal of the apatite phase, and changed the phase composition back to $\text{Ca}_2\text{Er}_8(\text{SiO}_4)_6\text{O}_2$ to dominate.

CEMSO19 & CEMSO20 samples

These two samples were treated with the calcination temperature at 1300°C and 1400°C, respectively. After the calcination, these two samples were somehow melted, so there were no powders obtained for characterization.

Summary

In conclusion, increasing the calcination temperature may not be used to remove the apatite $\text{Ca}_2\text{Er}_8(\text{SiO}_4)_6\text{O}_2$ phase. The calcination temperatures higher than 1300°C were found to melt the powders. Therefore, the experiments with increasing calcination time have been performed for further investigation.

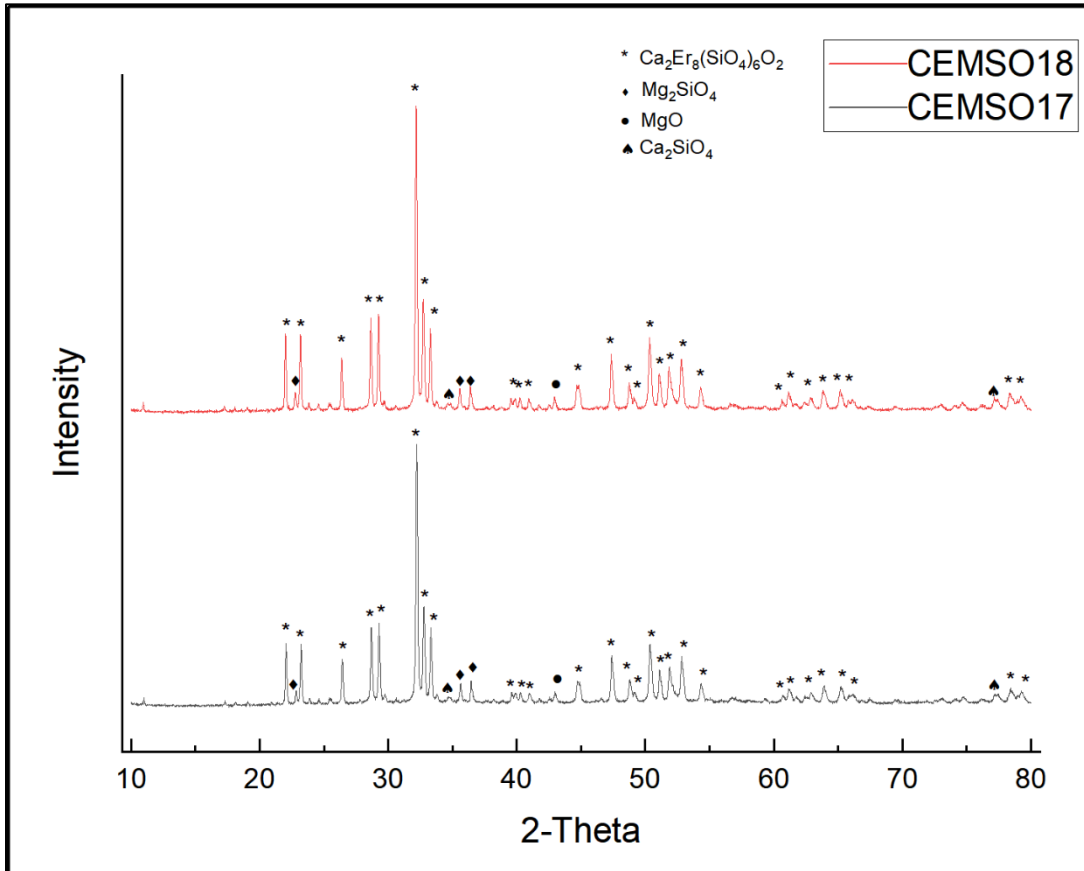


Figure 2.12 XRD spectra of CEMSO17 and CEMSO18 samples.

Increase of the calcination time

CEMSO21 & CEMSO22 samples

Sample CEMSO21 was calcinated at 1200°C for 10 h and another 10 h, which gave a total 20-hour calcination time. Sample CEMSO22 was calcinated at 1225°C for 10 h and another 10 h, which also gave a total 20-hour calcination time.

The XRD results for both of those samples are presented on Figure 2.13. The main peaks fit well with the theoretical garnet $\text{CaEr}_2\text{Mg}_2\text{Si}_3\text{O}_{12}$ phase, but the apatite $\text{Ca}_2\text{Er}_8(\text{SiO}_4)_6\text{O}_2$ phase still cannot be removed.

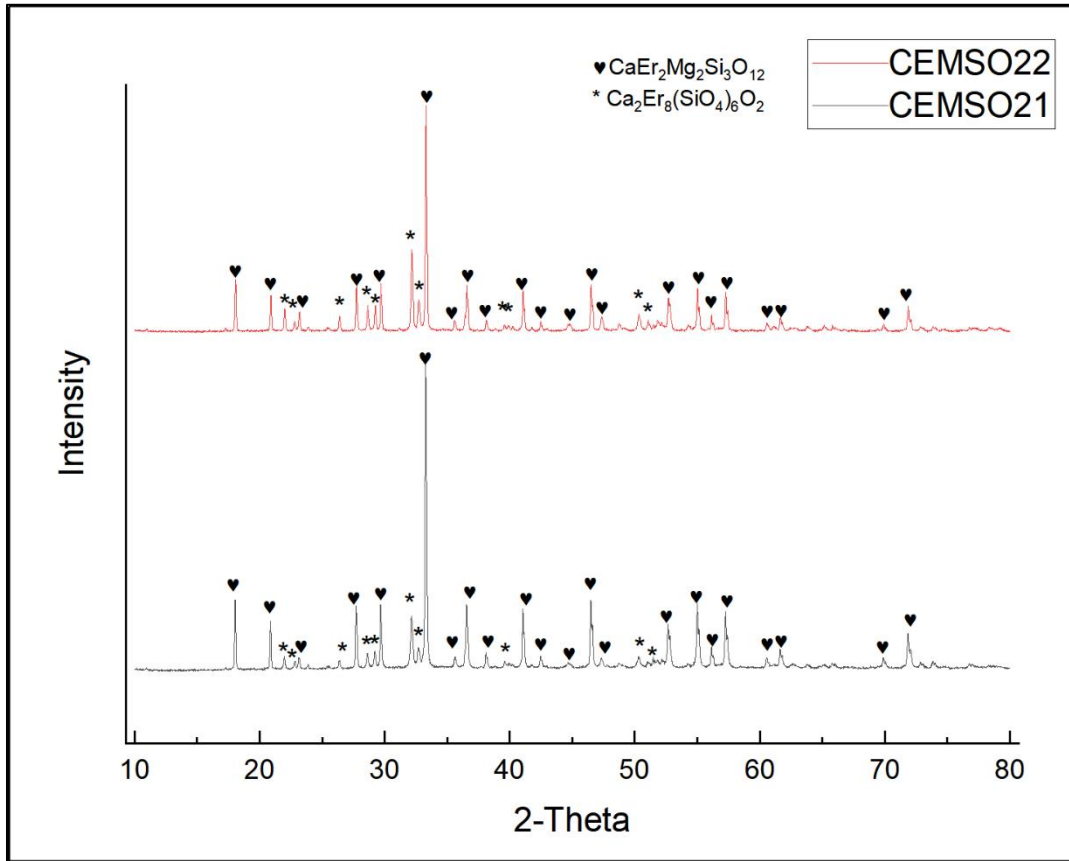


Figure 2.13 XRD spectra of CEMSO21 and CEMSO22 samples.

Comparison between the samples that contain the garnet phase

As mentioned above, CEMSO12, CEMSO16, CEMSO21, and CEMSO22 samples all contain $\text{CaEr}_2\text{Mg}_2\text{Si}_3\text{O}_{12}$ and $\text{Ca}_2\text{Er}_8(\text{SiO}_4)_6\text{O}_2$ phases (see Figure 2.8, Figure 2.11, and Figure 2.13). In order to further study the possibility of removing the apatite phase by increasing the calcination time, a comparison is made between these four samples, and the calcination parameters are listed in Table 2-11.

Comparison of the XRD patterns

The XRD patterns of the four samples are compared and shown on Figure 2.14. It was found that some peaks of $\text{Ca}_2\text{Er}_8(\text{SiO}_4)_6\text{O}_2$ phase tended to disappear with the increase of the calcination time (see Figure 2.14 CEMSO21). Therefore, further increasing the calcination time of CEMSO21 may be helpful for the removal of the apatite phase.

Table 2-11 The calcination parameters for CEMSO12, CEMSO16, CEMSO21, and CEMSO22 samples.

Sample Name	CEMSO12	CEMSO16	CEMSO21	CEMSO22
Calcination Temperature	1200°C	1225°C	1200°C	1225°C
Calcination Time	10 h	10 h	10 h + 10 h	10 h + 10 h

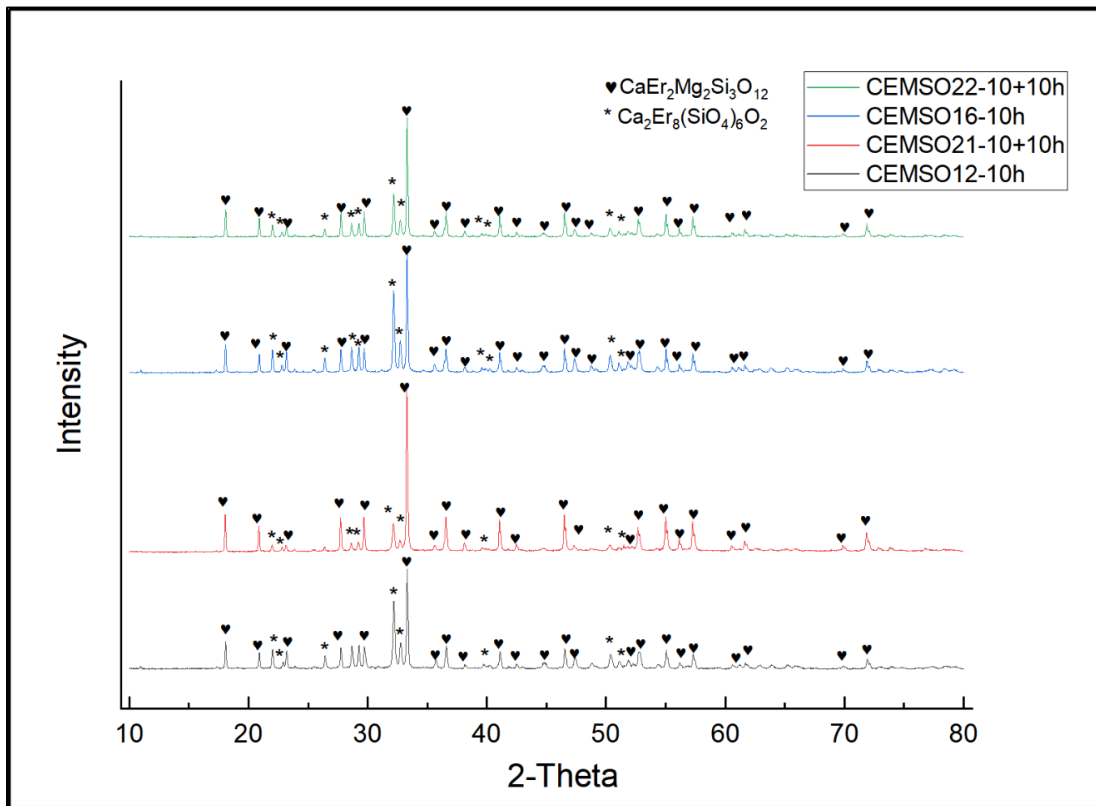


Figure 2.14 XRD spectra of CEMSO12, CEMSO16, CEMSO21 and CEMSO22 samples.

Next, CEMSO21 was further calcinated for another 10 hours, and CEMSO23 was obtained. As shown on Figure 2.15, it indicates that most of the peaks belong to $\text{CaEr}_2\text{Mg}_2\text{Si}_3\text{O}_{12}$ phase, and there is only one small peak which belongs to $\text{Ca}_2\text{Er}_8(\text{SiO}_4)_6\text{O}_2$ phase. Thus, longer calcination time is a promising way to remove the apatite $\text{Ca}_2\text{Er}_8(\text{SiO}_4)_6\text{O}_2$ phase.

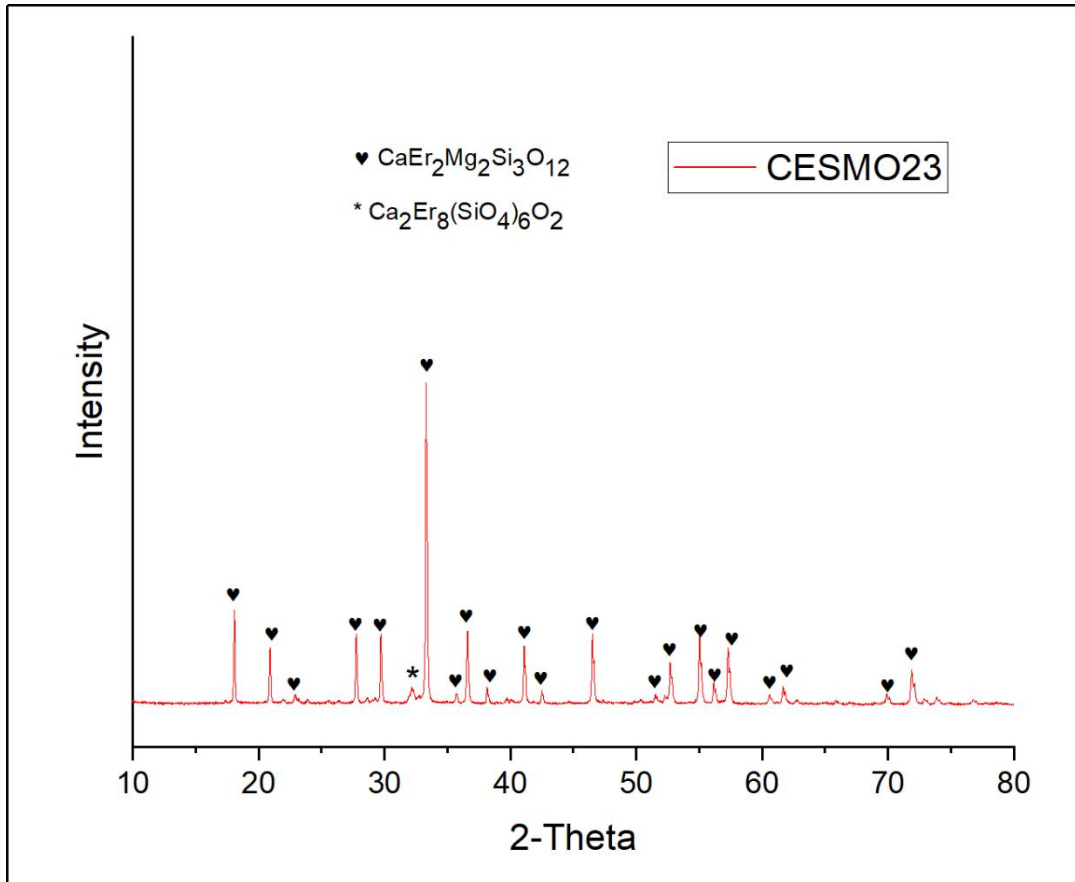


Figure 2.15 XRD spectra of CEMSO23.

Summary

The phase compositions of all the samples are listed in Table 2-12. It can be seen that samples CEMSO12, CEMSO16, CEMSO21, CEMSO22, and CEMSO23 contain both the targeted $\text{CaEr}_2\text{Mg}_2\text{Si}_3\text{O}_{12}$ phase and apatite $\text{Ca}_2\text{Er}_8(\text{SiO}_4)_6\text{O}_2$ phase. Among all these five samples, sample CEMSO23 is the most successful one, because the $\text{Ca}_2\text{Er}_8(\text{SiO}_4)_6\text{O}_2$ phase tends to be almost fully removed (see Figure 2.15). Therefore, the experimental conditions for sample CEMSO23 are

promising for the preparation of $\text{Ca}_2\text{Er}_8(\text{SiO}_4)_6\text{O}_2$ compound. The detailed conditions are listed here: the fuel-to-oxidizer ratio is 0.5, the reactants are mixed by the order of $\text{Ca}(\text{NO}_3)_2$, $\text{Er}(\text{NO}_3)_3$, $\text{CH}_6\text{N}_4\text{O}$, SiO_2 , and $\text{Mg}(\text{NO}_3)_2$, the content of $\text{Mg}(\text{NO}_3)_2$ is doubled, the stirring time is 1 h, the combustion reaction is maintained at 550°C for 15 min, and the calcination process is maintained at both 1200°C for 10 h + 10 h + 10 h (total 30 h). The results still indicate that further increasing the calcination time can fully remove the apatite $\text{Ca}_2\text{Er}_8(\text{SiO}_4)_6\text{O}_2$ phase.

Table 2-12 Phase composition of all the prepared samples.

Sample Name	Phase Composition
CEMSO1	$\text{Ca}_2\text{Er}_8(\text{SiO}_4)_6\text{O}_2$, Ca_2SiO_4 , Mg_2SiO_4 , and MgO
CEMSO2	$\text{Ca}_2\text{Er}_8(\text{SiO}_4)_6\text{O}_2$, Ca_2SiO_4 , Mg_2SiO_4 , and MgO
CEMSO3	$\text{Ca}_2\text{Er}_8(\text{SiO}_4)_6\text{O}_2$, Ca_2SiO_4 , Mg_2SiO_4 , and MgO
CEMSO4	$\text{Ca}_2\text{Er}_8(\text{SiO}_4)_6\text{O}_2$, Ca_2SiO_4 , Mg_2SiO_4 , and MgO
CEMSO5	$\text{Ca}_2\text{Er}_8(\text{SiO}_4)_6\text{O}_2$, Ca_2SiO_4 , Mg_2SiO_4 , and MgO
CEMSO6	$\text{Ca}_2\text{Er}_8(\text{SiO}_4)_6\text{O}_2$, Ca_2SiO_4 , Mg_2SiO_4 , and MgO
CEMSO7	$\text{Ca}_2\text{Er}_8(\text{SiO}_4)_6\text{O}_2$, Ca_2SiO_4 , Mg_2SiO_4 , and MgO
CEMSO8	$\text{Ca}_2\text{Er}_8(\text{SiO}_4)_6\text{O}_2$, Ca_2SiO_4 , Mg_2SiO_4 , and MgO
CEMSO9	$\text{Ca}_2\text{Er}_8(\text{SiO}_4)_6\text{O}_2$, Ca_2SiO_4 , Mg_2SiO_4 , and MgO
CEMSO10	$\text{Ca}_2\text{Er}_8(\text{SiO}_4)_6\text{O}_2$, Ca_2SiO_4 , Mg_2SiO_4 , and MgO
CEMSO11	$\text{Ca}_2\text{Er}_8(\text{SiO}_4)_6\text{O}_2$, Ca_2SiO_4 , Mg_2SiO_4 , and MgO
CEMSO12	$\text{CaEr}_2\text{Mg}_2\text{Si}_3\text{O}_{12}$ and $\text{Ca}_2\text{Er}_8(\text{SiO}_4)_6\text{O}_2$
CEMSO13	$\text{Ca}_2\text{Er}_8(\text{SiO}_4)_6\text{O}_2$, Ca_2SiO_4 , Mg_2SiO_4 , and MgO
CEMSO14	$\text{Ca}_2\text{Er}_8(\text{SiO}_4)_6\text{O}_2$, Ca_2SiO_4 , Mg_2SiO_4 , and MgO
CEMSO15	$\text{Ca}_2\text{Er}_8(\text{SiO}_4)_6\text{O}_2$, Ca_2SiO_4 , Mg_2SiO_4 , and MgO

Table 2-12 Phase composition of all the prepared samples (Cont).

Sample Name	Phase Composition
CEMSO16	$\text{CaEr}_2\text{Mg}_2\text{Si}_3\text{O}_{12}$ and $\text{Ca}_2\text{Er}_8(\text{SiO}_4)_6\text{O}_2$
CEMSO17	$\text{Ca}_2\text{Er}_8(\text{SiO}_4)_6\text{O}_2$, Ca_2SiO_4 , Mg_2SiO_4 , and MgO
CEMSO18	$\text{Ca}_2\text{Er}_8(\text{SiO}_4)_6\text{O}_2$, Ca_2SiO_4 , Mg_2SiO_4 , and MgO
CEMSO19	$\text{Ca}_2\text{Er}_8(\text{SiO}_4)_6\text{O}_2$, Ca_2SiO_4 , Mg_2SiO_4 , and MgO
CEMSO20	$\text{Ca}_2\text{Er}_8(\text{SiO}_4)_6\text{O}_2$, Ca_2SiO_4 , Mg_2SiO_4 , and MgO
CEMSO21	$\text{CaEr}_2\text{Mg}_2\text{Si}_3\text{O}_{12}$ and $\text{Ca}_2\text{Er}_8(\text{SiO}_4)_6\text{O}_2$
CEMSO22	$\text{CaEr}_2\text{Mg}_2\text{Si}_3\text{O}_{12}$ and $\text{Ca}_2\text{Er}_8(\text{SiO}_4)_6\text{O}_2$
CEMSO23	$\text{CaEr}_2\text{Mg}_2\text{Si}_3\text{O}_{12}$ and $\text{Ca}_2\text{Er}_8(\text{SiO}_4)_6\text{O}_2$

3 CONCLUSIONS & FUTURE WORK

In this research, several attempts have been made for the investigation of proper experimental conditions to prepare the targeted single-phased $\text{CaEr}_2\text{Mg}_2\text{Si}_3\text{O}_{12}$ garnet matrix. The sample CEMSO23 which mainly contains the $\text{CaEr}_2\text{Mg}_2\text{Si}_3\text{O}_{12}$ phase with only a small amount of the apatite $\text{Ca}_2\text{Er}_8(\text{SiO}_4)_6\text{O}_2$ phase is the most promising one (see Figure 2.15). Also, the experimental parameters for this sample are listed in Table 3-1. In addition, continuous increasing of the calcination time may potentially benefit the removal of the unwanted apatite $\text{Ca}_2\text{Er}_8(\text{SiO}_4)_6\text{O}_2$ phase.

Table 3-1 The experimental parameters for sample CEMSO23.

Sample Name	CEMSO23
f/o Ratio	0.5
Order	1. $\text{Ca}(\text{NO}_3)_2$ 2. $\text{Er}(\text{NO}_3)_3$ 3. $\text{CH}_6\text{N}_4\text{O}$ 4. SiO_2 5. $\text{Mg}(\text{NO}_3)_2 \cdot 2$
Stirring Time	1 h
Combustion Synthesis Parameters	550°C 15 min
Calcination Temperature	1200°C
Calcination Time	10 h + 10 h + 10 h

After this step, Europium can be doped into this single-phased $\text{CaEr}_2\text{Mg}_2\text{Si}_3\text{O}_{12}$ garnet matrix to prepare a red-emission Eu^{2+} -doped garnet phosphor.

REFERENCES

- [1] Y. N. Zhou, W. D. Zhuang, Y. S. Hu, R. H. Liu, Z. Q. Jiang, Y. H. Liu, Y. F. Li, Y. L. Zheng, L. Chen, and J. Y. Zhong, "A broad-band orange-yellow-emitting $\text{Lu}_2\text{Mg}_2\text{Al}_2\text{Si}_2\text{O}_{12}:\text{Ce}^{3+}$ phosphor for application in warm white light-emitting diodes," *Rsc Advances*, vol. 7, no. 74, pp. 46713-46720, 2017.
- [2] H. Guo, L. L. Sun, J. Liang, B. Li, and X. Y. Huang, "High-efficiency and thermal-stable Eu^{3+} -activated $\text{Ca}_3\text{Y}(\text{AlO})_3(\text{BO}_3)_4$ red-emitting phosphors for near-UV-excited white LEDs," *Journal of Luminescence*, vol. 205, pp. 115-121, Jan, 2019.
- [3] Y. Chen, Z. J. Wang, W. G. Ding, X. Li, Q. Bao, J. J. Liu, K. L. Qiu, X. Y. Meng, Z. P. Yang, and P. L. Li, "A single-phase white light emitting phosphor $\text{Ba}_3\text{Y}(\text{PO}_4)_3:\text{Ce}^{3+}/\text{Eu}^{2+}/\text{Mn}^{2+}$: Luminescence, energy transfer and thermal stability," *Journal of Luminescence*, vol. 210, pp. 322-334, Jun, 2019.
- [4] J. W. Chen, H. Y. Xiang, J. Wang, R. Wang, Y. Li, Q. S. Shan, X. B. Xu, Y. H. Dong, C. T. Wei, and H. B. Zeng, "Perovskite White Light Emitting Diodes: Progress, Challenges, and Opportunities," *Acs Nano*, vol. 15, no. 11, pp. 17150-17174, Nov, 2021.
- [5] N. Holonyak, and S. F. Bevacqua, "COHERENT (VISIBLE) LIGHT EMISSION FROM $\text{Ga}(\text{As}_1\text{-XPx})$ JUNCTIONS," *Applied Physics Letters*, vol. 1, no. 4, pp. 82-83, 1962.
- [6] M. G. Craford, "From Holonyak to Today," *Proceedings of the Ieee*, vol. 101, no. 10, pp. 2170-2175, Oct, 2013.
- [7] A. Paist, "New epoch in Estonian oil shale combustion technology," *Oil Shale*, vol. 21, no. 3, pp. 181-182, 2004.
- [8] S. Nakamura, M. Senoh, and T. Mukai, "P-GAN/N-INGAN/N-GAN DOUBLE-HETEROSTRUCTURE BLUE-LIGHT-EMITTING DIODES," *Japanese Journal of Applied Physics Part 2-Letters & Express Letters*, vol. 32, no. 1A-B, pp. L8-L11, Jan, 1993.
- [9] J. Cho, J. H. Park, J. K. Kim, and E. F. Schubert, "White light-emitting diodes: History, progress, and future," *Laser & Photonics Reviews*, vol. 11, no. 2, Mar, 2017.
- [10] Y. B. Liu, K. Zhang, B. R. Hyun, H. S. Kwok, and Z. J. Liu, "High-Brightness InGaN/GaN Micro-LEDs With Secondary Peak Effect for Displays," *Ieee Electron Device Letters*, vol. 41, no. 9, pp. 1380-1383, Sept, 2020.

- [11] N. Narendran, N. Maliyagoda, L. Deng, and R. Pysar, "Characterizing LEDs for general illumination applications: Mixed-color and phosphor-based white sources," *Proceedings of the Society of Photo-Optical Instrumentation Engineers (Spie)*. pp. 137-147, 2001.
- [12] Y. X. Qin, D. Y. Lin, and S. Y. Hui, "A Simple Method for Comparative Study on the Thermal Performance of LEDs and Fluorescent Lamps," *Ieee Transactions on Power Electronics*, vol. 24, no. 7, pp. 1811-1818, Jul, 2009.
- [13] Y. C. Chuang, Y. L. Ke, H. S. Chuang, C. C. Hu, and Ieee, "Single-Stage Power-Factor-Correction Circuit with Flyback Converter to Drive LEDs for Lighting Applications," *IEEE Industry Applications Society Annual Meeting*, 2010.
- [14] S. Ye, F. Xiao, Y. X. Pan, Y. Y. Ma, and Q. Y. Zhang, "Phosphors in phosphor-converted white light-emitting diodes Recent advances in materials, techniques and properties," *Materials Science & Engineering R-Reports*, vol. 71, no. 1, pp. 1-34, Dec, 2010.
- [15] J. Chen, S. Loeb, and J. H. Kim, "LED revolution: fundamentals and prospects for UV disinfection applications," *Environmental Science-Water Research & Technology*, vol. 3, no. 2, pp. 188-202, Mar, 2017.
- [16] Z. C. An, W. Liu, Y. H. Song, X. T. Zhang, R. J. Dong, X. Q. Zhou, K. Y. Zheng, Y. Sheng, Z. Shi, and H. F. Zou, "Color-tunable Eu²⁺,Eu³⁺ co-doped Ca₂₀Al₂₆Mg₃Si₃O₆₈ phosphor for w-LEDs," *Journal of Materials Chemistry C*, vol. 7, no. 23, pp. 6978-6985, Jun, 2019.
- [17] S. Muthu, F. J. P. Schuurmans, and M. D. Pashley, "Red, green, and blue LEDs for white light illumination," *Ieee Journal of Selected Topics in Quantum Electronics*, vol. 8, no. 2, pp. 333-338, Mar-Apr, 2002.
- [18] Z. T. Deng, D. Y. Gui, M. L. Wang, M. L. Tu, L. Xie, and Ieee, "Study on characterization of light aging of RGB LED packaging materials." pp. 252-256, 2018.
- [19] I. Moreno, U. Contreras, and R. I. Tzonchev, "Cluster configurations of red, green, and blue LEDs for white light illumination," *Proceedings of the Society of Photo-Optical Instrumentation Engineers (Spie)*. pp. 162-168, 2005.
- [20] J. S. Kuo, C. L. Kuyper, P. B. Allen, G. S. Fiorini, and D. T. Chiu, "High-power blue/UV light-emitting diodes as excitation sources for sensitive detection," *Electrophoresis*, vol. 25, no. 21-22, pp. 3796-3804, Nov, 2004.

- [21] H. P. Ji, L. Wang, M. S. Molokeev, N. Hirosaki, Z. H. Huang, Z. G. Xia, O. M. ten Kate, L. H. Liu, and R. J. Xie, "New garnet structure phosphors, $\text{Lu}_{3-x}\text{Y}_x\text{MgAl}_3\text{SiO}_{12}:\text{Ce}^{3+}$ ($x=0-3$), developed by solid solution design," *Journal of Materials Chemistry C*, vol. 4, no. 12, pp. 2359-2366, 2016.
- [22] P. Q. Jiang, Y. Peng, Y. Mou, H. Cheng, M. X. Chen, and S. Liu, "Thermally stable multi-color phosphor-in-glass bonded on flip-chip UV-LEDs for chromaticitytunable WLEDs," *Applied Optics*, vol. 56, no. 28, pp. 7921-7926, Oct, 2017.
- [23] Y. H. Kim, H. J. Kim, S. P. Ong, Z. B. Wang, and W. B. Im, "Cation-Size Mismatch as a Design Principle for Enhancing the Efficiency of Garnet Phosphors," *Chemistry of Materials*, vol. 32, no. 7, pp. 3097-3108, Apr, 2020.
- [24] Z. Zhou, S. Q. Liu, Y. N. Liu, M. Yokoyama, and Ieee, "A study of preparation and optical properties of the white OLEDs stacked with YAG and $\text{Sr}_2\text{Si}_5\text{N}_8$:Eu phosphors based Color Conversion Layers," *International Symposium on Next-Generation Electronics*, 2013.
- [25] C. Y. Shen, C. Zhong, and J. Z. Ming, "YAG: Ce^{3+} , Gd^{3+} nano-phosphor for white light emitting diodes," *Journal of Experimental Nanoscience*, vol. 8, no. 1, pp. 54-60, Jan, 2013.
- [26] E. F. Schubert, and J. K. Kim, "Solid-state light sources getting smart," *Science*, vol. 308, no. 5726, pp. 1274-1278, May, 2005.
- [27] H. T. Zhu, R. L. Fu, Y. H. Shi, Q. J. He, H. Wang, and X. H. Liu, "Multi-colour light emission based on pixel-array phosphor layer in LEDs," *Journal of Luminescence*, vol. 221, May, 2020.
- [28] Y. H. Wang, J. Y. Ding, Y. C. Wang, X. F. Zhou, Y. X. Cao, B. Ma, J. Y. Li, X. C. Wang, T. Seto, and Z. Y. Zhao, "Structural design of new $\text{Ce}^{3+}/\text{Eu}^{2+}$ -doped or co-doped phosphors with excellent thermal stabilities for WLEDs," *Journal of Materials Chemistry C*, vol. 7, no. 7, pp. 1792-1820, Feb, 2019.
- [29] Z. G. Xia, Z. H. Xu, M. Y. Chen, and Q. L. Liu, "Recent developments in the new inorganic solid-state LED phosphors," *Dalton Transactions*, vol. 45, no. 28, pp. 11214-11232, 2016.
- [30] A. Tiwari, and S. J. Dhoble, "Tunable lanthanide/transition metal ion-doped novel phosphors for possible application in w-LEDs: a review," *Luminescence*, vol. 35, no. 1, pp. 4-33, Feb, 2020.

- [31] Y. Ding, N. Guo, X. Lu, H. T. Zhou, L. Wang, R. Z. Ouyang, Y. Q. Miao, and B. Q. Shao, "None-rare-earth activated $\text{Ca}_{14}\text{Al}_{10}\text{Zn}_6\text{O}_{35}:\text{Bi}^{3+},\text{Mn}^{4+}$ phosphor involving dual luminescent centers for temperature sensing," *Journal of the American Ceramic Society*, vol. 102, no. 12, pp. 7436-7447, Dec, 2019.
- [32] L. Jiang, C. K. Chang, D. L. Mao, and C. L. Feng, "Concentration quenching of Eu^{2+} in $\text{Ca}_2\text{MgSi}_2\text{O}_7 : \text{Eu}^{2+}$ phosphor," *Materials Science and Engineering B-Solid State Materials for Advanced Technology*, vol. 103, no. 3, pp. 271-275, Oct, 2003.
- [33] Z. Y. Mao, Y. C. Zhu, Y. Zeng, L. Gan, and Y. Wang, "Concentration quenching and resultant photoluminescence adjustment for $\text{Ca}_3\text{Si}_2\text{O}_7:\text{Tb}^{3+}$ green-emitting phosphor," *Journal of Luminescence*, vol. 143, pp. 587-591, Nov, 2013.
- [34] H. S. Lee, and J. W. Yoo, "Yellow phosphors coated with TiO_2 for the enhancement of photoluminescence and thermal stability," *Applied Surface Science*, vol. 257, no. 20, pp. 8355-8359, Aug, 2011.
- [35] Q. L. Li, C. Chen, Y. Qiao, B. C. Yu, B. Q. Shen, and Y. P. Zhang, "High thermal stability of green-emitting phosphor $\text{NaBaB}_9\text{O}_{15}:\text{Tb}^{3+}$ via energy compensation," *Journal of Alloys and Compounds*, vol. 897, Mar, 2022.
- [36] L. N. Cao, W. Li, B. Devakumar, N. Ma, X. Y. Huang, and A. F. Lee, "Full-Spectrum White Light-Emitting Diodes Enabled by an Efficient Broadband Green-Emitting $\text{CaY}_2\text{ZrScAl}_3\text{O}_{12}:\text{Ce}^{3+}$ Garnet Phosphor," *Acs Applied Materials & Interfaces*, vol. 14, no. 4, pp. 5643-5652, Feb, 2022.
- [37] Y. M. Xu, Y. F. Dong, C. J. Tao, P. L. Li, and Z. J. Wang, "The high thermal stability of white emitting phosphor $\text{Mg}_2\text{Y}_2\text{Al}_2\text{Si}_2\text{O}_{12}:\text{Dy}^{3+},\text{Eu}^{3+},\text{La}^{3+}/\text{Lu}^{3+}$ for white light emitting diodes," *Luminescence*, vol. 37, no. 4, pp. 551-557, Apr, 2022.
- [38] J. M. Ha, E. Novitskaya, G. A. Hirata, C. H. Zhou, R. E. Ridley, O. A. Graeve, and J. McKittrick, "A Facile Method Using a Flux to Improve Quantum Efficiency of Submicron Particle Sized Phosphors for Solid-State Lighting Applications," *Ceramics-Switzerland*, vol. 1, no. 1, pp. 38-53, Sep, 2018.
- [39] J. K. Han, J. I. Choi, A. Piquette, M. Hannah, M. Anc, M. Galvez, J. B. Talbot, and J. McKittrick, "Phosphor Development and Integration for Near-UV LED Solid State Lighting," *Ecs Journal of Solid State Science and Technology*, vol. 2, no. 2, pp. R3138-R3147, 2013.

- [40] T. Krishnapriya, A. Jose, T. A. Jose, A. C. Saritha, C. Joseph, and P. R. Biju, "Investigation of the structural and photoluminescence properties of Eu^{3+} doped $\text{Na}_6\text{CaP}_2\text{O}_9$ phosphors for solid state lighting," *Materials Research Bulletin*, vol. 139, Jul, 2021.
- [41] Y. Jin, W. P. Qin, J. S. Zhang, Y. Wang, C. Y. Cao, J. S. Zhang, and X. G. Ren, "A Novel Red Phosphor ($\text{La}_3\text{PO}_7 : \text{Eu}^{3+}$) Prepared by Solid State Method," *Spectroscopy and Spectral Analysis*, vol. 28, no. 12, pp. 2768-2771, Dec, 2008.
- [42] K. S. Hong, and H. S. Yang, "Characterization and Photophysical Properties of Tricalcium Phosphates Prepared by Using the Solid-State Reaction Process," *Journal of the Korean Physical Society*, vol. 74, no. 3, pp. 236-240, Feb, 2019.
- [43] Z. Wei, Y. Ji, M. Zhu, W. Qu, Z. Feng, W. Guo, and J. Li, "Luminescence properties of garnet $\text{Y}_2\text{Mg}_2\text{Al}_2\text{Si}_2\text{O}_{12}:\text{Ce}^{3+}$ phosphors," *Chemical Physics Letters*, vol. 771, 2021.
- [44] T. Zorenko, V. Gorbenko, S. Witkiewicz, and Y. Zorenko, "Study of the luminescence of Eu^{2+} and Eu^{3+} states in $\text{Ca}_3\text{Ga}_2\text{Ge}_3\text{O}_{12}:\text{Eu}$ garnet using synchrotron radiation excitation," *Optical Materials*, vol. 99, 2020.
- [45] X. Huang, and H. Guo, "A novel highly efficient single-composition tunable white-light-emitting $\text{LiCa}_3\text{Mg}_3\text{V}_3\text{O}_{12}:\text{Eu}^{3+}$ phosphor," *Dyes and Pigments*, vol. 154, pp. 82-86, 2018.
- [46] I. Aritman, S. Yildirim, M. F. Ebeoglugil, M. Yurddaskal, K. Ertekin, and E. Celik, "Sol-gel synthesis, characterization, and photoluminescence properties of sub-micron $\text{Gd}_2\text{O}_2\text{SO}_4$ powders," *Journal of the Australian Ceramic Society*, vol. 53, no. 2, pp. 457-463, Oct, 2017.
- [47] R. Praveena, L. Shi, K. H. Jang, V. Venkatramu, C. K. Jayasankar, and H. J. Seo, "Sol-gel synthesis and thermal stability of luminescence of $\text{Lu}_3\text{Al}_5\text{O}_{12}:\text{Ce}^{3+}$ nano-garnet," *Journal of Alloys and Compounds*, vol. 509, no. 3, pp. 859-863, 2011.
- [48] A. Potdevin, G. Chadeyron, and R. Mahiou, " Tb^{3+} -doped yttrium garnets: Promising tunable green phosphors for solid-state lighting," *Chemical Physics Letters*, vol. 490, no. 1-3, pp. 50-53, 2010.
- [49] D. Song, C. Guo, and T. Li, "Luminescence of the self-activated vanadate phosphors $\text{Na}_2\text{LnMg}_2\text{V}_3\text{O}_{12}$ ($\text{Ln}=\text{Y}, \text{Gd}$)," *Ceramics International*, vol. 41, no. 5, pp. 6518-6524, 2015.

- [50] H. Bai, Y. Song, D. Li, Q. Ma, X. Dong, W. Yu, Y. Yang, J. Wang, G. Liu, and T. Wang, "Realizing white light emitting in single phased LaOCl based on energy transfer from Tm^{3+} to Eu^{3+} ," *Ceramics International*, vol. 44, no. 6, pp. 6754-6761, 2018.
- [51] M. Yang, H. You, Y. Jia, H. Qiao, N. Guo, and Y. Song, "Synthesis and luminescent properties of $NaLa(MoO_4)_2:Eu^{3+}$ shuttle-like nanorods composed of nanoparticles," *CrystEngComm*, vol. 13, no. 12, 2011.
- [52] L. Xu, X. Yang, H. Lu, C. Hu, and W. Hou, " $NaY(MoO_4)_2$ microcrystals with controlled faceting and their tunable photoluminescence properties after doping with Eu^{3+} ," *RSC Advances*, vol. 4, no. 26, 2014.
- [53] X. P. Chen, X. Y. Huang, and Q. Y. Zhang, "Concentration-dependent near-infrared quantum cutting in $NaYF_4:Pr^{3+}, Yb^{3+}$ phosphor," *Journal of Applied Physics*, vol. 106, no. 6, Sep, 2009.
- [54] R. J. Xie, N. Hirosaki, Y. Q. Li, and T. Takeda, "Rare-Earth Activated Nitride Phosphors: Synthesis, Luminescence and Applications," *Materials*, vol. 3, no. 6, pp. 3777-3793, Jun, 2010.
- [55] S. Georgescu, E. Cotoi, A. M. Voiculescu, O. Toma, and C. Matei, "REFLECTANCE SPECTRA OF $YVO_4:Eu^{3+}$ PHOSPHORS SYNTHESIZED BY DIRECT PRECIPITATION," *Romanian Journal of Physics*, vol. 55, no. 7-8, pp. 750-757, 2010.
- [56] J. B. Lian, W. G. Wang, B. X. Wang, and J. Li, "Photoluminescence of $(Gd_{1-x}Dy_x)_2O_2SO_4$ phosphors Synthesized by Homogeneous Precipitation Method," *Advanced Materials Research*. pp. 612-615, 2011.
- [57] B. K. Grandhe, V. R. Bandi, K. Jang, S. Ramaprabhu, S. S. Yi, and J. H. Jeong, "Enhanced red emission from $YVO_4:Eu^{3+}$ nano phosphors prepared by simple Co-Precipitation Method," *Electronic Materials Letters*, vol. 7, no. 2, pp. 161-165, Jun, 2011.
- [58] W. Pan, G. L. Ning, X. Zhang, J. Wang, Y. Lin, and J. W. Ye, "Enhanced luminescent properties of long-persistent $Sr_2MgSi_2O_7:Eu^{2+}, Dy^{3+}$ phosphor prepared by the co-precipitation method," *Journal of Luminescence*, vol. 128, no. 12, pp. 1975-1979, Dec, 2008.
- [59] Y. L. Yang, X. M. Li, W. L. Feng, W. L. Li, and C. Y. Tao, "Synthesis and Characteristic of $CaMoO_4:Eu^{3+}$ Red Phosphor for W-LED by Co-precipitation," *Journal of Inorganic Materials*, vol. 25, no. 10, pp. 1015-1019, Oct, 2010.

- [60] Z. J. Yu, X. W. Huang, W. D. Zhuang, X. Z. Cui, H. Q. He, and H. W. Li, "Co-precipitation preparation and luminescent behavior of (Y, Gd)BO₃ : Eu phosphor," *Journal of Rare Earths*, vol. 22, no. 6, pp. 829-832, Dec, 2004.
- [61] L. M. Chepyga, A. Osvet, I. Levchuk, A. Ali, Y. Zorenko, V. Gorbenko, T. Zorenko, A. Fedorov, C. J. Brabec, and M. Batentschuk, "New silicate based thermographic phosphors Ca₃Sc₂Si₃O₁₂:Dy, Ca₃Sc₂Si₃O₁₂:Dy,Ce and their photoluminescence properties," *Journal of Luminescence*, vol. 202, pp. 13-19, 2018.
- [62] Y. Tratsiak, Y. Bokshits, A. Borisevich, M. Korjik, A. Vaitkevičius, and G. Tamulaitis, "Y₂CaAlGe(AlO₄)₃:Ce and Y₂MgAlGe(AlO₄)₃:Ce garnet phosphors for white LEDs," *Optical Materials*, vol. 67, pp. 108-112, 2017.
- [63] J. S. Liao, L. L. Nie, L. F. Zhong, Q. J. Gu, and Q. Wang, "Co-precipitation synthesis and luminescence properties of K₂TiF₆:Mn⁴⁺ red phosphors for warm white light-emitting diodes," *Luminescence*, vol. 31, no. 3, pp. 802-807, May, 2016.
- [64] C. G. Ma, W. Zheng, L. G. Jin, and L. M. Dong, "Fluorescence and preparation of Sr-2(P₂O₇):Ce,Tb phosphate by co-precipitation method," *Rare Metals*, vol. 32, no. 4, pp. 420-424, Aug, 2013.
- [65] X. Li, H. Y. Wang, L. Guan, Y. J. Fu, Z. Guo, K. S. Yuan, L. C. Tie, Z. P. Yang, and F. Teng, "Influence of pH value on properties of YPO₄:Tb³⁺ phosphor by co-precipitation method," *Journal of Rare Earths*, vol. 33, no. 4, pp. 346-349, Apr, 2015.
- [66] Y. Shi, Q. W. Chen, and J. L. Shi, "Effect of precipitants on morphologies of Lu₂O₃ phosphors by co-precipitation process," *Journal of Inorganic Materials*, vol. 23, no. 4, pp. 824-828, Jul, 2008.
- [67] M. H. M. Abdelrehman, R. E. Kroon, A. Yousif, H. Ahmed, and H. C. Swart, "Luminescence properties of Yb³⁺ and Er³⁺ co-doped into Gd₂O₃:Bi³⁺ phosphor powder," *Journal of Alloys and Compounds*, vol. 902, May, 2022.
- [68] N. N. N. Roslan, W. A. W. Razali, A. R. Tamuri, H. Azhan, and Z. Mohamed, "Synthesis of green phosphor SrAl₂O₄: Eu²⁺, Dy³⁺: Rietveld refinement and optical properties," *Chalcogenide Letters*, vol. 19, no. 2, pp. 83-91, Feb, 2022.
- [69] A. S. Mukasyan, P. Epstein, and P. Dinka, "Solution combustion synthesis of nanomaterials," *Proceedings of the Combustion Institute*, vol. 31, pp. 1789-1795, 2007.

- [70] S. T. Aruna, and A. S. Mukasyan, "Combustion synthesis and nanomaterials," *Current Opinion in Solid State & Materials Science*, vol. 12, no. 3-4, pp. 44-50, Jun-Sep, 2008.
- [71] C. M. Mehare, N. S. Dhoble, C. Ghanty, and S. J. Dhoble, "Photoluminescence and thermoluminescence characteristics of $\text{CaAl}_2\text{Si}_4\text{O}_{12}:\text{Dy}^{3+}$ new phosphor prepared by combustion synthesis," *Journal of Molecular Structure*, vol. 1227, 2021.
- [72] J. Li, K. Qiu, J. Li, W. Li, Q. Yang, and J. Li, "A novel broadband emission phosphor $\text{Ca}_2\text{KMg}_2\text{V}_3\text{O}_{12}$ for white light emitting diodes," *Materials Research Bulletin*, vol. 45, no. 5, pp. 598-602, 2010.
- [73] C. Zhao, J. Yu, Y. Zhang, H. Gong, B. Xie, X. Lin, M. Sheng, J. Mao, and J. Jing, "Microwave-induced solution combustion synthesis and luminescent properties of nano-sized powders with different Nd concentrations," *Ceramics International*, vol. 46, no. 11, pp. 17891-17895, 2020.
- [74] K. Uematsu, K. Toda, and M. Sato, "Preparation of $\text{YVO}_4 : \text{Eu}^{3+}$ phosphor using microwave heating method," *Journal of Alloys and Compounds*, vol. 389, no. 1-2, pp. 209-214, Mar, 2005.
- [75] K. Uematsu, A. Ochiai, K. Toda, and M. Sato, "Characterization of $\text{YVO}_4 : \text{Eu}^{3+}$ phosphors synthesized by microwave heating method," *Journal of Alloys and Compounds*, vol. 408, pp. 860-863, Feb, 2006.
- [76] A. Toda, K. Uematsu, T. Ishigaki, K. Toda, and M. Sato, "Morphology control of phosphors synthesized by microwave heating method," *Key Engineering Materials*. pp. 233-+, 2010.
- [77] H. K. Jung, D. W. Lee, K. Y. Jung, and J. H. Boo, "Fabrication of dense $\text{BaMgAl}_{10}\text{O}_{17} : \text{Eu}^{2+}$ phosphor particles by spray pyrolysis," *Journal of Alloys and Compounds*, vol. 390, no. 1-2, pp. 189-193, Mar, 2005.
- [78] J. L. Wu, X. Wang, G. H. Peng, Z. H. Liang, and X. F. Wang, "Spherical $\text{SrMoO}_4:\text{Eu}^{3+}$ Phosphors Prepared by Spray Pyrolysis," *Advanced Materials Research*. pp. 93-+, 2014.
- [79] M. J. Kim, J. H. Park, K. Y. Lee, S. Lee, G. S. Han, H. J. Song, H. Shin, T. K. Ahn, and H. S. Jung, "Cerium-Doped Yttrium Aluminum Garnet Hollow Shell Phosphors Synthesized via the Kirkendall Effect," *Acs Applied Materials & Interfaces*, vol. 6, no. 2, pp. 1145-1151, Jan, 2014.

- [80] P. V. Tumram, P. R. Kautkar, S. P. Wankhede, P. D. Belsare, and S. V. Moharil, "Combustion Synthesis of Some Cr³⁺-Activated Aluminate Phosphors," *Physics of the Solid State*, vol. 63, no. 7, pp. 1104-1112, Jul, 2021.
- [81] M. Ayvacikli, "Characterization of a Green-Emitting Copper-Doped Barium Aluminate Phosphor," *Spectroscopy Letters*, vol. 47, no. 7, pp. 504-511, Aug, 2014.
- [82] L. C. Chen, Z. L. Tseng, W. W. Chang, and Y. W. Lin, "Warm white light-emitting diodes using organic-inorganic halide perovskite materials coated YAG:Ce³⁺ phosphors," *Ceramics International*, vol. 44, no. 4, pp. 3868-3872, Mar, 2018.
- [83] V. Tucureanu, A. Matei, and A. M. Avram, "Synthesis and characterization of YAG:Ce phosphors for white LEDs," *Opto-Electronics Review*, vol. 23, no. 4, pp. 239-251, Dec, 2015.
- [84] J. Zhong, W. Zhuang, X. Xing, L. Wang, Y. Li, Y. Zheng, R. Liu, Y. Liu, and Y. Hu, "Blue-shift of spectrum and enhanced luminescent properties of YAG: Ce³⁺ phosphor induced by small amount of La³⁺ incorporation," *Journal of Alloys and Compounds*, vol. 674, pp. 93-97, 2016.
- [85] J. Xu, W. W. Chen, R. J. Zeng, and D. L. Peng, "A Carbon-free sol-gel method for preparation of Lu₃Al₅O₁₂: Ce³⁺ phosphors for potential applications in laser scintillators and LEDs," *Materials Letters*, vol. 133, pp. 1-4, Oct, 2014.
- [86] R. Nagaraj, A. Raja, and S. Ranjith, "Synthesis and luminescence properties of novel red-emitting Eu³⁺ ions doped silicate phosphors for photonic applications," *Journal of Alloys and Compounds*, vol. 827, Jun, 2020.
- [87] M. Iwaki, K. Sugimoto, M. Watanabe, K. Uematsu, K. Toda, and M. Sato, "High thermal stable blue-emitting alkali silicate phosphor, Eu²⁺-activated Na₂Mg₂Si₆O₁₅," *Journal of Ceramic Processing Research*, vol. 20, no. 3, pp. 205-210, Jun, 2019.
- [88] J. S. Kim, O. H. Kwon, J. W. Jang, S. H. Lee, S. J. Han, J. H. Lee, and Y. S. Cho, "Long-Term Stable, Low-Temperature Remote Silicate Phosphor Thick Films Printed on a Glass Substrate," *Acs Combinatorial Science*, vol. 17, no. 4, pp. 234-238, Apr, 2015.
- [89] L. E. Muresan, A. I. Cadis, I. Perhaita, O. Ponta, O. Pana, L. Trinkler, B. Berzina, and V. Korsaks, "Influence of vinyltriethoxysilane concentration on structural and luminescent characteristics of cerium doped yttrium based silicate phosphors," *Ceramics International*, vol. 41, no. 10, pp. 13179-13188, Dec, 2015.

- [90] I. A. Turkin, M. V. Keskinova, M. M. Sychov, K. A. Ogurtsov, K. Hara, Y. Nakanishi, and O. A. Shilova, "Cathodoluminescent Properties and Particle Morphology of Eu-Doped Silicate Phosphors Synthesized in Microwave Furnace," *Advances in Intelligent Systems and Computing*. pp. 339-346, 2017.
- [91] R. Yu, M. He, N. Xie, H. M. Noh, B. K. Moon, B. C. Choi, and J. H. Jeong, "Photoluminescence Properties of a New Orange-Red-Emitting Sm³⁺-Doped Potassium Calcium Silicate Phosphor," *Science of Advanced Materials*, vol. 9, no. 3-4, pp. 514-518, Mar, 2017.
- [92] Y. Liu, W. Zhuang, Y. Hu, and W. Gao, "Improved photoluminescence of green-emitting phosphor Ca₃Sc₂Si₃O₁₂:Ce³⁺ for white light emitting diodes," *Journal of Rare Earths*, vol. 28, no. 2, pp. 181-184, 2010.
- [93] G. Li, D. Deng, Y. Li, Q. Wang, Y. Hua, and S. Xu, "Luminescence properties of Mn²⁺ ions doped Lu₂CaMg₂Si₃O₁₂ garnet phosphors," *Journal of Rare Earths*, vol. 30, no. 3, pp. 193-196, 2012.
- [94] Y. Chu, Q. Zhang, J. Xu, Y. Li, and H. Wang, "An orange emitting phosphor Lu₂-CaMg₂Si_{2.9}Ti_{0.1}O₁₂:xCe with pure garnet phase for warm white LEDs," *Journal of Solid State Chemistry*, vol. 229, pp. 213-218, 2015.
- [95] Y. Chen, D. Feng, S. Xu, S. Zeng, and X. Wei, "Synthesis and photoluminescence of Eu²⁺ doped Lu₂CaMg₂Si₃O₁₂ garnet phosphors," *Materials Letters*, vol. 164, pp. 180-182, 2016.
- [96] H. L. Ngee, T. Hatsumori, K. Uematsu, T. Ishigaki, K. Toda, and M. Sato, "Synthesis of phosphate phosphor for a white LED," *Physics Procedia*. pp. 171-183, 2009.
- [97] K. N. Shinde, and S. J. Dhoble, "5d-4f transition in new phosphate-based phosphors," *Luminescence*, vol. 27, no. 1, pp. 69-73, Jan-Feb, 2012.
- [98] A. Toda, K. Uematsu, T. Ishigaki, K. Toda, and M. Sato, "Synthesis and luminescence property of new phosphate phosphor, RbPO₃:Tb," *Materials Science and Engineering B-Advanced Functional Solid-State Materials*, vol. 173, no. 1-3, pp. 168-170, Oct, 2010.
- [99] K. N. Shinde, S. J. Dhoble, and A. Kumar, "Synthesis of novel Dy³⁺ activated phosphate phosphors for NUV excited LED," *Journal of Luminescence*, vol. 131, no. 5, pp. 931-937, May, 2011.

- [100] G. F. Ju, Y. H. Hu, L. Chen, X. J. Wang, and Z. F. Mu, "Recent progress in Eu²⁺-activated phosphate persistent phosphors," *Optical Materials*, vol. 36, no. 11, pp. 1920-1923, Sep, 2014.
- [101] J. Sun, X. Zhang, and H. Du, "Combustion synthesis and luminescence properties of blue NaBaPO₄:Eu²⁺ phosphor," *Journal of Rare Earths*, vol. 30, no. 2, pp. 118-122, 2012.
- [102] X. Yang, J. Chen, C. Chai, S. Zheng, and C. Chen, "Near ultraviolet excited white light emitting diode (WLED) based on the blue LiCaPO₄:Eu²⁺ phosphor," *Optik*, vol. 198, 2019.
- [103] D. Kim, B. R. Lee, S. H. Park, B. C. Choi, J. H. Kim, and J. H. Jeong, "Cation substitution induced excellent quantum efficiency and thermal stability in (Ca_{1-x}Sr_x)₉La(PO₄)₇:Eu²⁺ phosphors," *New Journal of Chemistry*, vol. 43, no. 31, pp. 12325-12330, 2019.
- [104] F. Lei, B. Yan, and H. H. Chen, "Solid-state synthesis, characterization and luminescent properties of Eu³⁺-doped gadolinium tungstate and molybdate phosphors: Gd(2-x)MO₆:Eu-x(3+) (M = W, MO)," *Journal of Solid State Chemistry*, vol. 181, no. 10, pp. 2845-2851, Oct, 2008.
- [105] J. Czajka, Z. Piskula, A. Szczeszak, and S. Lis, "Structural, morphology and luminescence properties of mixed calcium molybdate-tungstate microcrystals doped with Eu³⁺ ions and changes of the color emission chromaticity," *Optical Materials*, vol. 84, pp. 422-426, Oct, 2018.
- [106] M. Y. Guan, X. H. He, T. M. Shang, J. H. Sun, and Q. F. Zhou, "Hydrothermal synthesis of ultrathin Bi₂MO₆ (M=W, Mo) nanoplates as new host substances for red-emitting europium ion," *Progress in Natural Science-Materials International*, vol. 22, no. 4, pp. 334-340, Aug, 2012.
- [107] Y. Hu, W. Zhuang, H. Ye, D. Wang, S. Zhang, and X. Huang, "A novel red phosphor for white light emitting diodes," *Journal of Alloys and Compounds*, vol. 390, no. 1-2, pp. 226-229, 2005.
- [108] C.-H. Chiu, M.-F. Wang, C.-S. Lee, and T.-M. Chen, "Structural, spectroscopic and photoluminescence studies of LiEu(WO₄)_{2-x}(MoO₄)_x as a near-UV convertible phosphor," *Journal of Solid State Chemistry*, vol. 180, no. 2, pp. 619-627, 2007.
- [109] S. Verma, K. Verma, D. Kumar, B. Chaudhary, S. Som, V. Sharma, V. Kumar, and H. C. Swart, "Recent advances in rare earth doped alkali-alkaline earth borates for solid state lighting applications," *Physica B-Condensed Matter*, vol. 535, pp. 106-113, Apr, 2018.

- [110] S. P. Hargunani, R. P. Sonekar, R. S. Palaspagar, P. Patil, and S. K. Omanwar, "Blue Luminescent Phosphor $\text{Sr}_3\text{Y}_1\text{-X}(\text{BO}_3)_3\text{:Bi-X(3+)}$ for WLED Applications," 2019.
- [111] G. Li, Q. Cao, Z. Li, Y. Huang, and H. Jiang, "Solution combustion synthesis and luminescence properties of $(\text{Y,Gd})\text{Al}_3(\text{BO}_3)_4\text{:Eu}^{3+}$ phosphors," *Journal of Rare Earths*, vol. 28, no. 5, pp. 709-712, 2010.
- [112] İ. Pekgözlü, "A novel UV-emitting phosphor: $\text{LiSr}_4(\text{BO}_3)_3\text{:Pb}^{2+}$," *Journal of Luminescence*, vol. 143, pp. 93-95, 2013.
- [113] J. T. Ingle, A. B. Gawande, R. P. Sonekar, S. K. Omanwar, Y. Wang, and L. Zhao, "Combustion synthesis and optical properties of Oxy-borate phosphors $\text{YCa}_4\text{O}(\text{BO}_3)_3\text{:RE}^{3+}$ ($\text{RE}=\text{Eu}^{3+}$, Tb^{3+}) under UV, VUV excitation," *Journal of Alloys and Compounds*, vol. 585, pp. 633-636, 2014.
- [114] M. S. Jang, Y. H. Choi, S. Wu, T. G. Lim, and J. S. Yoo, "Material properties of the Ce^{3+} -doped garnet phosphor for a white LED application," *Journal of Information Display*, vol. 17, no. 3, pp. 117-123, 2016.
- [115] T. L. Deng, S. R. Yan, and J. G. Hu, "Effect of Calcination Temperature on Up-Conversion Photoluminescence of the $\text{GdAlO}_3\text{:Er}^{3+}$, Yb^{3+} Phosphor," *Ecs Journal of Solid State Science and Technology*, vol. 4, no. 3, pp. R48-R53, 2015.
- [116] K. A. Koparkar, N. S. Bajaj, and S. K. Omanwar, "Effect of calcination temperature on structural and optical properties of europium (III) doped $\text{SrO-Y}_2\text{O}_3$ phosphor," *Journal of Materials Science-Materials in Electronics*, vol. 26, no. 5, pp. 2748-2753, May, 2015.
- [117] S. Chong, B. J. Riley, E. T. Nienhuis, D. Lee, and J. S. McCloy, "Syntheses and Crystal Structures of Rare-Earth Oxyapatites $\text{Ca}_2\text{RE}_8(\text{SiO}_4)_6\text{O}_2$ ($\text{RE} = \text{Pr}$, Tb , Ho , Tm)," *Journal of Chemical Crystallography*, vol. 51, no. 3, pp. 293-300, Sep, 2021.